A review on B/A measurement methods with a clinical perspective

A review on *B/A* measurement methods with a clinical perspective

Anastasiia Panfilova, Ruud J. G. van Sloun, Hessel Wijkstra, Oleg A. Sapozhnikov, and Massimo Mischi

Citation: The Journal of the Acoustical Society of America **149**, 2200 (2021); doi: 10.1121/10.0003627
View online: https://doi.org/10.1121/10.0003627
View Table of Contents: https://asa.scitation.org/toc/jas/149/4
Published by the Acoustical Society of America

JASA REVIEW-ARTICLE

A review on *B/A* measurement methods with a clinical perspective

Anastasiia Panfilova,[1,a)] Ruud J. G. van Sloun,[1] Hessel Wijkstra,[1,b)] Oleg A. Sapozhnikov,[2,c)] and Massimo Mischi[1]
[1]*Electrical Engineering Department, Faculty of Electrical Engineering, Eindhoven University of Technology, Groene Loper 35612 AE, Eindhoven, The Netherlands*
[2]*Department of Acoustics, Physics Faculty, Moscow State University, Leninskie Gory, Moscow 119991, Russia*

ABSTRACT:
The nonlinear parameter of ultrasound *B/A* has shown to be a useful diagnostic parameter, reflecting medium content, structure, and temperature. Despite its recognized values, *B/A* is not yet used as a diagnostic tool in the clinic due to the limitations of current measurement and imaging techniques. This review presents an extensive and comprehensive overview of the techniques developed for *B/A* measurement of liquid and liquid-like media (e.g., tissue), identifying the methods that are most promising from a clinical perspective. This work summarizes the progress made in the field and the typical challenges on the way to *B/A* estimation. Limitations and problems with the current techniques are identified, suggesting directions that may lead to further improvement. Since the basic theory of the physics behind the measurement strategies is presented, it is also suited for a reader who is new to nonlinear ultrasound. © *2021 Acoustical Society of America*. https://doi.org/10.1121/10.0003627

(Received 31 July 2020; revised 21 December 2020; accepted 12 February 2021; published online 2 April 2021)
[Editor: James F. Lynch] Pages: 2200–2237

I. INTRODUCTION

In the last several decades, ultrasound propagation has been treated as a nonlinear phenomenon (Duck, 2002). The importance of nonlinear propagation effects has been recognised in medical ultrasound for predicting/modelling heat deposition in tissue, relevant for safety regulations, as well as defining optimal settings for high-intensity focused ultrasound therapy (Carstensen *et al.*, 1980; Cartersen, 1998; Duck and Starritt, 1983; Filonenko and Khokhlova, 2001; Ginter *et al.*, 2002; Goss and Fry, 1981; Jackson *et al.*, 2013; Muir and Carstensen, 1980) and lithotripsy (Cleveland and McAteer, 2007). In addition, tissue harmonic imaging has found wide application, improving the resolution of images with respect to those obtained in fundamental mode (Burns *et al.*, 2000; Ma *et al.*, 2005; Shen and Li, 2001; Zhang and Gong, 2006). Furthermore, stemming from a different underlying mechanism, contrast agents have become a useful tool in the clinic, generating a strong nonlinear signal when isonified and allowing for the extraction of information about vascular perfusion and dispersion (Panfilova *et al.*, 2019; van Sloun *et al.*, 2017).

Apart from the established medical applications of nonlinearity, new ultrasound modalities for the quantification of the parameter of nonlinearity (Madigosky *et al.*, 1981) *B/A* have been continuously developed for the last few decades in an effort to bring it to the clinic. This parameter characterizes the degree of nonlinearity of a medium. Studies of aqueous solutions have concluded that *B/A* is influenced by the chemical composition and molecular structure of the solutes (Gong *et al.*, 1993; Sarvazyan *et al.*, 1990; Sehgal *et al.*, 1986a), and were found to be useful to assess the structure of silicone oil used in eye surgery (Zhe *et al.*, 2014). It has also been shown to be useful for tissue characterization, demonstrating distinct values for fatty (Law *et al.*, 1985), malignant, healthy, and cirrotic tissue in the liver (Errabolu *et al.*, 1988; Gong *et al.*, 1993; Sehgal *et al.*, 1984; Sehgal *et al.*, 1986a). Since these different tissue conditions are also associated with different compositions, several papers have developed models defining *B/A* depending on the constituents of the studied substance (Apfel, 1983; Everbach *et al.*, 1991), leading to works estimating tissue content from its *B/A* value combined with additional parameters (e.g., speed of sound, compressibility) (Apfel, 1986; Errabolu *et al.*, 1987; Gong *et al.*, 1993; Sehgal *et al.*, 1986a).

In studies with the same chemical composition, it was shown that *B/A* increases with structural hierarchy of tissue (e.g., intact liver vs homogenized liver) (Law *et al.*, 1981, 1983; Zhang *et al.*, 1991) and that *B/A* was sensitive to structural changes in tissue caused by disease (Gong *et al.*, 1993; Zhang and Gong, 1999). Moreover, there have been indications that *B/A* reflects the quasilattice structure of water, i.e., the ratio of bound to unbound water molecules (Sehgal *et al.*, 1986b; Yoshizumi *et al.*, 1987), altered in malignant tissues (Chung *et al.*, 2008; Nikolini *et al.*, 1987) and skin disease (Takenouchi *et al.*, 1986).

B/A has also been used to quantify the nonlinear scattering properties of ultrasound contrast agents (Verboven,

[a)]Electronic mail: A.P.Panfilova@tue.nl
[b)]Also at: Department of Urology, Amsterdam University Medical Centers location AMC, Meibergdreef 9, 1105 AZ, Amsterdam, The Netherlands.
[c)]Also at: Center for Industrial and Medical Ultrasound, Applied Physics Laboratory, University of Washington, 1013 Northeast 40th Street, Seattle, WA 98105.

https://doi.org/10.1121/10.0003627

2017; Wu and Tong, 1998; Xia, 2019). From a different perspective, B/A is sensitive to temperature, increasing for most liquids as the temperature increases (Khelladi *et al.*, 2009; Lu *et al.*, 2001) and increasing as tissue is heated (Choi *et al.*, 2011; Jackson *et al.*, 2014; Liu *et al.*, 2008; Lu *et al.*, 2004; Sehgal *et al.*, 1986a). Even though some works show a small B/A increment when tissue is coagulated (Jackson *et al.*, 2014; Saito and Kim, 2011), others state the contrary (Choi *et al.*, 2011; Lu *et al.*, 2004). Several works demonstrated that the B/A profile in tissue follows the temperature profile, generating images of the temperature distribution through B/A (Ichida *et al.*, 1983; Liu *et al.*, 2008; Lu *et al.*, 2004) and suggesting B/A as a tool for high intensity focused ultrasound (HIFU) treatment monitoring (Dongen and Verweij, 2008; Varray *et al.*, 2011b). Besides this, there is evidence that some tumors exhibit an increased temperature compared to surrounding parenchyma (Fear *et al.*, 2002), and that glucose administration is able to raise their temperature by 7 °C (Jain *et al.*, 1984), suggesting that the temperature distribution may help to identify tumor location. This body of evidence fortifies the motivation to develop B/A measurement methods, whether it is for assessment of biological liquids or nonlinear imaging aimed at tissue diagnosis or temperature monitoring.

It was demonstrated that B/A is proportional to the change of sound speed accompanied by an adiabatic change in pressure [Eq. (4)]. This dependency forms the basis of the thermodynamic method for measuring B/A (Beyer, 1960; Everbach and Apfel, 1995; Lu *et al.*, 1998; Sehgal *et al.*, 1984; Zhang and Dunn, 1991; Zhu *et al.*, 1983). In this framework, one records speed of sound changes in the substance when it is subjected to different static pressures. This method is considered to be accurate (Everbach and Apfel, 1995; Hamilton and Blackstock, 1998; Zhang and Dunn, 1991); however, it is also the most cumbersome, requiring a temperature controlled environment and a special cell, where the pressure can be varied. This technique can only yield a single, averaged B/A value for the whole bulk of the studied medium.

The method for aqueous solutions observes the subtle B/A changes for varying solute concentrations of biological compounds (Chalikian *et al.*, 1992; Sarvazyan *et al.*, 1990). Modifying the setup for the thermodynamic method, the inventors of the aqueous solution method enabled accurate velocity measurement for a small sample volume of 1 mL and derived an equation with differential parameters between the solution and the solvent, rather than absolute values. Keeping the main disadvantages of the thermodynamic method, this technique is the most accurate of all B/A measurement methods.

The finite amplitude method (FAM) exploits the dependency of the speed of sound on B/A and the excess medium density (or particle velocity, or excess pressure). Due to this dependency [Eq. (5)], the peaks of the sinusoidal US wave travel faster than the valleys. This leads to nonlinear distortion of the wave, equivalent to the generation of higher harmonics in the frequency spectrum. Consequently, nonlinear attenuation of the wave increases due to energy transfer from the fundamental component to the higher harmonics, which experience stronger attenuation than the fundamental. This way, the energy of a nonlinear wave is attenuated to a higher extent than that of a small-signal linear wave. FAMs exploit all these alterations, quantifying distortion through direct observation of the wave profile (Hunter *et al.*, 2016; Mikhailov and Shutilov, 1959; Takahashi, 1995), through harmonic content (Adler and Hiedemann, 1962; Beyer, 1960; Fujii *et al.*, 2004; Gong *et al.*, 1989; Law *et al.*, 1985; Liu *et al.*, 2008; Shklovskaya-Kordi, 1963; Varray *et al.*, 2011b; Wallace *et al.*, 2007; Zhang and Gong, 1999; Zhang and Dunn, 1987) or by observing nonlinearly induced attenuation (Byra *et al.*, 2017; Hikata *et al.*, 1980; Kashkooli *et al.*, 1987; Nikoonahad and Liu, 1989). This family of methods counts the largest number of publications of all. Even though FAMs are less accurate than the thermodynamic method, they require a much simpler measurement setup and have high potential for a clinical application, enabling B/A tomography for in-transmit measurements and a few echo-mode imaging strategies.

The parametric array method requires transmission of two, typically collinear, beams that generate secondary waves at the sum and difference frequencies. The amplitude of these waves is proportional to the medium B/A (Barrière and Royer, 2001; Bereza *et al.*, 2008; Nakagawa *et al.*, 1984; Zhang *et al.*, 2001a). The secondary beams are narrow, less prone to diffraction than those observed with FAM, and do not have side lobes. Parametric array tomography allows for higher resolution, compared to finite amplitude tomography (Gong *et al.*, 2004; Wang *et al.*, 2003). No echo-mode imaging has been performed with this method.

The pump wave method registers the speed of sound change of a low-amplitude high-frequency wave when another high-amplitude low-frequency wave modulates the pressure in the medium (Ichida *et al.*, 1983; Kato and Watanabe, 1994; Sato *et al.*, 1985). Uniquely, this method allows for a reconstruction of the B/A profile along the path of the low-amplitude high-frequency wave from a through-transmission measurement. A particular case of this method, the second order ultrasound field technique (SURF), has been utilized to acquire echo-mode images representing the B/A distribution (Fukukita *et al.*, 1996; Kvam *et al.*, 2019b).

The method of phase conjugated beams (Krutyansky *et al.*, 2007; Preobrazhensky and Pernod, 2003) utilizes a wave phase conjugater to reverse the beam insonating it and reradiate its amplified version back to the source. The amplitude of the harmonics of the reradiated beam reflects the B/A of the propagation medium. Phase conjugation provides the unique capability to compensate for phase distortion of the wave and achieves high-quality retrofocusing. Only C-scan images of isoechogenic phantoms have been acquired with this method. The possibility of echo-mode imaging is excluded.

The vast body of literature devoted to nonlinear ultrasound has already provided material for several review papers. Beyer (1973), Duck (2002), Hamilton and

Blackstock (1998), Muir and Carstensen (1980) discuss the origins of nonlinearity and the way it manifests itself with further consequences in practical applications. Some of these (Beyer, 1973; Hamilton and Blackstock, 1998) introduce separate equations for different states of matter: gas, liquid, and solids. Hamilton and Blackstock (1998) and Naugolnykh (2009) wrote historical reviews on the evolution of nonlinearity in ultrasound. Zheng *et al.* (1999) wrote a review on material characterization with the help of nonlinear acoustics, devoting a significant portion of it to solids. (Bjørnø, 1986, 2005, 2010; Hamilton and Blackstock, 1998; Zhang and Gong, 2006) are review papers that summarize the progress in B/A measurement methods either over a short time span, devote their attention mainly to a specific measurement strategy, or provide a brief general overview of the main concepts of the existing methods. A concise review of most techniques for B/A measurement has been given by Sato and Yamakoshi more than 30 years ago (Sato and Yamakoshi, 1986). Varray *et al.* (2011a) presented a review of FAMs that have the potential to be extended to echo-mode regarding the parametric array and pump wave method as one of the above.

This review aims at presenting an extensive and comprehensive up to date overview of B/A measurement and B/A imaging methods of liquids and liquid-like media (e.g., tissue). Importantly, it gives more focus to methods that are relevant for a medical application and discusses the most common pitfalls in this context. By identifying blind spots and limitations we aim at suggesting directions of research that may bring B/A to the clinic. This review paper is further separated into the following sections: Sec. II, theoretical background; Sec. III, Thermodynamic method; Sec. IV, method for aqueous solutions; Sec. V, FAM; Sec. VI, parametric array; Sec. VII, pumping waves; Sec. VIII, phase conjugate beam, and Sec. IX, conclusion.

Section II explains the origin of B/A, presents the most utilized wave equations of nonlinear acoustics, and gives a short overview of the main B/A measurement groups of methods. The sections devoted to various methods (Secs. III–VIII) start with a short introduction of the governing equations and the first published works, followed by the resulting developments, subdivided depending on the adopted measurement strategies. In cases where this has been accomplished, the sections are concluded with studies that presented B/A images. Since the review introduces the basic theory required to understand the physics behind the presented measurement strategies, it is also suited for a reader who is new to nonlinear ultrasound.

II. THEORETICAL BACKGROUND

A. *B/A* origin

An ultrasound wave consists of a series of compressions and rarefactions. Linear acoustics views density as linearly dependent on pressure. However, this is an approximation, and ultrasound propagation, in general, is a nonlinear process. The adiabatic equation of state expresses the pressure-density relation with the Taylor expansion series (Beyer, 1960; Coppens *et al.*, 1965; Hamilton and Blackstock, 1998),

$$P = P_0 + \rho_0 \left(\frac{\partial P}{\partial \rho}\right)_{0,s} \frac{\rho - \rho_0}{\rho_0} + \frac{{\rho_0}^2}{2} \left(\frac{\partial^2 P}{\partial \rho^2}\right)_{0,s} \left(\frac{\rho - \rho_0}{\rho_0}\right)^2 + \cdots. \tag{1}$$

Here, P and P_0 are instantaneous and hydrostatic pressures, ρ and ρ_0 are instantaneous and equilibrium densities of the medium under investigation and the partial derivatives are taken about the equilibrium state (indicated by the subscript 0) and constant entropy (indicated by subscript s). One can define

$$A = \rho_0 \left(\frac{\partial P}{\partial \rho}\right)_{0,s} = \rho_0 {c_0}^2, \tag{2}$$

where c_0 is the small-signal speed of sound, and

$$B = {\rho_0}^2 \left(\frac{\partial^2 P}{\partial \rho^2}\right)_{0,s}, \tag{3}$$

making

$$\frac{B}{A} = \frac{\rho_0}{{c_0}^2} \left(\frac{\partial^2 P}{\partial \rho^2}\right)_{0,s} = \frac{\rho_0}{{c_0}^2} \left(\frac{\partial c^2}{\partial \rho}\right)_{0,s} = 2\rho_0 c_0 \left(\frac{\partial c}{\partial P}\right)_{0,s}. \tag{4}$$

The relative importance of second-order nonlinear effects to linear effects can be expressed with the nonlinear parameter B/A or the alternative nonlinear coefficient (Varray *et al.*, 2011a), expressed as $\beta = 1 + (B/2A)$ for liquid and liquid-like media (e.g., tissue).

As stated previously (Beyer, 1973; Hamilton and Blackstock, 1998), one may differentiate Eq. (1) by ρ and, by substituting the speed of sound $c^2 = (\partial P/\partial \rho)_s$, obtain

$$\frac{c}{c_0} = 1 + \frac{B}{2A}\left(\frac{\rho - \rho_0}{\rho_0}\right) = 1 + \frac{B}{2A}\frac{u}{c_0} \tag{5}$$

for a plane progressive wave, illustrating that the local speed of sound c is dependent on B/A and u, the particle velocity. The former is an oscillating disturbance, induced by ultrasound propagation. This explains the origin of accumulating wave distortion, leading to saw-tooth waves: the compressional part of the wave (the high density region, with positive particle velocity and positive excess pressure) travels faster than the rarefractional part, contributing to wave distortion proportionally to B/A.

Tables I and II summarize the measured B/A values for liquids and animal tissues. As one can see, at atmospheric pressure and room temperature B/A is in the range of 5–11 for most liquids and liquid-like media.

https://doi.org/10.1121/10.0003627

TABLE I. Liquids. This table presents B/A values of some pure liquids at atmospheric pressure and in a temperature range of 20 °C–30 °C. When several studies are stated, all of them were included in the column "*Studies*" and only one value was chosen to be stated in the column "B/A."

Medium	B/A	Studies
Water	5.1	Beyer, 1960; Davies *et al.*, 2000; Zhu *et al.*, 1983
Methanol	9.7	Lu *et al.*, 1998
Ethylene glycol	9.9	Zhang and Dunn, 1991
Ethanol	10.4	Lu *et al.*, 1998
Carbon tetrachloride	8.3	Davies *et al.*, 2000; Zhu *et al.*, 1983
Glycerol	10.1	Harris *et al.*, 2007; Khelladi *et al.*, 2009; Zeqiri *et al.*, 2015
Methanol	9.6	Coppens *et al.*, 1965; Lu *et al.*, 1998; Plantier *et al.*, 2002b
Glycerine	9.4	Mikhailov and Shutilov, 1960
Corn oil	11.4	Harris *et al.*, 2007; Kujawska *et al.*, 2003
Linseed oil	9	Kujawska *et al.*, 2003
Silicone oil	11	Takahashi, 1995
Olive oil	10.7	Saito and Kim, 2011
Hyper-branched silicone oil	8.5	Zhe *et al.*, 2014
Linear silicone oil	9.7	Zhe *et al.*, 2014
1-propanol	9.5	Banchet *et al.*, 2000
1-butanol	9.7	Banchet *et al.*, 2000; Saito and Kim, 2011; Saito *et al.*, 2005
Benzyl alcohol	10.4	Akiyama, 2000; Saito, 1993a; Saito *et al.*, 2005
1-pentanol	10.0	Banchet *et al.*, 2000
1-hexanol	10.2	Banchet *et al.*, 2000
1-heptanol	10.6	Banchet *et al.*, 2000
1-octanol	10.7	Banchet *et al.*, 2000
1-nonanol	10.8	Banchet *et al.*, 2000
1-decanol	10.7	Banchet *et al.*, 2000
N-butanol	11.2	Lu *et al.*, 1998; Plantier *et al.*, 2002b; Shklovskaya-Kordi, 1963
1-propanol	10.3	Fukukita *et al.*, 1996
N-propanol	10.7	Coppens *et al.*, 1965; Lu *et al.*, 1998
1,2-propanediol	11.5	Zorebski and Zorebski, 2009
Acetone	9.2	Coppens *et al.*, 1965

TABLE II. Animal tissues and fluids.

Medium	B/A	Studies
Bovine liver	7.8	Dunn *et al.*, 1982; Law *et al.*, 1981
	6.2–8	Law *et al.*, 1985
	8.1	Saito, 1993a
Homognized bovine liver	6.8	Dunn *et al.*, 1982; Law *et al.*, 1981
	7.2	Jackson *et al.*, 2014
Beef brain	7.6	Law *et al.*, 1985
Beef heart	6.7–7.4	Law *et al.*, 1985
Homogenized porcine liver	6.5	Kujawska *et al.*, 2003
	6.6	Gong *et al.*, 1989
Porcine liver	7	Saito, 1993a
	7.6	Choi *et al.*, 2011
	6.9	Gong *et al.*, 1993
	7.1, 6.9	Gong *et al.*, 1989
	7.2	Liu *et al.*, 2008; Lu *et al.*, 2004
	6.5	Gong *et al.*, 2004
	6.8	Zhang and Gong, 1999
	6.3	Zhang *et al.*, 1996
Porcine liver	6.5	Wang *et al.*, 2003
	7.3	Zhang *et al.*, 2001b
Pathologic porcine liver	7.4–10.3	Gong *et al.*, 2004; Gong *et al.*, 1993; Wang *et al.*, 2003; Zhang and Gong, 1999; Zhang *et al.*, 2001b; Zhang *et al.*, 1996
Porcine whole blood	6.3	Dunn *et al.*, 1982; Law *et al.*, 1981
	6.3	Gong *et al.*, 1989
	6	Kujawska *et al.*, 2003
Porcine fat	10.9–11.3	Law *et al.*, 1985
	9.6	Saito, 1993a
	10.8, 10.9	Gong *et al.*, 1989
	9.7	Liu *et al.*, 2008
	10.7	Zhang *et al.*, 2001b
	11	Gong *et al.*, 2004
	9.1	Zhang *et al.*, 1996
	11	Wang *et al.*, 2003
Porcine muscle	7.5–8.1	Law *et al.*, 1985
Porcine muscle	5.8	Lu *et al.*, 2004
Porcine heart	7.1, 6.8	Gong *et al.*, 1989
Porcine kidney	6.9, 6.3	Gong *et al.*, 1989
Porcine kidney	7.1	Zhang and Gong, 1999
Pathologic porcine kidney	7.1–8.1	Zhang and Gong, 1999
Porcine spleen	6.9, 6.3	Gong *et al.*, 1989
	6.9	Zhang and Gong, 1999
Porcine tongue	6.5, 6.8	Gong *et al.*, 1989
In vivo cat liver	6.5–7.0	Zhang and Dunn, 1987
Cat liver	6.4–6.9	Zhang and Dunn, 1987
Human liver	6.5	Sehgal *et al.*, 1984
Human breast fat	9.2	Sehgal *et al.*, 1984
Human multiple myeloma	5.6	Sehgal *et al.*, 1984
Fresh human blood	6.0	Gong *et al.*, 1989
Different kinds of body fats	9.6–10.8	Errabolu *et al.*, 1987
Human liver	6.3	Sehgal *et al.*, 1986a
Pathologic human liver	5.7–8.7	Sehgal *et al.*, 1986a

B. Main wave equations

To obtain the equations governing the propagation of ultrasound waves in fluid homogeneous media one may refer to the equation of motion, the continuity equation, the heat transfer equation, and the equation of state [Eq. (1)] (Naugolnykh and Ostrovskii, 1998). For an ultrasound wave, together these equations describe the relationship between the spatially varying quantities of pressure, particle velocity, density, as well as heat transfer, related to loss. When these equations model ideal fluid (lossless fluid) and only linear terms are kept, one may derive the well-known wave equation Crocker (1997),

$$\frac{\partial^2 P(z,t)}{\partial z^2} - \frac{1}{{c_0}^2}\frac{\partial^2 P(z,t)}{\partial t^2} = 0, \tag{6}$$

in one-dimensional (1D) space, where we chose to describe the pressure variation P, dependent on the coordinate z and

TABLE II. (*Continued*)

Medium	*B*/*A*	Studies
Human whole blood	6.3	Xu *et al.*, 2003
Bovine serum albumin solutions (various concentrations)	5.2–7.4	Dunn *et al.*, 1982; Law *et al.*, 1981, 1985; Zhu *et al.*, 1983
Hemoglobin solutions (various concentrations)	5.2–7.7	Dunn *et al.*, 1982; Law *et al.*, 1981
Milk	5.1, 5.9	Gong *et al.*, 1989
Egg yolk	8.9	Zhang *et al.*, 1996
	8.3	Zhang *et al.*, 2001b
	9.1	Errabolu *et al.*, 1987
	9.5	Saito, 1993a
Egg white	5.8	Saito, 1993a
	6.4	Zhang *et al.*, 1996
	6.3	Zhang *et al.*, 2001b
	5.2	Errabolu *et al.*, 1987

time t. When second order nonlinear effects are considered [e.g., equation of state given in the form of Eq. (1)] and propagation in three-dimensional (3D) space is addressed, one can obtain the Westervelt equation (Westervelt, 1963),

$$\nabla^2 P - \frac{1}{c_0{}^2}\frac{\partial^2}{\partial t^2}P = -\frac{\beta}{\rho_0 c_0{}^4}\frac{\partial^2 P^2}{\partial t^2}, \tag{7}$$

where $\nabla^2 = \partial^2/\partial x^2 + \partial^2/\partial y^2 + \partial^2/\partial z^2$ is the Laplacian. The term on the right-hand of Eq. (7) models cumulative nonlinear effects, while local nonlinear effects are neglected here (Hamilton and Blackstock, 1998; Jeong *et al.*, 2016), implying that the Westervelt equation is valid at propagation distances further than a few wavelengths from the source. Equation (7) models sound propagation of plane waves or quasi-plane waves, like directional beams (Devaney, 1980; Hamilton and Blackstock, 1998) in homogeneous lossless media. It was further expanded to include loss in a weakly thermoviscous fluid (Hamilton and Blackstock, 1998; Naugolnykh and Ostrovskii, 1998; Sapozhnikov, 2015; Szabo, 1994b; Tjotta and Tjotta, 1981),

$$\nabla^2 P - \frac{1}{c_0{}^2}\frac{\partial^2}{\partial t^2}P = -\frac{\delta}{c_0{}^4}\frac{\partial^3 P}{\partial t^3} - \frac{\beta}{\rho_0 c_0{}^4}\frac{\partial^2 P^2}{\partial t^2}, \tag{8}$$

where $\delta = 2c_0{}^3\alpha/\omega^2$ is sound diffusivity, proportional to α, the attenuation coefficient. Importantly, loss in a weakly thermoviscous fluid assumes attenuation to be proportional to the squared frequency of the wave f^2 (Hamilton and Blackstock, 1998; Naugolnykh and Ostrovskii, 1998; Szabo, 1994b; Tjotta and Tjotta, 1981). This is valid for some liquids (e.g., water, certain oils; Chanamai and McClements, 1998; Chavrier *et al.*, 2006; Naugolnykh and Ostrovskii, 1998; Szabo, 1994a); however, most biological media exhibit a nearly linear attenuation-frequency dependence (Cai *et al.*, 1992; Duck, 1990; Goss *et al.*, 1979; Purrington and Norton, 2012). Alternative time-domain equations exist, incorporating arbitrary attenuation (Cai *et al.*, 1992; Szabo, 1994b), more appropriate for, e.g., tissues. No exact analytical solution to the Westervelt equation exists. However, expressions in the form of integrals have been obtained in Jeong *et al.* (2016) for the case of weak nonlinearity with the help of the Green's function and when approximating the source pressure as a sum of Gaussian beams (Wen and Breazeale, 1988).

A somewhat simpler description of nonlinearity and attenuation was provided by Zabolotskaya and Khokhlov (1969) and Kuznetsov (1970). Derived from the same original equations as the Westervelt equation, the Khokhlov-Zabolotskaya-Kuznetsov (KZK) equation [Eq. (9)] makes the additional assumption of the parabolic approximation that holds for "acoustic sources which are many wavelengths across and for field points that are not too close to the source or too far off axis" (Jeong *et al.*, 2016),

$$\frac{\partial^2 P}{\partial \tau \partial z} = \frac{\delta}{2c_0{}^3}\frac{\partial^3 P}{\partial \tau^3} + \frac{\beta}{2\rho_0 c_0{}^3}\frac{\partial^2 P^2}{\partial \tau^2} + \frac{c_0}{2}\nabla_{tr}{}^2 P. \tag{9}$$

Here, $\nabla_{tr}^2 = \partial^2/\partial x^2 + \partial^2/\partial y^2$ is the transverse Laplacian and τ is the retarded time $\tau = t - (z/c_0)$. The terms on the right side of the equation from left to right represent wave attenuation, nonlinearity, and diffraction effects (Zhao and McGough, 2014). The diffraction effect describes the deviation of the field from a plane wave, due to finite source geometry and is somewhat elaborated on in Sec. V B 1. An explicit solution to the KZK equation for the case of weak nonlinearity has been derived in Froysa (1994), Jeong *et al.* (2015), and Ji *et al.* (2011).

The simplest equation describing combined effects of nonlinearity and thermoviscous loss is the Burgers equation (Burgers, 1948),

$$\frac{\partial P}{\partial z} - \frac{\beta}{\rho_0 c_0{}^3}P\frac{\partial P}{\partial \tau} = \frac{\delta}{2c_0{}^3}\frac{\partial^2 P}{\partial \tau^2}. \tag{10}$$

It considers only plane progressive waves, and therefore, does not account for the diffraction effects. Just as for the Westervelt equation, another form of Eq. (10) can be adopted for biological tissues and liquids, accounting for an arbitrary frequency dependence of attenuation (Blackstock, 1985; Chavrier *et al.*, 2006; Chen and Holm, 2004). The lossless Burger's equation is derived by setting the attenuation coefficient $\alpha = 0$ (and therefore $\delta = 0$) to zero,

$$\frac{\partial P}{\partial x} - \frac{\beta}{\rho_0 c_0{}^3}P\frac{\partial P}{\partial \tau} = 0. \tag{11}$$

The exact solutions to the lossy and lossless Burger's equations are known, derived by Fubini-Ghiron (1935) and Keck and Beyer (1960), respectively. These solutions are presented further in this review (Sec. V B). Unlike the Burgers equation, the Westervelt and KZK equations are mainly solved numerically, providing much more accurate predictions of the pressure field (Demi *et al.*, 2011; Doinikov

https://doi.org/10.1121/10.0003627

et al., 2014; Purrington and Norton, 2012; Zhao *et al.*, 2014). At the same time, solutions of the Burgers equation provide simple formulas for the fundamental and higher harmonic pressures. Diffraction affects can be accounted for in the solutions in a *post hoc* manner.

III. THERMODYNAMIC METHOD

It has been shown in Eq. (4) that B/A is proportional to the change in sound velocity occurring with an isentropic (adiabatic) change of hydrostatic pressure. The term isentropic refers here to a process where no heat or matter is abstracted or conveyed to the system from outside. Once the derivative in Eq. (4) is expanded, as previously demonstrated (Beyer, 1960; Hamilton and Blackstock, 1998; Rudnick, 1958),

$$\frac{B}{A} = 2\rho_0 c_0 \left(\frac{\partial c}{\partial P}\right)_{0,T} + \frac{2c_0 Tq}{\rho_0 C_P}\left(\frac{\partial c}{\partial T}\right)_{0,P}. \tag{12}$$

B/A can be expressed through the change in sound velocity caused by isothermal pressure and isobaric temperature (T) changes. The parameter $q = (1/V)(\partial V/\partial T)_P$ is the isobaric volume coefficient of thermal expansion and C_P is the specific heat at constant pressure. B/A is sometimes referred to in the literature as the adiabatic nonlinear parameter, while the first term on the right-hand side of Eq. (12) is referred to as the isothermal nonlinear parameter (Errabolu *et al.*, 1988; Varray, 2011) $(B/A)'$,

$$\left(\frac{B}{A}\right)' = 2\rho_0 c_0 \left(\frac{\partial c}{\partial P}\right)_{0,T}. \tag{13}$$

The remaining term in Eq. (12) is referred to as the isobaric nonlinear parameter,

$$\left(\frac{B}{A}\right)'' = \frac{2c_0 Tq}{\rho_0 C_P}\left(\frac{\partial c}{\partial T}\right)_{0,P}. \tag{14}$$

In general, the thermodynamic methods can be classified into two groups, where B/A is determined either from Eq. (12), as it was initially done, or from Eq. (4). Within these groups, the strategies to measure the speed of sound c differ. All studies carried out with the thermodynamic method require a velocimeter: a vessel of known length L, comprising the test liquid and the transmitter-receiver equipment, inserted in a liquid-filled pressure vessel, e.g., water (Law *et al.*, 1983, 1985) or oil (Greenspan and Tschiegg, 1957, 1959; Wilson, 1959) that is in turn submerged in a bath with controlled temperature (Fig. 1).

A. Traditional thermodynamic technique

The traditional thermodynamic technique determines B/A *via* Eq. (14). The required speed of sound measurement can be performed with different techniques, allowing to infer the travel time (time of flight) t_{tr} of the wave through the velocimeter of known length L (Fig. 1). All the identified

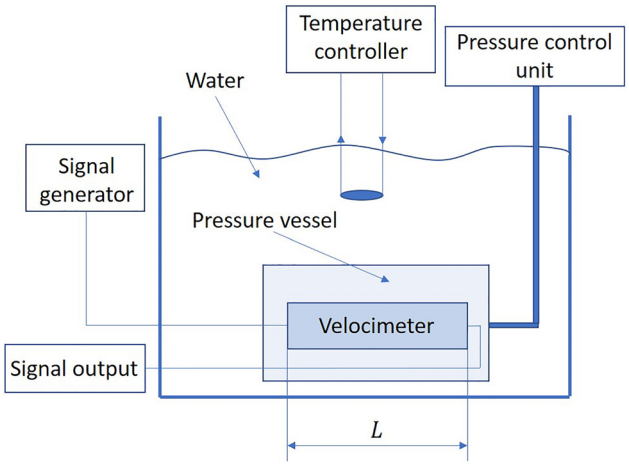

FIG. 1. (Color online) Schematic simplified diagram of the typical setup used for a thermodynamic B/A measurement. More detailed representations can be found in Holton *et al.* (1968) and Law *et al.* (1985).

works utilizing the traditional thermodynamic technique are summarized in Table III, stating the utilized technique and the parameter directly measured, as well as the specified measurement uncertainty and the investigated media.

The first paper reporting the determination of B/A by the thermodynamic method (Beyer, 1960) used thermodynamic data previously acquired by other scientists (Greenspan and Tschiegg, 1957, 1959; Wilson, 1959) for several liquids. In Greenspan and Tschiegg (1957, 1959) and Wilson (1959), t_{tr} was inferred with the help of a sing-around circuit (Ficken and Hiedemann, 1956; Zorebski *et al.*, 2005). This circuit allows for triggering of the generator to send a pulse once the preceding pulse is received and, therefore, to infer t_{tr} through the pulse repetition frequency (PRF). In this work, to improve the accuracy of the measurement Greenspan and Tschiegg (1957, 1959) and Wilson (1959) adjusted the PRF of the generator so that a new pulse was transmitted when the echoes of the previously transmitted pulse were superimposed on the receiver. This way, the device allowed determining the speed of sound from the pulse transit time t_{tr}, inferred from the PRF and the distance travelled by the pulse (L) equal to twice the length of the vessel,

$$c = 2L/t_{tr}. \tag{15}$$

Hagelberg *et al.* (1967) and Holton *et al.* (1968) performed the speed of sound c measurement in water with the pulse-echo method: using one transducer as the source and receiver, where t_{tr} was inferred from the interval between echoes reflected from an acoustic mirror positioned at the other end of the vessel.

Law *et al.* (1983) measured the coefficient of nonlinearity of biological solutions and soft tissues. Since for the studied substances, values of q and C_p in Eq. (12) were not known, the authors used the well-known values for water: the values for tissues measured in former studies showed a difference with water up to 30%, and as previously

TABLE III. Summary of works that measured B/A with the traditional thermodynamic technique. The indicators *liquid* and *tissue* refer to measurement uncertainties for liquids and tissues, respectively. Uncertainty (*Uncert.*,%) is stated in percent of the measured values.

Study	Measured parameter	Uncert., %	Investigated media
Beyer, 1960; Greenspan and Tschiegg, 1957, 1959; Wilson, 1959	PRF, sing-around circuit	—	Water, ethyl alcohol
Coppens *et al.*, 1965	PRF, sing-around citcuit	<3 (liquid)	Organic liquids, water-alcohol mixtures
Hagelberg *et al.*, 1967; Holton *et al.*, 1968	t_{tr}, pulse-echo m.	—	Water
Madigosky *et al.*, 1981	PRF, sing-around circuit	—	Fluorocarbon fluids
Law *et al.*, 1983	t_{tr}	3 (liquid), 5 (tissue)	Biological solutions, soft tissues
Law *et al.*, 1985	t_{tr}	3 (liquid), 5 (tissue)	Biological solutions, soft tissues
Zorebski and Zorebski, 2009	t_{tr}, pulse echo-overlap m.	3 (liquid)	Lower alkanediols
Zorebski *et al.*, 2016	PRF, sing-around circuit, pulse-echo-overlap m.	3 (liquid)	Ionic liquid

discovered, the term $(B/A)''$ contributed only 3% to the B/A value. The speed of sound was inferred from a direct measurement of the time of flight based on the display of the oscilloscope, showing the driving and received signals. Law *et al.* (1985) observed no dependence of B/A on solute molecular weight in dextran solutions and a linear dependency on solute concentration. The authors postulated that nonlinearity is a result of solute-solvent interactions. The authors also identified that homogenization of tissue reduced B/A and, in general, B/A showed an increasing trend with the specimen's structural hierarchy. It is worth mentioning that this paper presents a comprehensible diagram and description of the apparatus used.

Zorebski and Zorebski (2009) utilized the pulse-echo-overlap method (Greenspan and Tschiegg, 1957; Zorebski *et al.*, 2005) to determine the speed of sound in lower alkenediols by extracting the PRF at conditions of overlapping echoes coming back from a reflector. The authors acquired B/A at pressures up to 100 MPa and temperatures from 21 to 46 °C. Zorebski *et al.* (2016) extended the range of studied temperatures, measuring B/A from 16 to 46 °C.

The accuracy of the traditional thermodynamic techniques, taking into account further measurement uncertainties (e.g., temperature and pressure), resulted in a global uncertainty of the B/A estimation within 3% for liquid and 5% for tissue (Table III). The higher uncertainty for tissue samples accounts for the inhomogeneous speed of sound (Law *et al.*, 1985). The studies conducted with the traditional thermodynamic method revealed that B/A'' is much smaller compared to B/A' (constituting less than 5% for fluorocarbon fluids (Madigosky *et al.*, 1981), 9% of B/A for the liquids studied in Zorebski and Zorebski (2009), and 12% of the pressure-dependent term for methanol-water mixtures (Coppens *et al.*, 1965). Besides this, B/A' has shown to be always positive, while B/A'' can exhibit positive and negative values depending on the studied material. Hagelberg *et al.* (1967) and Holton *et al.* (1968) illustrated that for a range of temperatures up to 80 °C and a very wide range of pressures B/A of water has small variability (from 4.1 to 6.8), and increases monotonically with temperature for a pressure value of 1 atm. Coppens *et al.* (1965) demonstrated that B/A of alcohol mixtures show low variability with temperature. Madigosky *et al.* (1981) reported fluorocarbon fluids to have the highest nonlinearity reported so far ($B/A = 13$). Law *et al.* (1983, 1985) demonstrated the dependence of B/A on the chemical composition of biological solutions as well as the structural hierarchy of biological material.

B. Isentropic thermodynamic technique

The isentropic thermodynamic technique, also referred to as the improved thermodynamic method (Gong *et al.*, 1989; Lu *et al.*, 1998; Plantier *et al.*, 2002a), makes use of Eq. (4) rather than Eq. (12). It requires a rapid (1–3 s) change of pressure to eliminate significant heat transfer with the test vessel. This way, the pressure change can be regarded as an isentropic process. As noted by Zhu *et al.* (1983), this technique is simpler than its predecessor, since it eliminates the need for measurements at different temperature points. Moreover, as Sehgal *et al.* (1984) indicated, the traditional thermodynamic method requires knowledge of q and C_p, which are "not known with great precision for most soft tissues." The uncertainty of the early isentropic phase method is estimated to be 4% (Everbach and Apfel, 1995). However, the development of this method is connected to the improvement in the techniques measuring the speed of sound, permitting to reduce the uncertainty to <1% (Table IV). It is velocity measurement techniques that account for the variability of the isentropic phase methods. Therefore, the following section is divided into subsections according to the measured parameter through which the speed of sound is inferred, that being phase ϕ, voltage U_p, frequency f, or the time of flight t_{tr} of a pulse. A summary of the identified works, utilizing the isentropic thermodynamic technique, is presented in Table IV.

The most frequently used are phase measurement techniques, providing more accurate speed of sound estimations compared to earlier methods used in the framework of the traditional thermodynamic technique (Table III). A few others, deriving speed of sound from frequency information, or estimating the time of flight of a pulse, are also used. A detailed explanation follows below.

1. Phase measurements

Among the first publications using the isentropic thermodynamic technique are Emery *et al.* (1979) and

https://doi.org/10.1121/10.0003627

TABLE IV. Summary of strategies to measure B/A with the isentropic thermodynamic technique. The uncertainty (*Uncert.*, %) of the B/A measurement is stated in percent of the measured value for tissues and liquids.

Measured parameter	Studies	Uncert., %	Investigated media
Phase ϕ	Zhu *et al.*, 1983	2.5 (liquid)	Liquids, e.g., water, bovine serum albumin solution
	Gong *et al.*, 1989	4 (liquid), 7 (tissue)	Biological solutions and soft tissues
	Sehgal *et al.*, 1984; Sehgal *et al.*, 1986a	3 (tissue)	Normal and malignant human tissues
	Sehgal *et al.*, 1986b	1 (liquid)	Monohydric alcohol-water solutions
	Errabolu *et al.*, 1987	-	Livers, fat, egg, oils
	Errabolu *et al.*, 1988	3	Human and animal fats, simple mixtures (e.g., skim milk)
Voltage ΔU_p	Lu *et al.*, 1998	2.2 (liquid)	Water, organic liquids
	Plantier *et al.*, 2002a	2 (liquid)	Water
	Plantier *et al.*, 2002b	2 (liquid)	Primary alcohols
	Plantier *et al.*, 2003	<2.2 (liquid)	Alkanes
	Khelladi *et al.*, 2009	2 (liquid)	Glycerol
	Zhe *et al.*, 2014	<2 (liquid)	Silicone oils
Transmit time Δt_{tr}	Zhang and Dunn, 1991	0.7 (liquid)	Water, dextrose, ethylene glycol
	Zhang *et al.*, 1991	Tissues not assessed separately	Cat and rat livers, liver suspensions
Frequency f	Everbach and Apfel, 1995	0.85 (liquid)	Aqueous buffers, protein solutions, lipid oils, emulsions
	Davies *et al.*, 2000	1 (liquid)	Liquids

Zhu *et al.* (1983), measuring B/A of liquids. The authors considered the measurement isentropic, as the applied pressure changes were small (varying from 1 to 2 atm) and too fast (≈2.0 s) for a significant heat exchange. The speed of sound change is connected to the wave's transit time t_{tr} and the distance between transducers L *via* Eq. (16) (Zhu *et al.*, 1983),

$$\left(\frac{\partial c}{\partial P}\right) = -\frac{L}{{t_{tr}}^2}\left(\frac{\partial t_{tr}}{\partial P}\right). \tag{16}$$

Equation (16) allows us to determine B/A based on Eq. (4) as

$$\frac{B}{A} = -\frac{2\rho_0 {c_0}^2}{t_{tr}}\left(\frac{\Delta t_{tr}}{\Delta P}\right)_s. \tag{17}$$

To detect the change in transit time t_{tr}, Zhu *et al.* (1983) chose to conduct phase measurements: they compared the phase of the received tone burst to that of a reference signal with a phase mixer and acquired Δt_{tr} with the help of a delay line. Since $\Delta\varphi = \omega\Delta t_{tr}$ and $t_{tr} = L/c_0$, B/A was determined according to

$$\frac{B}{A} = -\frac{2\rho_0 {c_0}^3}{\omega L}\left(\frac{\Delta\varphi}{\Delta P}\right)_s, \tag{18}$$

where L is the length of the ultrasound path through the liquid. Equation (16) forms the basis of all phase measurement techniques, which in general produced more accurate results compared to earlier strategies. A follow-up paper (Gong *et al.*, 1989) of one of the authors of Zhu *et al.* (1983) used the same version of the method to measure B/A of biological solutions and soft tissues. Gong *et al.* (1989) confirmed the results obtained by Law *et al.* (1985) for homogenized liver versus whole liver, as well as biological solutions, observing that B/A increases with the structural hierarchy of the specimen.

a. Pressure-jump method. Sehgal *et al.* (1984) presented the pressure jump method. During the pressure increase, the phase of the received signal was monitored. The speed of sound was inferred from Eq. (18). After the pressure change, the system was allowed to equilibrate to the ambient temperature and the authors could also measure the isothermal nonlinear parameter $(B/A)'$. Sehgal *et al.* (1984) and Sehgal *et al.* (1986a) used the method described above, transmitting ultrasound in continuous-wave mode. This configuration was "most suitable for attenuating media" (Sehgal *et al.*, 1984) as tissue since high attenuation avoided the formation of standing waves. Sehgal *et al.* (1984) measured B/A of several human tissues. They demonstrated that fatty breast tissue had a substantially higher value than parenchymal liver tissue, and that multiple myeloma had a substantially lower B/A compared to normal parenchymal liver tissue. Sehgal *et al.* (1986a) showed that B/A of fatty liver is higher compared to normal, while cirrotic and tumorous B/A is lower than for normal liver. Sehgal *et al.* (1984) and (1986a) are the only papers, to the best of our knowledge, reporting B/A for malignant tissues.

In Errabolu *et al.* (1987), Errabolu *et al.* (1988), and Sehgal *et al.* (1986b), the adiabatic nonlinear parameter and the isothermal nonlinear parameter were measured with the pressure-jump method, detecting the phase change [Eq. (18)] of a shock-excited pulse. Sehgal *et al.* (1986b) reported B/A of alcohol-water mixtures. Since alcohols have smaller speed of sound and larger B/A, their addition to water was expected to increase B/A. This was not the case for low concentrations of alcohol. Such an effect on B/A was attributed to the effects of solvent-solute interactions, and alteration in the water-molecule structure due to the addition of alcohol. The authors speculated that, since tissue is composed of 60%–80% of water, changes in the state of tissue due to the change in unbound-bound water ratio must have been reflected in its B/A, creating another opportunity for determining tissue properties based on B/A. Errabolu

et al. (1988) demonstrated that human and animal fat tissues are highly nonlinear, with B/A values ranging between 10 and 12. Moreover, in the range of temperatures from 20 to 37 °C, B/A vs temperature exhibits a positive or flat trend. Errabolu *et al.* (1987) proposed a two-component model (fat and nonfat), able to predict the fat percentage based on the measured B/A and speed of sound. The model was tested for livers, fats, oil, and egg mixtures.

b. Phase derivation from output voltage. Lu *et al.* (1998) utilized a highly sensitive phase comparison technique by transmitting a tone burst signal and producing small pressure changes below 2 atm to liquids. This technique (like Zhu *et al.*, 1983) also utilizes a phase mixer. However, different from other methods, the phase change is inferred from the amplitude of the phase detector rather than with a delay line. The measurements are done for small phase changes (below $\pi/20$), where the output voltage of the phase detector (mixer) U_p is linearly dependent on signal phase ϕ. Therefore, the phase change of the detector signal, ΔU_p, can be described through the phase change $\Delta\phi$ as

$$\Delta U_p = kA_1A_2\Delta\phi, \tag{19}$$

where A_1 and A_2 are the amplitudes of the received and the reference signal that are mixed in the phase detector, and k is a constant characterizing the phase detector. This way, ΔU_p can be utilized to estimate B/A as

$$\frac{B}{A} = -\frac{2\rho_0 {c_0}^3}{\omega L}\frac{1}{kA_1A_2}\left(\frac{\Delta U_p}{\Delta P}\right)_s. \tag{20}$$

The maximum pressure change was adjusted to maintain a linear relation between voltage and phase. Lu *et al.* (1998) report the technique to have an uncertainty of 2.2%.

This strategy was used to measure B/A of several liquids (Khelladi *et al.*, 2009; Lu *et al.*, 1998; Plantier *et al.*, 2002a,b; Zhe *et al.*, 2014). A few of these studies (Khelladi *et al.*, 2009; Plantier *et al.*, 2002a,b, 2003) enabled B/A measurement at pressures up to 100 MPa and temperatures up to 100 °C.

2. Transmit time

Zhang and Dunn (1991) developed an isentropic thermodynamic method capable of measuring B/A of 4-mL sample volumes. This system is important for situations when samples are products of biochemical reactions with small yields or pathological tissue areas which may be of limited locus/size. The distance between the source and receiver in the velocimeter was only 1 cm. The speed of sound was determined with Eq. (17) by calculating the time delay from cross correlation of the transmitted and received pulses. Since the receiver was in the near field, an error was introduced in the velocity measurements; however, the authors stated that their system was nevertheless able to measure within an error of 0.7%, confirmed by measurement of three mixtures.

Zhang *et al.* (1991) used the above described setup (Zhang and Dunn, 1991) to determine the influence of structural parameters on B/A. Performing measurements of cat and rat liver tissue as well as suspensions acquired from these livers, the authors altered their structure physically and biochemically, and reached the conclusion that structural dependence of B/A "exists at all three levels of biological structure, viz., the tissue level, the cellular level and the molecular level. The relative contributions due to structural features is 26% at the tissue level, 20% at the cellular level, and 15% at the macromolecular level."

3. Frequency measurement

Everbach and Apfel (1995) automated the measurement of speed of sound, allowing for the performance of thousands of acquisitions on a sample in a reasonable time. The utilized interferometer consisted of a receiving and source transducer. A phase-locked loop circuit was used to correct for the frequency of the transmitted pulse by Δf so that a constant phase relationship was kept at the receiver transducer as the speed of sound changed in the medium. Since Δf required to keep the phase constant can be defined by

$$\Delta f/f_0 = \Delta c/c_0, \tag{21}$$

B/A can be expressed as

$$\frac{B}{A} = 2\rho_0 {c_0}^2\left(\frac{\Delta f}{f_0\Delta P}\right)_s, \tag{22}$$

where f_0 and ρ_0 are the initial frequency and density. A pressure of 180 kPa (1.85 atm) was generated in the measurement cell and then released. During this release (3 s) the source transducer transmitted 20-cycle tone bursts at 11 frequencies. Contrary to Sehgal *et al.* (1984) and Sehgal *et al.* (1986a), attenuation was an undesired effect for an interferometer, as the measurements were performed for a range of organic and aqueous solutions. The presented method is reported to have an accuracy of about 1%.

Davies *et al.* (2000) also measured the change in frequency associated with the pressure change [Eq. (22)]. Contrary to Everbach and Apfel (1995), they performed continuous wave phase locking since the continuous wave approach avoids the uncertainty of pulse onset identification. As the system was developed for small-volume samples, the authors encountered near-field problems (Zhang and Dunn, 1991) in an early setup when using phase locking in double-disk interferometers. To overcome this problem, they utilized a cylindrical piezoelectric cavity resonator which, coupled with the developed electronic system, "provided a real-time measurement of the change in speed of sound as function of frequency." The authors applied a 2-s pressure sweep from 0 to 200 kPa during which 100 data frequencies $f = f_0 + \Delta f$ were acquired. This system was reported to produce uncertainty of less than 1% for B/A.

https://doi.org/10.1121/10.0003627

IV. METHOD FOR AQUEOUS SOLUTIONS

Sarvazyan *et al.* (1990) noted that the B/A errors were too large to study solute-solvent mixtures with a small amount of solvent. Most biological compounds cannot be diluted in high concentrations in aqueous solutions due to the low solubility. The B/A change in the possible range of concentration is estimated to be approximately 1% (Sarvazyan *et al.*, 1990), within the error span of the most accurate thermodynamic techniques (see Tables III and IV). For this reason, Sarvazyan *et al.* (1990) developed a differential method that rather than measuring absolute values, estimated the differences between the solute and the solution, which is a common approach in chemical relaxation kinetics (Eggers and Funck, 1973). The accuracy of the relative measurements of the nonlinearity parameter achieved by this method was 0.3%.

The theory was derived by differentiating Eq. (12) for the traditional thermodynamic method, resulting in the following expression:

$$\frac{\Delta B/A}{C}\frac{1}{2\rho_0 c_0} = \frac{1}{C}\Delta\left(\frac{\partial c}{\partial P}\right)_T + ([U]+[\rho])\left(\frac{\partial c}{\partial P}\right)_{T_0} + \frac{\gamma_0 T_0}{\rho_0 C_p}\left[\frac{1}{C}\Delta\left(\frac{\partial c}{\partial T}\right)_{P_0} + ([c]+[\gamma]-[C_p])\times\left(\frac{\partial c}{\partial T}\right)_{P_0}\right], \quad (23)$$

where capital C is the solute concentration, values attributed to the solvent are denoted by subscript 0, and Δ refers to the difference between the solution and the solvent for the corresponding expressions. $[c]$, $[\rho]$, $[\gamma]$, $[C_p]$ are relative specific increments of speed of sound, solution density, thermal expansion coefficient, and heat capacity at constant pressure, respectively,

$$[c]=\frac{\Delta c}{c_0 C}, \quad [\rho]=\frac{\Delta\rho}{\rho_0 C}, \quad [\gamma]=\frac{\Delta\gamma}{\gamma_0 C}, \quad [C_p]=\frac{\Delta C_p}{C_{P_0} C}. \quad (24)$$

Parameters $[\rho]$, $[\gamma]$, $[C_p]$ are known from literature, leaving $[c]$, $\Delta(\partial c/\partial P)_T$, and $\Delta(\partial c/\partial T)_P$ as the values to be measured, given that the solvent parameters with subscript 0 are known.

The setup used in Sarvazyan (1982) is typical for the thermodynamic method (Sec. III). However, several important modifications were made. The measurement cell was represented by a four-channel resonator cell, each with a volume as small as 0.2 mL, all filled with the test liquids. Simultaneous velocity measurements in these chambers were made by the resonator method with an acoustic interferometer. Standing waves form in the cells at resonance frequencies at which the distance between transducers is equal to a whole number of half-wavelengths. This results in amplitude peaks at these frequencies (amplitude frequency characteristic), as well as a particular phase dependence of the received signal on the frequency (phase-frequency characteristic). The authors inferred Δc from the phase frequency characteristic, identifying the shift in resonance frequency Δf to keep the phase constant at its inflection point [Eq. (21)]. The resonator method is the only technique that can be applied for such small-volume samples (Sarvazyan, 1991). Different from previous thermodynamic studies (Sec. III), the authors introduced a reference cell with the solvent, placed in the same thermostated volume as the solution. This lowered the requirement for the temperature stability of the system.

The above work was employed to assess the acoustic properties of solutions of amino acids and proteins, giving insight into the molecular origins of B/A. For instance, the authors discovered that an increase in the number of charged groups that favor bonds with water molecules augments B/A, while CH_2 groups decrease it due to decreased accessibility of water to such molecules. The authors also noted a strong sensitivity of B/A to a replacement of a single atomic group within a molecule, compared to ultrasound velocity and density. These observations demonstrated that B/A may be a useful indicator of molecular structure and hydration of biomolecules in solutions. This method enables measurement of the smallest amounts of sample reported and provides the highest measurement accuracy (0.3%) reported until now (Sec. IX, Table VIII). A follow-up paper studied temperature dependencies of B/A of aqueous amino acid solutions (Chalikian *et al.*, 1992).

V. FAM

As demonstrated in Sec. II, the speed of an ultrasound wave at a point in space and time is dependent on B/A (or β) and the excess density (or particle velocity) at that point and time. Due to this, as the wave propagates it distorts, which was shown to be equivalent to the generation of higher harmonics (integers of the transmitted frequency) in the frequency domain (Fubini-Ghiron, 1935; Keck and Beyer, 1960; Krasilnikov *et al.*, 1957). As higher harmonics grow, the fundamental component is depleted due to the energy transfer from the fundamental harmonic to the higher harmonics.

All FAMs register the wave after a certain propagation distance in a medium (e.g., Fig. 2) and derive B/A from cumulative nonlinear effects observed in the registered signal. The FAMs can be classified into three main groups: deriving B/A directly from the wave's shape, from the second harmonic component, and from the fundamental component. A detailed description of each family of methods follows below. The theory presented in the introductory

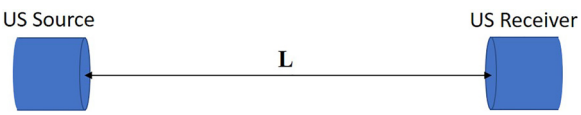

FIG. 2. (Color online) Schematic of the most common through-transmission setup used to measure B/A with many FAMs. Here, L is the path in the studied medium. In reflection-mode imaging, the receiver is substituted by a reflector plate, and the source transducer acts as the receiver.

sections (Secs. V C 1 and V B 1) of the FAM groups concerns only weak nonlinearity (the shock parameter $\sigma = [2\pi f P_1(0) z\beta/\rho_0 {c_0}^3] \leqslant 1$), since the pressure amplitudes that demonstrate strong nonlinearity are above the safety regulations for assessment of biological media. Table V, presented below, summarized all the identified FAM works and the utilized strategies to measure B/A.

A. Wave shape

1. Light diffraction method

The earliest works observing the wave shape to infer B/A were performed with optical methods (Fig. 3). When an optical wave propagates in a direction perpendicular to the ultrasonic beam, the initially flat wave front of the optical wave is modulated in phase according to the velocity profile of the US wave, possibly distorted due to nonlinear propagation.

This way, measurement of the diffraction of light allows for the reconstruction of the US wave's velocity profile and quantification of distortion by extracting w_0 or w_1 from its shape (Fig. 4), and thereby derivation of B/A.

This method was implemented by Mikhailov and Shutilov (1960) and Shutilov (1959) and yielded B/A for water and several other optically transparent liquids. More recently, Takahashi (1995) also utilized the waveshape to quantify B/A through the assessment of w_0 or w_1. In this case, the signal was received with a hydrophone, while the source pressure was determined from the diffraction pattern of light emitted by a laser. This way, the setup was a hybrid of those presented in Figs. 2 and 3. Other works are also known (Nomoto and Negishi, 1965), using the diffraction of light to capture the nonlinear distortion of ultrasound waves and extract B/A.

2. Modelling of the wave profile

Chavrier *et al.* (2006), Hunter *et al.* (2016), Jackson *et al.* (2014), and Jeong *et al.* (2016) utilized the setup presented in Fig. 2, where the signal passed through a medium of length L and was received by a hydrophone or a transducer. Chavrier *et al.* (2006), Hunter *et al.* (2016), and Jackson *et al.* (2014) fit nonlinear waveforms of the received pulses with the Burger's equation, where B/A (and α) was the fit parameter. These works use large source transducers (e.g., 10 cm in diameter; see Jackson *et al.*, 2014) to avoid edge diffraction effects, eliminating the need for diffraction correction and justifying the use of the Burger's equation which cannot account for diffraction. Conversely, Jeong *et al.* (2016) developed multi-Gaussian beam models based on a quasilinear approximation of the Westervelt equation and the KZK equation (Jeong *et al.*, 2015), including both diffraction and attenuation effects. This allowed describing the pressure fields of the fundamental and 2nd harmonic with no restrictions for the source size or the distance range. From a single measurement set at distances from 2 to 20 cm, the authors extracted the attenuation coefficients at the fundamental α_1 and 2nd harmonic frequency α_2, as well as the β value by fitting a model to the observed pressure profiles. A calibration procedure for $P_1(0)$ was required. Works inferring B/A through the wave profile require broadband receivers, able to capture the wave shape accurately.

B. Second harmonic measurements

1. Basic theory

The amplitudes of the higher harmonics in the preshock region ($\sigma \leqslant 1$) of a plane wave in a lossless medium are given by Fox and Rock (1941), Fubini-Ghiron (1935), and Hamilton and Blackstock (1998),

$$P_n(\sigma) = \left[\frac{2P_1(0)}{n\sigma}\right] J_n(n\sigma), \tag{25}$$

where n is a positive integer indicating the number of the harmonic: the fundamental $P_1(0)$ at the source and higher harmonics $P_{2,3,\ldots}$; and σ is the shock parameter $\sigma = 2\pi f P_1(0) z\beta/\rho_0 {c_0}^3$. Equation (25) is the Fubini solution (Fubini-Ghiron, 1935) of the lossless Burgers equation [Eq. (11)]. By expanding the Bessel function as a power series and neglecting the high order terms, the amplitude of the 2nd harmonic can be expressed as

$$P_2(z) = \left(\frac{B}{A} + 2\right) \frac{\pi f z {P_1}^2(0)}{2\rho_0 {c_0}^3}. \tag{26}$$

This equation illustrates that the amplitude of the 2nd harmonic increases proportionally to B/A, to the distance z from the source, and the frequency of the transmitted signal f. It also shows a quadratic dependence on the transmitted pressure amplitude $P_1(0)$ at the source.

Later, this theory was further developed to include losses in two alternative ways. The first one was based on the assumption that the attenuation of the fundamental and higher harmonics are independent of each other. Furthermore, the change of the 2nd harmonic amplitude was ascribed to its harmonic generation due to nonzero B/A value and its small-signal absorption (neglecting energy transfer to higher harmonic components) (Thuras *et al.*, 1935). The following expression is the solution to the equation describing the change of the 2nd harmonic:

$$P_2(z) = \frac{(2 + B/A)\pi f}{2\rho_0 {c_0}^3} {P_1}^2(0) \frac{e^{-\alpha_2 z} - e^{-2\alpha_1 z}}{2\alpha_1 - \alpha_2}, \tag{27}$$

where α_1 and α_2 are the attenuation coefficients of the fundamental and its harmonic. Here, no assumption about the frequency dependence of attenuation has been made, therefore, the formula is valid for liquids and tissues. This expression can be further simplified (Dunn *et al.*, 1982) when assuming $(\alpha_2 - 2\alpha_1)z$ to be small,

$$P_2(z) = \frac{(2 + B/A)\pi f z}{2\rho_0 {c_0}^3} {P_1}^2(0) e^{-(\alpha_1 + (\alpha_2/2))z}. \tag{28}$$

The previous simplification leads to an error of 1% when the value $(\alpha_2 - 2\alpha_1)z$ is $<1/2$ (Dunn *et al.*, 1982). Equation (28)

https://doi.org/10.1121/10.0003627

TABLE V. Intercomparison of FAMs. The table discusses the main principle, advantages and disadvantages, and accuracy of FAM variations in their initial form, developed for B/A estimation as a global parameter. In the column *Uncert.*, %, the measurement error is stated for liquids, tissues, or phantoms (tissue-mimicking or layers of liquid), respectively. The column *Images* states whether or not any experimental works presented B/A images, therefore, visualizing B/A distribution rather than a single global B/A value. $P_1(0)$, source pressure; P_2, 2nd harmonic pressure.

Main Groups	Subgroup	Main principle	Advantages	Disadvantages	Uncert., %	Images
Wave shape	Light diffraction. Sec. V A 1	Assessment US wave shape through diffraction of light	- Accurate, - No *per se* assumptions about the harmonic content of the signal is needed	- Complicated setup that includes a laser and an optical receiving system	7–8 (liquid) (Mikhailov and Shutilov, 1960) <8 (liquid) (Kashkooli *et al.*, 1987)	—
	Modelling of the wave profile. Sec. V A 2	Fit pulse waveforms to nonlinear models	- No *per se* assumptions about the harmonic content of the signal is needed	- Requires $P_1(0)$ (calibration) -Broadband receiver needed	10 (liquid, tissue) (Chavrier *et al.*, 2006; Hunter *et al.*, 2016; Jackson *et al.*, 2014), 5 (liquid) (Jeong *et al.*, 2016)	—
Second harmonic measurement	2nd harmonic maximum. Sec. V B 2 a	Experimentally identifying the distance from the source of P_2 maximum	- No clear advantages identified	- only for viscous liquids - Measurements at several distances	—	—
Second harmonic measurement	Extrapolation scheme. Sec. V B 2 b	Extrapolating $[\frac{P_2(x)}{xP_1(0)^2}]$ to zero distance from the source	- Does not need any attenuation measurement	- Requires transducer calibration to estimate $P_1(0)$ - Measurements at several distances	10 (liquid) (Adler and Hiedemann, 1962), 8 (liquid, tissue) (Law *et al.*, 1985) 2–11 (liquid) (Wallace *et al.*, 2007), 10 (liquid) (Law *et al.*, 1981; Dunn *et al.*, 1982)	—
	Single measurement. Sec. V B 2 c	Measuring the 2nd harmonic amplitude at a distance	- One measurement at one distance is sufficient for B/A estimation	- Requires transducer calibration to estimate $P_1(0)$ and an extra α measurement	4 (liquid) (Cobb, 1983), <8 (tissue) (Zhang and Dunn, 1987)	Echo-mode: (van Sloun *et al.*, 2015)
	Source $P_1(0)$ -P_2 characteristic. Sec. V B 2 d	Fitting a line to P_2 depending on the source pressure	- Requires measurements at only one distance	- Requires transducer calibration to estimate $P_1(0)$, α (unless can be neglected)	7.5 (liquid) (Chitnalah *et al.*, 2007), 3 (liquid) (Pantea *et al.*, 2013), 12 (liquid) (Panfilova *et al.*, 2018)	—
Second harmonic measurement	Comparative method. Sec. V B 2 e	Comparing P_2 in the sample to that in a reference medium at a fixed distance from the source	- Requires measurements at only one distance - No source calibration needed - Potential to mitigate diffraction effects	- Source pressure in the studied medium may be altered, compared to the reference medium (due to different acoustic impedances of the media)	< 3 (tissue) (Yu *et al.*, 2014), 8 (liquid) (Gong *et al.*, 1984), 3 (liquid) (Zhang *et al.*, 1991)	Echo-mode: (Toulemonde *et al.*, 2015; Varray *et al.*, 2011b)
	FAIS. Sec. V B 2 f	Extracting β from the ratio $\frac{P_{2x}}{P_{20}}$ (with the sample in the path between the source and the receiver and without)	- As for the comparative method - Requires little sample volume	—	8 (liquid) (Gong *et al.*, 1984), <8 (liquid, phantom) (Dong *et al.*, 1999), < 10 (liquid) (Harris *et al.*, 2007), <5 (tissue, liquid) (Kujawska *et al.*, 2003)	Tomography: (Zhang *et al.*, 1996), (Zhang and Gong, 1999), reflection tomography and echo-mode C-scans: (Gong *et al.*, 2004)
Second harmonic measurement	Transmission line method. Sec. V B 2 g	Measuring the fundamental saturation as source pressure is increased	- No transducer calibration required	- Acquisitions at several source-receiver separation distances	20 (liquid) (Kushibiki *et al.*, 1997), <2 (liquid) (Dong *et al.*, 2006)	—

TABLE V. (*Continued*)

Main Groups	Subgroup	Main principle	Advantages	Disadvantages	Uncert., %	Images
Fundamental	Sec. V C	Measuring the fundamental saturation as source pressure is increased	- One measurement distance - Transmit and reception at the same frequency	- Transducer calibration required, - For tissue may require high $P_1(0)$ for an accurate B/A estimation	10 (liquid) (Kashkooli *et al.*, 1987),	Echo-mode: [Nikoonahad and Liu, 1990)]

is particularly applicable to tissue since tissue attenuation exhibits a nearly linear frequency dependence (Duck, 1990; Goss *et al.*, 1979).

An alternative way to take attenuation into account was proposed (Blackstock, 1966; Keck and Beyer, 1960) when solving the Burger's equation [Eq. (10)] for the weakly nonlinear case characterized by a Goldberg number $G = 2\pi f P_0 \beta/\rho_0 {c_0}^3 \alpha < 1$ (Hamilton and Blackstock, 1998),

$$P_2(z) = \left(\frac{B}{A} + 2\right) \frac{\pi f {P_1}^2(0)}{2\alpha \rho_0 {c_0}^3} (e^{-2\alpha z} - e^{-4\alpha z}), \tag{29}$$

where α is the attenuation coefficient of the fundamental wave. The Golberg number reflects the balance between the nonlinear processes and the absorption processes (Duck, 2002). Equation (29) applies to weakly thermoviscous fluids (Sec. II B).

The theory above, as already mentioned, was developed for plane waves. Due to this, most studies use a plane piston source as a signal transmitter and perform the measurements in the near field at distances closer than the Rayleigh distance F_d ($F_d = \pi r^2/\lambda$, where r is the source radius and λ is the signal wavelength; Kuntz *et al.*, 1983). In reality, however, even the near field of a plane piston source differs from an ideal plane wave, due to interference of signals originated from different locations of the source (Huygens principle). These effects are diffraction effects (Duck, 2002) and result in a complicated diffraction pattern of pressure amplitude oscillations, demonstrated in Fig. 5. Only a very small triangular region of the near field remains truly a plane wave: in the proximity of the source the plane wave and the edge wave do not yet interfere (Kramer *et al.*, 1988). It is also worth mentioning that the second harmonic beam is somewhat narrower than the fundamental beam. This can be fully appreciated at greater distances in Duck (2002), where the pressure distributions are presented up to the far field.

The deviation from plane wave theory can be accounted for by the diffraction correction term. For example, Dunn *et al.* (1982) considered both attenuation and diffraction effects, leading to the following expression for the 2nd harmonic:

$$P_2(z) = \frac{(2 + B/A)\pi f z}{2\rho_0 {c_0}^3} {P_1}^2(0) e^{-(\alpha_1 + (\alpha_2/2)z)} F(z), \tag{30}$$

where $F(z)$ is the diffraction correction factor, described in detail in Ingenito and Williams (1971) and Williams (1951). Alternatively, the diffraction corrections developed using Multi-Gaussian beams have also been utilized (Haumesser and Meulen, 2019; Jeong *et al.*, 2017; Jeong *et al.*, 2015; Jeong *et al.*, 2016).

The theory above serves the basis of the FAMs. Numerous works have estimated B/A through 2nd harmonic measurement [Eqs. (26)–(30)]. In most of these methods, the 2nd harmonic is measured in the near field of a plane piston source, enabling the plane wave approximation. Therefore, these conditions are implied throughout this section (Sec. V B) unless otherwise stated. These

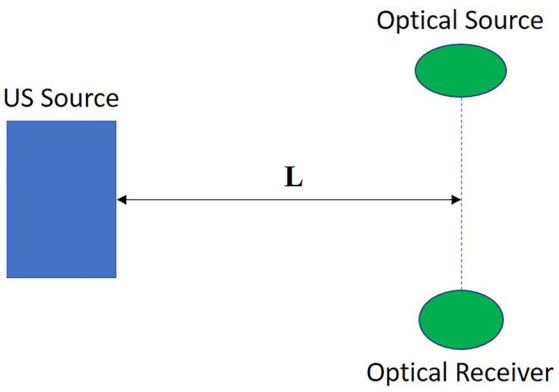

FIG. 3. (Color online) Schematic illustration of the setup used in optical methods/light diffraction methods for B/A measurement (top view). Detailed representations of such setups can be found in Adler and Hiedemann (1962) and Mikhailov and Shutilov (1959).

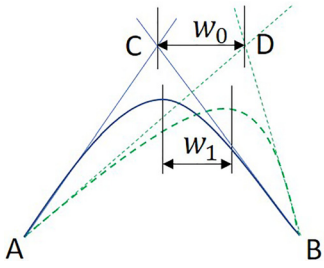

FIG. 4. (Color online) Illustration of the waveform deformation. The image shows the positive half-cycles of an undistorted sinus wave (solid line), and of a distorted wave (dashed line), where the distance w_1 is the distance between the maxima of these waves, and w_0 is the distance between points C and D, which are the intersections of the tangents at points A and B.

https://doi.org/10.1121/10.0003627

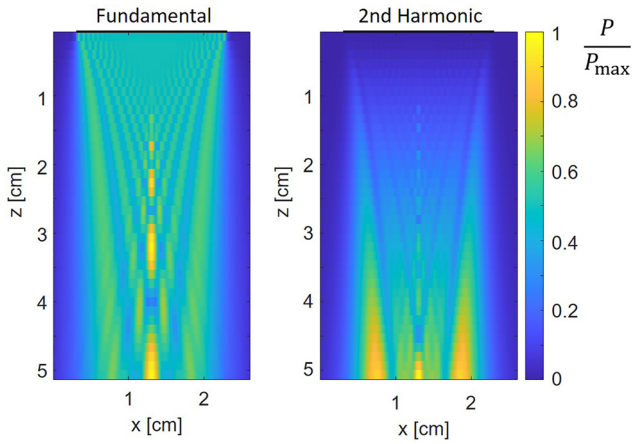

FIG. 5. (Color online) Simulated pressure distributions along the diagonal of a circular plane piston source up to 5 cm away from the source. The fundamental and the 2nd harmonic pressure amplitudes are normalized to their maximum amplitude values, the position of the source is indicated by the black line. The simulation was performed in *k-Wave*, MATLAB™ (Treeby and Cox, 2010) for a source with a radius of 10 mm, transmitting a Gaussian 10-cycles pulse at 2.25 MHz with an amplitude of 0.1 MPa, in 3D space.

methods are presented in two sections: measurements of homogeneous media (Sec. V B 2) and heterogeneous media (Sec. V B 3).

2. B/A measurement of homogeneous media

The studies discussed in this section assume invariant B/A along the beam path in the medium, yielding a single B/A value. All the strategies suitable for bulk estimation of B/A through 2nd harmonic measurement are presented below. All the presented works, unless otherwise mentioned, utilized the setup as in Fig. 2. Unlike the wave shape method, in this case, the receiver has to be responsive at the 2nd harmonic of the fundamental signal, transmitted by the source.

a. Second harmonic maximum. Equation (29) formed the basis for one of the early B/A measurement approaches (Beyer, 1960; Keck and Beyer, 1960). One can find the distance to the source where the 2nd harmonic reaches its maximum value by differentiating Eq. (29) with respect to z and finding the zero crossing. Once the coordinate of the 2nd harmonic maximum is determined experimentally, B/A can thus be calculated.

b. Extrapolation scheme. Other strategies utilized the lossless formulation in Eq. (26). It has been experimentally verified (Krasilnikov *et al.*, 1957) that at distances close to the source, the dependence of the 2nd harmonic on the distance z and the pressure at the source $P(0)$ follows the lossless model described by Eq. (26) also in a dissipative medium. Therefore, one can derive B/A by extrapolating the 2nd harmonic amplitude at zero distance from the source,

$$\frac{B}{A} = \frac{2\rho_0 c_0^3}{\pi f}\left[\frac{P_2(z)}{zP_1(0)^2}\right]_{zP_1(0)=0} - 2. \tag{31}$$

For this purpose, Adler and Hiedemann (1962) utilized the optical setup (Fig. 3) to measure the transmitted fundamental signal $P_1(0)$ and the 2nd harmonic at different distances from the source transducer. Extrapolation of $[P_2(z)/zP_1(0)^2]$ to $z=0$, as in Fig. 6, yielded B/A for water and m-Xylene.

Law *et al.* (1981) and Dunn *et al.* (1982) utilized a much simpler setup (Fig. 2), measuring the 2nd harmonic amplitude P_2 and $P_1(0)$ with an additional planar transducer, also employed in all the following studies unless otherwise mentioned. For this purpose, a calibration procedure of the receiver is required, allowing us to convert measured voltage to pressure values and to determine $P_1(0)$. Extrapolating $[P_2(z)/zP_1(0)^2]$ to zero distance from the source, they obtained B/A for several biological solutions as well as whole liver. When comparing their values to glycerol and glycerin, previously obtained by the thermodynamic method (Coppens *et al.*, 1965), they concluded that this technique has an uncertainty of 10%.

Dunn *et al.* (1982) introduced attenuation in the expression for the 2nd harmonic [Eq. (28)], showing that $[P_2(z)/zP_1(0)^2]$ decreases exponentially with distance in the proximity of the transducer. Moreover, they were the first ones to consider diffraction effects [Eq. (30)] that manifested themselves in the calibration procedure (Williams, 1951) of the receiver as well as in the quantification of the 2nd harmonic (Ingenito and Williams, 1971). Law *et al.* (1985) followed the same procedure as Dunn

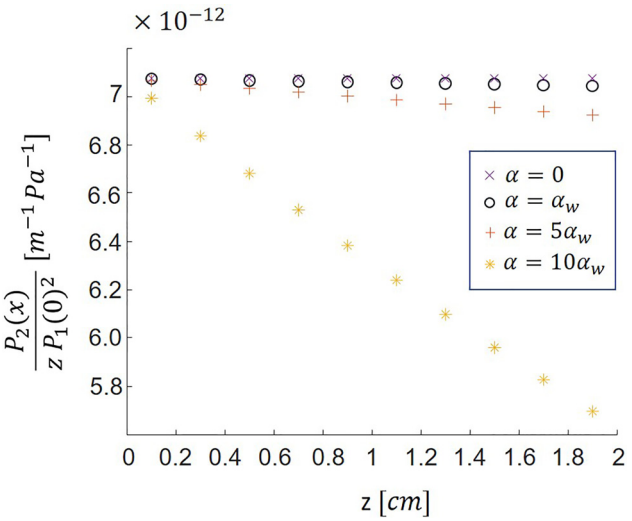

FIG. 6. (Color online) Simulated curves for media with the same acoustic parameters as for water but different attenuation. The graph illustrates the dependance of $[P_2(z)/zP_1(0)^2]$ on z for a lossless medium, a medium with an attenuation coefficient as that of water α_w, and media with much higher attenuation than that of water ($5\alpha_w$ and $10\alpha_w$). The curves simulate Eq. (27) at close distances from the source, when transmitting a frequency of 2 MHz and a pressure of 0.5 MPa.

et al. (1982) to measure B/A of tissues, requiring the tissue sample to be sliced in order to obtain measurements at several distances.

The extrapolation scheme has an important advantage: it avoids measurements of the attenuation coefficient of the medium. As illustrated in Fig. 6, even if the attenuation value of the medium under study changes, the curves intersect at the same point, provided that the other acoustic parameters are equivalent. This method is sometimes referred to as the pullback method (Wallace *et al.*, 2007).

c. Single measurement. Equations (27)–(30) also enable measuring B/A from a single measurement once the attenuation coefficients at the fundamental α_1 and harmonic α_2 frequencies are known. After first estimating the attenuation coefficients, Cobb (1983) estimated B/A, taking diffraction of the 2nd harmonic (Ingenito and Williams, 1971) into account [for the case of transducers of equal size, Eq. (27)]. The authors noted that the approximation given by Eq. (28), justifying the extrapolation scheme, may lead to errors of 7% in samples such as water and glycerin (Dunn *et al.*, 1982). Zhang and Dunn (1987) utilized Eq. (30) to estimate B/A from a single acquisition, finding that there is no significant difference between B/A of *in vivo* and *ex vivo* cat livers. In Haumesser and Meulen (2019), the second harmonic was measured after its reflection from an aluminium plate that replaced the receiver in a typical through-transmission setup (Fig. 2). The reflection mode method increased the propagation path of the signal in the studied medium. This way an accurate B/A measurement could be acquired for a reduced amount of the investigated liquid. Li *et al.* (2017) presented a through-transmission method for B/A measurement of fluids, utilizing focused transducers to transmit and receive acoustic signals. Diffraction corrections were derived for focused receiver and source and a simple calibration procedure of the receiver was proposed. This enabled estimating B/A of water within an 8% error for multiple distances.

d. Source pressure-harmonic characteristic. Panfilova *et al.* (2018) and Pantea *et al.* (2013) determined B/A of water based on Eqs. (27) and (28) by fitting a line to the dependence of the 2nd harmonic amplitude on the fundamental pressure $P_1(z)$. They require no attenuation measurement since they account for attenuation by using the fundamental and 2nd harmonic values at the measurement point. Pantea *et al.* (2013) reported more extensive work, performing the fit for a larger range of distances and making use of the extrapolation scheme or pullback method (Sec. V B 2 b).

Meulen and Haumesser (2008) implemented this method in echo-mode by the employment of a reflector, concluding that the reflector must have an impedance higher than that of the studied fluid. This ensures that the 2nd harmonic components generated during forth and backpropagation interfere constructively, and B/A quantification is possible. Otherwise, these components add out of phase.

Similarly, Chitnalah *et al.* (2007) recorded the 2nd harmonic in reflection mode at different source pressures but reflected from the interface of two liquids. They took into account attenuation and diffraction correction, decomposing the source function into a series of Gaussian beams.

e. Comparative method. **Transmission mode comparative method.** The first record of the comparative method was found in Gong *et al.* (1963). Its aim is to avoid absolute pressure measurements and therefore a receiver calibration procedure. The idea of the method is to compare the 2nd harmonic signal relative to that generated in a medium with a known B/A when the measurements are performed at the same source pressure and distance L from the source (Fig. 2). This way, when describing the 2nd harmonic component with Eq. (26) for both media, and taking their ratio, one can derive that

$$\left(\frac{B}{A}\right)_m = \frac{P_{2m}}{P_{20}}\frac{(\rho_0 c_0^3)_m}{(\rho_0 c_0^3)_0}\left(\left(\frac{B}{A}\right)_0 + 2\right) - 2, \tag{32}$$

where the subscripts m and 0 denote the medium under study and the reference medium, respectively. In this first study, the reference liquid was acetone, with a density and speed of sound close to that of the studied nitrogen. However, most studies use water as the reference medium, as its B/A is well known and attenuation can be neglected. Gong *et al.* (1984) and Zhang *et al.* (1991) utilized the same technique, with the latter work also accounting for diffraction effects.

Wallace *et al.* (2007) used a hybrid of the extrapolation and comparative methods. The authors compared the ratio $[V_2(z)/zV_1(0)^2]_{zV_1(0)=0}$ of isopropanol to that of water, where V_1 and V_2 are the voltages associated with the fundamental and the 2nd harmonic. Differently from previous works, the authors took into account the fact that the generated source pressure actually depends on the medium where the source is immersed (also explained in Jackson *et al.*, 2014), defined by the transmission coefficient between the transducer material and the medium [see also Eq. (34)]. Besides this, they introduced a steel delay line in front of the transmitting transducer. Since steel has a speed of sound that is approximately four times higher than in water, the resulting diffraction pattern is compressed compared to that in water. this allowed positioning the natural focus inside or right after the path in steel. As a result, Wallace *et al.* (2007) satisfy the plane wave approximation by measuring in the far field, requiring no further diffraction corrections.

Yu *et al.* (2014) performed an evaluation of the comparative technique, including simulations and a phantom experiment for homogeneous tissue. The simulation study utilized a linear probe as the source and measured β for 3 tissue types at different distances. The experiment showed that the estimated β did not depend significantly on the measurement distance, demonstrating the method's robustness. The authors took into account tissue attenuation [Eq. (28)]. In this work, the formula for B/A was derived from the special

https://doi.org/10.1121/10.0003627

case of the comparative method: the finite amplitude insert substitution (FAIS) technique explained below in Sec. V B 2 f). This resulted in an erroneous formula. However, since the transmission coefficients of the studied tissues were close to unity, the introduced error was very small. The authors assessed their technique to be within 3% of uncertainty.

Reflection mode comparative method. Kourtiche *et al.* (2001) used the same transducer to transmit the fundamental and receive the 2nd harmonic reflected from a reflector plate. In this case, the 2nd harmonic generation occurs both ways. The authors also performed an analysis of the electromechanical behavior of the transducer at different transmit frequencies. A transducer generates a "clean" and strong fundamental around its resonance frequency. At the same time, it must be sensitive enough to detect the 2nd harmonic of the transmitted signal. Therefore, a favorable trade-off frequency region must be determined for B/A estimation. Besides this, a transducer usually shows different sensitivities in transmission and in receiving. These are influenced by the impedance of the transducer, which varies with signal frequency and the impedance of the medium. The authors showed that neglecting these effects can lead to errors in β estimation and that there is a frequency range where B/A can be estimated most accurately. This work is relevant for all echo-mode developments as well as transmission mode measurements utilizing identical transducers as source and receiver.

f. FAIS method. **Transmission mode FAIS.** The FAIS method was motivated by the idea of avoiding absolute pressure measurements, similar to the comparative method. Some authors classify the comparative method (Sec. V B 2 e) as a particular case of FAIS (Yu *et al.*, 2014), which in reality was developed later. In light of this, it should be noted that the equation utilized for the comparative method should not be derived as a general case of the FAIS. With FAIS, the medium under study is inserted in a water path and does not have the same length as the reference medium (water), in most cases resulting in 2 reflection interfaces (Fig. 7). Initially, Shklovskaya-Kordi (1963) developed this method based on the Fubini solution [Eq. (26)] for measurement of internal pressure through B/A. When the source pressure and distance between the source and receiver (L) are fixed (in this work kept within the near field distance to adhere to the plane wave approximation), the amplitude of the 2nd harmonic in a water path P_{20}, whose B/A is known, is compared to that when a sample of thickness d is inserted in this path P_{2m}. Through the ratio P_{2m}/P_{20}, we can calculate B/A as (Gong *et al.*, 1984),

$$\left(\frac{B}{A}\right)_m = \left(\frac{P_{2m}}{P_{20}}\frac{L}{dD'D''} - \frac{L}{d} + 1\right)\frac{(\rho_0 c_0{}^3)_m}{(\rho_0 c_0{}^3)_0}\frac{1}{D''}\left[\left(\frac{B}{A}\right)_0 + 2\right] - 2, \tag{33}$$

where D' and D'' are the sound transmission coefficients from water to the sample and from the sample to water, respectively,

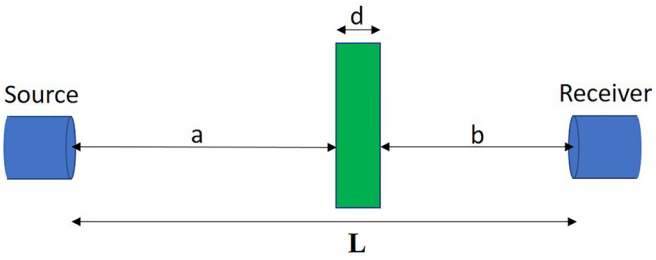

FIG. 7. (Color online) Setup for the FAIS method.

$$D' = \frac{2(\rho_0 c_0)_0}{(\rho_0 c_0)_0 + (\rho_0 c_0)_m};\quad D'' = \frac{2(\rho_0 c_0)_m}{(\rho_0 c_0)_0 + (\rho_0 c_0)_m}. \tag{34}$$

Equation (33) is only valid when the investigated medium is nearly lossless. Moreover, the formula was derived merging the 2nd harmonic contribution from water before the sample and after it, which is justified if the acoustic impedance of the medium is close to water. Alternatively, the medium can be placed very close to the receiver, making the 2nd harmonic generation in the water path after the sample negligible. Because of this, the sample is conventionally positioned close to the receiver in all FAIS modifications. As for the comparative method, FAIS does not require transducer calibration for recovery of the absolute pressure values since the pressure ratio term is equivalent to the received voltage ratio. Gong *et al.* (1989) built on this method, introducing an attenuation correction in Eq. (28) aimed at measuring B/A of tissue, making the assumption that $(\alpha_2 - 2\alpha_1)z$ is small, valid for most tissues as they have a nearly linear frequency dependence (Duck, 1990; Goss *et al.*, 1979). The resulting expression is

$$\left(\frac{B}{A}\right)_m = \left[\frac{P_{2m}}{P_{20}}\frac{L}{d}e^{(\alpha_1+(1/2)\alpha_2)d} - \left(\frac{L}{d} - 1\right)e^{(\alpha_1-(1/2)\alpha_2)d}D'D''\right] \times \frac{(\rho_0 c_0{}^3)_m}{(\rho_0 c_0{}^3)_0}\frac{1}{D''^2 D'}\left[\left(\frac{B}{A}\right)_0 + 2\right] - 2. \tag{35}$$

Here, one can see that a measurement of the attenuation coefficient at the fundamental α_1 and the harmonic α_2 is required for B/A determination. Besides this, Gong *et al.* (1989) also introduced a diffraction correction which for most biological tissues (speeds of sound: 1400–1600 m/s) they quantified to be within 2%. However, it must be noted that, in general, for liquids with a speed of sound further away from that of water, the diffraction correction can introduce significant errors (e.g., 5% error for ethanol).

Wu and Tong (1998) measured B/A of contrast agents. Since B/A of contrast agents can be on the order of hundreds and thousands, the harmonic component generated in water can be neglected for the configuration in Fig. 7. This resulted in a simpler expression. No diffraction correction was used, possibly due to the assumption of a similar speed of sound in contrast agents to that of water (not stated).

Dong *et al.* (1999) derived a formula analogous to Eq. (35), however, they utilized the general expression for

attenuation in Eq. (27). Dong *et al.* (1999) positioned the sample and the receiver in the extreme far field of the source, another region of the piston field where the plane wave approximation may be considered valid. The authors removed all harmonic content generated in the near field by placing an acoustic absorber before the sample. Yet, due to the absorber, the insonifying amplitude is expected to have been low, and the resulting distortion weak. Cortela *et al.* (2020) and King *et al.* (2011) utilized the same configuration as Dong *et al.* (1999) to measure B/A of gellan gum-based tissue-mimicking phantoms. Choi *et al.* (2011) utilized the same formula as Dong *et al.* (1999) in a setup where no acoustic absorber was used. They presented the temperature dependence of B/A of porcine liver.

Harris *et al.* (2007) proposed another setup that allowed avoiding diffraction correction. Their solution was a large source transducer (8 cm in diameter), which provided a broad plane wave region, without diffraction effects. Figure 5 demonstrates such a triangular region in the proximity of the transducer, where the field is stable.

Kujawska *et al.* (2003) introduced a modified FAIS method. A model of the ratio P_{2m}/P_{20} depending on sample thickness d was fit to experimental data when using a small receiver (0.4 mm in diameter). The best fit of the data provided an estimate B/A for liquids and homogenized tissue. The current approach required no plane wave assumption.

Zeqiri *et al.* (2015) conducted a detailed analysis of the influence of several factors on the accuracy of B/A measurement with the FAIS, e.g., sample positioning with respect to the receiver, source pressure amplitude, and sample thickness.

Reflection mode FAIS. Lu *et al.* (2004) utilized FAIS in reflection mode, transmitting and receiving with the same compound transducer whose inner ring served as the source, and outer ring received the signal from a reflector plate. In this case, the authors needed to take into account 2nd harmonic generation in the forward and backward path, making the calculations more complex. It is of notice that for FAIS, the transducer sensitivity is not altered by the studied medium. The authors showed a strong dependence of B/A in porcine liver and muscle on temperature, suggesting the possibility of temperature monitoring through B/A during HIFU.

Nonlinear acoustic microscopy. Acoustic microscopy allows studies of small-volume samples (e.g., 0.1 mL; Saito, 2010). It utilizes high frequency sources (14–19 MHz) in conjunction with acoustic lenses that provide a short focal distance (e.g., 2.3 mm; Germain *et al.*, 1989). Altogether, this produces appreciable nonlinear effects in the focal spot already at such short distances. All the studies in this field have adapted the comparative and FAIS techniques using water as a reference medium and either completely filling the space by the sample, or positioning it only in the focal region, surrounded by water.

Banchet *et al.* (2000), Banchet and Cheeke (2000), and Germain *et al.* (1989) developed an acoustic microscope for the measurement of B/A. The 2nd harmonic was detected by a planar transducer. Its generation was assumed to be confined to the focal region and was described with plane wave theory utilizing Eq. (28). This system also allowed measuring sound velocities; however, parameters like density and attenuation needed to be measured beforehand to enable calculations with Eq. (28).

Additional work in this direction was performed in Saito (1993a,b, 2010), Saito and Kim (2011), and Saito *et al.* (2005). The final setup of the developed system utilized the source as a receiver, detecting the signal from a reflector. The authors made use of Gaussian beam theory that models the field as a series of beams whose spatial pressure distribution is described by the Gaussian function (Kim *et al.*, 2006). This system allowed measurement of B/A as well as linear acoustic parameters, including sample density. At the latest stage of development, Saito and Kim (2011) generated two-dimensional (2D) images of B/A and linear acoustic parameters by mechanically translating the samples of biological tissues (e.g., fat vs nonfat; coagulated vs normal), showing that tissue B/A was variable on a microscale and exhibited different variation patterns than the linear parameters (e.g., attenuation, density). In Saito (2010) and Saito and Kim (2011) the authors observed good reproducibility of their measurements (within 1%) and stated the measurement error to be within 10%, typical for FAMs.

g. Transmission line method. Dong *et al.* (2006) and Kushibiki *et al.* (1997) introduced a novel method utilizing frequencies as high as 100–200 MHz. The specimen was positioned between two SiO_2 buffer rods with transducers at their outer ends. SiO_2 has a negative β: its 2nd harmonic shows an opposite phase compared to that generated in liquid. This way, when acquiring P_2 for different sample lengths, at a certain point the 2nd harmonic was cancelled out completely. The authors utilized plane wave theory [Eq. (27)], incorporating diffraction and dispersion in Kushibiki *et al.* (1997), showing that this gives more stable B/A estimates. The major advantage of this method is that no pressure measurement is needed. However, the observed β for water was 20% higher than the value reported in literature. This was ascribed by the authors to uncertainties in the properties of SiO_2.

3. B/A imaging

The studies discussed in this section consider B/A estimation in heterogeneous media. First, the section performing through-transmission measurements is presented. In this case, the image is reconstructed with computer tomography (CT) once the through-transmission measurement is repeated for several sample rotation and translation configurations (Fig. 8). The reconstruction is obtained by use of the Radon transform with the resulting image resolution being determined by the number of employed rotation angles. The reflection-mode measurement follows the same scheme, however, using the source as the receiver. After transmission through the tissue, the signal is reflected from a reflective plate on the opposite side of the sample. Echo-mode imaging is the last family of methods presented in this section. In this case, the signal is received by the source transducer as it is reflected along its

https://doi.org/10.1121/10.0003627

propagation path in tissue, due to tissue inhomogeneities. This distinction between reflection-mode and echo-mode imaging will be further used in this review.

a. B/A tomography. Zhang and Gong (1994, 1999) and Zhang *et al.* (1996) implemented B/A tomography based on the FAIS method. When considering a heterogeneous medium, the received 2nd harmonic amplitude at a distance L from the source is the result of its propagation path where different values of $\beta, \alpha_1, \alpha_2$ correspond to every z,

$$P_{2m}(L) = \frac{\pi f_2 P_1(0)^2}{2(\rho_0 {c_0}^3)_m} \int_0^L \beta_m(z) \exp\left(\int_0^z -2\alpha_1(z)dz - \int_z^L \alpha_2(z)dz \right) dz, \tag{36}$$

where the indice m refers to the medium under investigation. In order to avoid conversion to absolute pressure values, the authors also measure the amplitude of the 2nd harmonic $P_2(L)$ in a homogeneous reference medium with a known β. The reference medium was water, making it possible to apply the lossless Fubini solution [Eq. (26)],

$$P_{20}(L) = \frac{\pi f_2 P_1(0)^2}{2(\rho_0 {c_0}^3)_0} L\beta_0. \tag{37}$$

This way, when the sample is placed in the water path between the source and the receiver, the ratio of the received 2nd harmonics is defined by

$$P = \frac{P_{2m}(L)}{P_{20}(L)} = \frac{(\rho_0 {c_0}^3)_0}{(\rho_0 {c_0}^3)_m \beta_0} \int_0^L \beta_m(z) \times \exp\left(\int_0^z -2\alpha_1(z)dz - \int_z^L \alpha_2(z)dz \right) dz. \tag{38}$$

The implemented CT system allowed for rotation of the sample and translation of the source and receiver (hydrophone) along the sample length (Fig. 8). The receiver was positioned in the near field of the transmitting transducer. The obtained projection images of the ratio P [Eq. (38)] were transferred to the β domain by the filtered convolution method and then corrected by multiplying with the attenuation matrix describing the sample's attenuation in space (estimated by attenuation tomography with the same setup). This work showed promising results; however, the authors concluded that attenuation and velocity estimates required further improvement. Yu *et al.* (2014) also simulated B/A tomography based on Eq. (38), modified for the case of an attenuating reference medium and utilizing a filtered back projection algorithm.

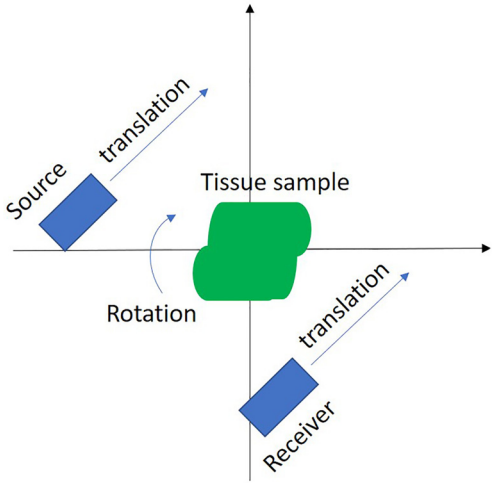

FIG. 8. (Color online) Top view of the typical CT scanning system. Multiple signal acquisitions are performed for various sample rotation configurations and multiple source-receiver translations.

b. β tomography in reflection mode. Gong *et al.* (2004) extended their previous work (Zhang *et al.*, 1996) to reflection tomography. The tissue sample was positioned in water between the source and a reflective plate, where the reflective plate replaced the receiver in Fig. 8. Equation (38) was extended, now containing nonlinear generation and attenuation terms for the forward and backward path. Figure 9 presents an example of an image acquired in this work. In this image, we can see a two-layered tissue structure with porcine liver surrounded by porcine fat, submerged in water.

c. β imaging in echo-mode. Reflection mode imaging poses additional challenges, compared to transmission tomography. In the latter case, the recorded signal has travelled through the whole bulk of the tissue, and therefore, the effect of varying scatterer density within the medium is averaged out. However, when utilizing echo-mode β imaging, the strength of the reflected echoes is, to a large extent, defined by the scatterer density at each reflection point (Waag, 1984), masking information about other acoustic properties. To cancel out the scatterer effect, scientists normalized the recorded signal to a signal that is assumed to have an analogous scattering pattern. Three different reference signals have been identified in literature. One utilizes an additional signal, transmitted at the 2nd harmonic frequency. Another utilizes the second harmonic amplitude reflected from a scattering homogeneous reference medium. The last reference signal is the reflected fundamental component of the received pulse.

Akiyama (2000) and Fujii *et al.* (2004) found a way to mitigate the influence of scatterers by assuming that the scatterer distribution affects a signal of a certain frequency in the same way, whether it is the generated 2nd harmonic at $2f_0$ of the fundamental at f_0, or whether it is the transmitted fundamental at $2f_0$. The authors assumed that the 2nd harmonic is generated only in transmission, and not on the way back when reflected from scatterers due to low amplitudes of the reflected signal. Attenuation was taken into account in both directions of propagation, leading to

$$P_{2h}(z) = {P_0}^2(f_0) \exp\left(-2\int \alpha(f_0, z)dz - \int \alpha(2f_0, z)dz \right) \gamma(2f_0, z) \int \frac{(B/A+2)2\pi f_0}{4\rho_0 {c_0}^3} dz, \tag{39}$$

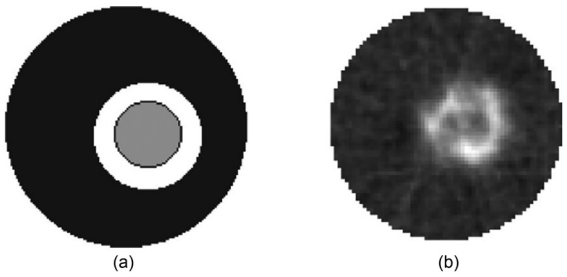

FIG. 9. Reprinted from Gong *et al.* (2004). (a) Model of the imaged media: porcine liver surrounded with porcine fat, submerged in water. (b) The acquired reflection-mode tomographic image, utilizing the finite amplitude insert-substitution method.

where ρ and c are medium properties, assumed constant and $\gamma(2f_0, z)$ is the backscattering characteristic term. The received fundamental when transmitting a 2nd pulse at $2f_0$ is also proportional to $\gamma(2f_0, z)$, and $\int \alpha(2f_0, z)dz$. Therefore, the ratio of the generated 2nd harmonic to the fundamental at the frequency of the 2nd harmonic cancels out the backscattering and the attenuation at $2f_0$ terms. The authors extracted $h(z)$, a parameter defined by B/A, speed of sound and density of the medium with the following equation:

$$h(z) = \frac{A_0(0, 2f_0)}{P_0{}^2(0, f_0)} \frac{d}{dz}\left[\frac{P_{2h}(z)}{P_{2f}(z)}\right], \tag{40}$$

where P_0 and A_0 are pressures at the source when transmitting at f_0 and $2f_0$, respectively. Signals $P_{2h}(z)$ and $P_{2f}(z)$ are the received 2 harmonic and fundamental at $2f_0$, correspondingly. It is important to note that the studies mentioned above retrieved one single value of h, fitting a line to the ratio $P_{2h}(z)/P_{2f}(z)$ observed throughout the whole sample depth. Besides a phantom study, Fujii *et al.* (2004) conducted an *in vivo* clinical study with 41 patients, using h as a single-valued indicator of liver fat content.

A similar strategy was followed by Gong *et al.* (2004) and Liu *et al.* (2008) who acquired C-scan images of the B/A profile, modifying Eq. (40),

$$\frac{B}{A}(z) = \frac{4\rho_0 c_0{}^3}{\omega} \frac{A_0(0, 2f_0)}{P_0{}^2(0, f)} \frac{d}{dz}\left[\frac{P_{2h}(2f_0, z)}{P_{2f}(2f_0, z))}\right] - 2, \tag{41}$$

assessing the local slope of the ratio $P_{2h}(2f_0, z)/P_{2f}(2f_0, z)$ of the echoes reflected by tissue. The authors showed very promising discrimination capabilities, when imaging heterogeneous tissue models in the plane perpendicular to the beam propagation direction, by mechanically scanning their system point by point. No capabilities of B/A discrimination in depth of the sample were presented.

Varray *et al.* (2011b) extended the comparative method [Eqs. (36) and (27)] to enable imaging of heterogeneous media in echo mode. By taking several acquisition lines in the filtered 2nd harmonic image as a reference, the authors normalized the 2nd harmonic response of the whole image to construct a β image. The images of two phantoms with inclusions were acquired with the ULA-OP scanner (X-Phase), transmitting a focused beam. Experimental images acquired with this strategy in other works (Toulemonde *et al.*, 2014; van Sloun *et al.*, 2015) are presented in Figs. 10 and 11. van Sloun *et al.* (2015) eliminated the influence of scatterer density, expressing $\beta(z) = f(P_{2h}(z)/P_f(z))$ as a function of the ratio of the received amplitudes of the 2nd harmonic to the fundamental, derived from the 1D lossy Westervelt equation [Eq. (8)]. The proposed approach was called "the harmonic ratio method." Simulations were performed with the iterative nonlinear contrast source approach, capable of modelling 3D fields in complex media (Demi *et al.*, 2011). The modelled media exhibited different β and α values with the same constant speed of sound and density. The resulting images showed good contrast. A more realistic tissue-mimicking phantom acquisition was performed with the ULA-OP scanner, acquiring 128 radio frequency (RF) lines. van Sloun *et al.* (2015) compared the proposed method to the extended comparative method (Varray *et al.*, 2011b) and direct estimation of β from the 2nd harmonic amplitude [Secs. V B 2 c and V B 1, Eqs. (27)–(30)]. The two phantom layers had different oil content and were, therefore, expected to have different β. The resulting normalized β images of the phantom for the three studied strategies are presented in Fig. 10. All methods showed capable of distinguishing two layers with different oil content. However, the strategy proposed in van Sloun *et al.* (2015) showed more homogeneous estimates for both layers and better consistency over depth. Unfortunately, no follow-up experimental work further confirmed the applicability of this method in a realistic clinical setting.

Another *in silico* work Toulemonde *et al.* (2014) proposed utilizing the extended comparative method (Varray *et al.*, 2011b) on compounded B-mode images acquired with high frame rate plane wave imaging. Utilizing plane waves allowed imaging at various depths compared to focused beams (Varray *et al.*, 2011b) while compounding reduced the speckle. Moreover, to reduce the speckle, filtered second harmonic images were normalized by the corresponding filtered fundamental images. These normalized second harmonic signals were compared to those of the reference medium to extract the B/A distribution. This way, Toulemonde *et al.* (2014) proposed utilizing two types of signals to reduce the influence of scatterers on B/A estimation: the fundamental of the received signal and the received 2nd harmonic of a reference medium. This approach resulted in a more accurate B/A reconstruction of a simple B/A distribution than with the original extended comparative method in Varray *et al.* (2011b). Nevertheless, B/A images of a simulated medium with a complex B/A distribution were greatly degraded by the remaining speckle pattern for both methods. Further, this approach was extended to multi-taper coherent plane wave compounding (Toulemonde *et al.*, 2015) using several orthogonal apodizations for plane wave beamforming, creating several speckle patterns for each steering angle. Toulemonde *et al.* (2015) presented B/A images of *in silico* and experimental phantoms, showing a better B/A delineation compared to previous approaches

https://doi.org/10.1121/10.0003627

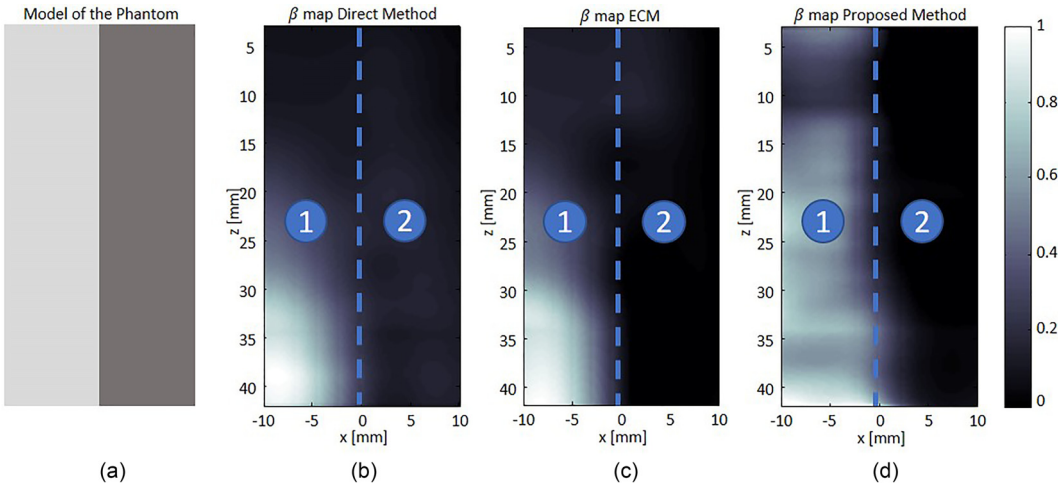

FIG. 10. (Color online) (a) Model of the imaged gelatin-based tissue-mimicking phantom with two layers of different oil content. Reprinted from van Sloun *et al.* (2015), with the permission of AIP Publishing. (b) Direct method. (c) Extended comparative method, proposed in Varray *et al.* (2011b). (d) Harmonic ratio method proposed in van Sloun *et al.* (2015).

(Toulemonde *et al.*, 2014; Varray *et al.*, 2011b). Experimental images of a three-layered tissue-mimicking phantom are presented in Fig. 11.

C. Fundamental nonlinear absorption

1. Basic theory

When observing an increase in absorption with signal intensity (Fox and Rock, 1941), this was first attributed to cavitation. Later, however, it was recognized (Fox and Wallace, 1954) to be the result of energy transfer from the fundamental to higher harmonics. Moreover, as nonlinear effects grow with the source amplitude [e.g., Eq. (26)], nonlinear attenuation increases along with them, limiting the power that can be possibly delivered to a certain depth (Fig. 12) (Hikata *et al.*, 1980; Kashkooli *et al.*, 1987).

In the shock-free or pre-shock region ($\sigma < 1$) of a lossless medium, the fundamental component of a plane wave will decrease according to Eq. (42) due to energy transfer to higher harmonics (Fubini-Ghiron, 1935),

$$P_1(z) = P_0\left(1 - \frac{1}{8}\sigma^2\right) = P_0\left(1 - \frac{1}{2}\left[\frac{\left(1 + \frac{1}{2}\frac{B}{A}\right)z\pi f_0}{\rho_0 {c_0}^3}P_0\right]^2\right). \quad (42)$$

Additional small-signal attenuation losses can be accounted for by the Keck and Beyer solution (Keck and Beyer, 1960) for the fundamental.

Another way to account for both effects of small-signal attenuation and nonlinear depletion of plane waves was proposed by Bartram (1972) and Rudnick (1952), introducing spatial changes that are ascribed to the rate of heat production due to fluid heating by the shock fronts and energy loss between shocks,

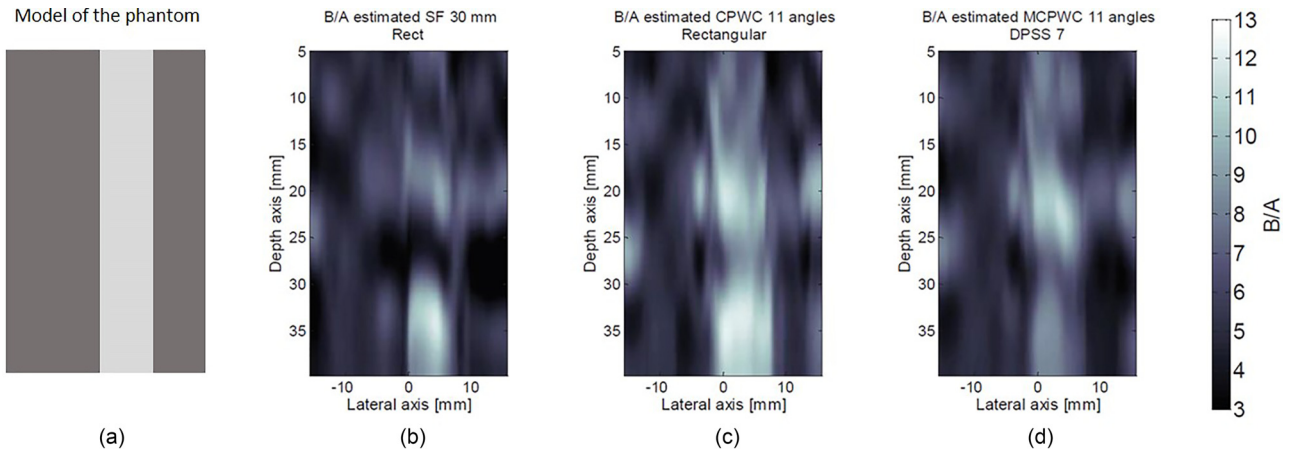

FIG. 11. (Color online) (a) Model of the imaged gelatin-based tissue-mimicking phantom with a layer of greater oil content than in the side regions. Reprinted from Toulemonde *et al.* (2015) with the permission of AIP Publishing. (b) Image acquired with the extended comparative method, utilizing a focused beam (Varray *et al.*, 2011b). (c) Extended comparative method, making use of plane wave compounding (Toulemonde *et al.*, 2014). (d) Extended comparative method, utilizing multitaper coherent plane wave compounding (Toulemonde *et al.*, 2015).

$$\frac{dP(z)}{dz} = -\alpha P - \frac{\beta f \pi}{\rho_0 {c_0}^3} P^2. \tag{43}$$

The equation above was first introduced for weak shock theory ($\sigma > 3$); however, it has also been adapted by Kashkooli *et al.* (1987) to describe the fundamental amplitude change at $\sigma < 3$, the proposed solution being

$$P(z) = P(0)e^{-\alpha z}\left[1 + \frac{(1 - e^{-\alpha z})\beta \pi f P(0)}{\alpha \rho_0 {c_0}^3}\right]^{-1}. \tag{44}$$

When the source pressure is low, the dominating term in Eq. (44) is the first one on the right hand side, describing small-signal attenuation, and corresponding to the linear region in Fig. 12. However, as the source pressure increases, the harmonics grow, depleting the fundamental harmonic as described by the 2nd term in Eq. (44) and corresponding to the saturating process in Fig. 12.

2. B/A measurement of homogeneous media

a. Transmission mode. Hikata *et al.* (1980) and Kashkooli *et al.* (1987) used the finite amplitude loss technique (FALT) based on Eq. (44). The authors performed a transmission measurement, where the dependence of the received signal pressure $P(z)$ on the intensity of the transmitted signal pressure $P(0)$ was recorded at a fixed distance. When expressing the dependence of $P(0)/P(z)$ *via* $P(0)$, they extracted β from the slope of this linear dependence. The authors discuss the trend of the FALT to yield values, higher than those acquired with the thermodynamic method (Sec. III) and from light diffraction (Sec. V A 1). Even though limited to homogeneous media, the method is rather simple, requiring a pair of transducers with a similar resonance frequency. The internal consistency of the measurements was stated to be 10% (Kashkooli *et al.*, 1987).

b. Echo-mode. Byra *et al.* (2017) applied the lossless plane wave theory [Eq. (42)] to determine B/A of water.

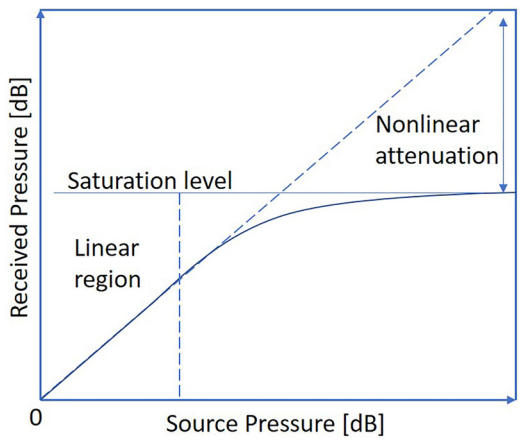

FIG. 12. (Color online) A response curve showing the phenomenon of saturation as the source power is increased, for a lossless medium. Experimental curves can be found in Hikata *et al.* (1980) and Kashkooli *et al.* (1987).

Typical for echo-mode imaging, it was assumed that the backscattered waves travelled linearly. The Verasonics research scanner (Verasonics, Inc.) equipped with a linear array probe L12–5 was used to image a set of reflecting wires positioned at different depths in water. By sending progressively increasing pressure values, the authors were able to observe a portion of the fundamental saturation (Fig. 12) and by fitting Eq. (42) to this curve extract water's β.

3. B/A imaging

All B/A imaging works, based on the registration of the fundamental amplitude, were performed in echo-mode. Iinuma (1988) patented the approach of detecting fundamental saturation already in 1988 when utilizing an array transducer. A simple approximate equation was used to describe the received pressure P_{rec}, depending on the transmitted pressure P_{trans},

$$P_{rec} = \frac{P_{trans}}{1 + aP_{trans}}, \tag{45}$$

where a is the parameter reflecting nonlinear effects, equal to 0 if nonlinear effects are absent.

Nikoonahad and Liu (1990) utilized a similar approach. However, actual B/A values were determined and a single-frequency pulse was used. The authors utilized the approximate analytical solution to a nonlinear differential equation in terms of density fluctuations (Tjotta and Tjotta, 1981), determining B/A from the fundamental depletion of echoes as the source pressure was progressively increased. Diffraction effects were cancelled out by taking the ratio of two signals received at different source pressures. The theory was validated with simulations and an experimental measurement in ethylene glycol after a calibration procedure in water. The authors also showed in Nikoonahad and Liu (1989) that it was possible to resolve B/A of a phantom with heterogeneous liquid layers by taking track of the pulse's history and using a recursive algorithm. Nikoonahad and Liu (1989) stated that the applicability of the method to tissue still had to be investigated, since the high viscous losses in tissue may not allow for sufficient fundamental depletion at safe pressure levels.

Aiming to enable real-time B/A assessment, Fatemi and Greenleaf (1996) adapted the theory from Nikoonahad and Liu (1990), limiting the number of transmissions to two: one at a low amplitude in the linear regime, and another at a high amplitude with prominent nonlinear phenomena. The authors generated images in which shadows reflected nonlinearity of preceding regions, in a manner in which attenuation manifests itself on B-mode images, as well as relative B/A images. The authors imaged the nonlinearity of ethanol and water, as well as fat-muscle structures, and tissue-water and tissue-contrast agent structures, concluding that the method can effectively identify regions of elevated nonlinearity.

In conclusion, several works utilizing the depletion of the fundamental to measure B/A have been presented.

https://doi.org/10.1121/10.0003627

Utilizing the fundamental is practical, since in most pulse-echo systems the receiving transducer has a relative bandwidth of 50%–70%, making it challenging to detect harmonics with a good signal-to-noise ratio (SNR) (Fatemi and Greenleaf, 1996).

VI. PARAMETRIC ARRAY

The concept of the parametric array was introduced to acoustics by Westervelt (1963), stating that two collimated coaxial acoustic beams, approximated by plane waves, generate the sum and difference frequency waves (secondary waves). The secondary waves represent narrow beams, whose amplitude is proportional to the parameter of nonlinearity β of the propagation medium and rises linearly with distance from the probe z_0,

$$P_s(z_0) = -\frac{S_0{\omega_s}^2}{4\pi\rho_0{c_0}^4}\beta P_1(0)P_2(0) \times \int_0^{z_0}\frac{\exp(-(\alpha_1+\alpha_2)z-\alpha_s(z_0-z))}{z_0-z}dz. \quad (46)$$

Equation (46) is intended for homogeneous media, where P_s and α_s are the pressure amplitude and attenuation coefficient of the secondary wave, $P_1(0)$ and $P_2(0)$ are amplitudes of primary beams at the source, α_1 and α_2 are their attenuation coefficients, and S_0 is the beam cross-sectional area of the primary beams. The difference frequency wave undergoes lower attenuation compared to the sum component. Therefore, if two source frequencies are close to each other, the difference frequency wave is simpler to detect compared to the sum component. In the contrary situation, the sum component may be more favorable since P_s is proportional to ω_s. Detection of the difference or sum frequency component provides a means of β measurement, called the parametric array method. The section below summarizes the evolution and progress made regarding its application. Table VI presents all the identified works, utilizing the parametric array method to measure B/A.

The possibility of β measurement with the parametric array was first demonstrated in Nakagawa *et al.* (1984), when the finite amplitude and thermodynamic methods were already actively used and compared (Law *et al.*, 1983, 1985). In a configuration when a dual-frequency voltage pulse was transmitted by a transducer and detected by a hydrophone in a transmit-mode configuration, the authors estimated β of an agar gel phantom by comparing the amplitude of the difference frequency wave in water to that of an agar gel phantom. Here, attenuation effects were taken into account, and β was estimated as an average uniform value. In the same paper, Nakagawa *et al.* (1984) extended this method to CT using a conventional system (Fig. 8), generating the first CT images acquired with the parametric array method. This work was further continued in Nakagawa *et al.* (1986), confirming that attenuation and β images could be acquired with the proposed system and discovering that the estimation of attenuation was heavily influenced by refraction, causing errors in β reconstruction. Nakagawa *et al.* (1986) and Nakagawa *et al.* (1984) used the Westervelt equation to model the secondary wave propagation [Eq. (46)]. Since an accurate estimation of S_0 poses a problem, the β value can only be estimated when comparing the secondary wave sound pressure generated in the sample to that of a medium with a known β. Arnold *et al.* (1987) and Nakagawa *et al.* (1986) simplified the analysis of the parametric array method by describing it with the Burgers equation [Eq. (10)] rather than the Lighthill's exact equation for arbitrary fluid motion used by Westervelt (Westervelt, 1963). The solution of the Burgers equation for homogeneous media is

$$P_s(z_0) = -\frac{\omega_s P_1(0)P_2(0)}{\rho_0{c_0}^3}\beta \times \int_0^{z_0}\exp[-(\alpha_1+\alpha_2)z-\alpha_s(z_0-z)]dz. \quad (47)$$

This allowed for direct β reconstruction from the registered primary wave amplitudes, and estimated attenuation

TABLE VI. Summary of parametric array works.

Study	Type of assessment, imaged parameter	Investigated media	Uncert., %
Nakagawa *et al.*, 1984	Single measurement (for homogeneous Media), $\frac{\beta}{\beta_{ref}}$, tomography, $\frac{\beta}{\beta_{ref}}$	Agar gel phantom	—
Arnold *et al.*, 1987; Nakagawa *et al.*, 1986	Tomography, β	Phantoms with inclusions	—
Cai *et al.*, 1992	*In silico* diffraction tomography, β	Simulated weakly, moderately, and strongly scattering objects	—
Zhang *et al.*, 2001a	*In silico* tomography, β	Simulated fluids, biological tissues	<1 (*in silico* experiment)
Zhang *et al.*, 2001b	Tomography, β	Tissue phantoms with water, porcine liver and fat, pathologic liver; boiled egg	10 (tissue)
Wang *et al.*, 2003	Reflection tomography, β	Normal and pathological porcine liver	5 (tissue)
Barrière and Royer, 2000, 2001	Single measurement (for homogeneous liquid media), β	Ethanol, water	2–5 (liquid)
Bereza *et al.*, 2008; Burov *et al.*, 2006	Tomography (noncollinear parametric interaction), variation of β	Wool fibre, hog fat in water	—

compensation. Just as for previous studies, the source of errors in primary wave data and the attenuation correction term were attributed to diffraction or refraction effects. Diffraction tomography was proposed as a solution to this problem. The possibilities of diffraction tomography were studied based on theory and simulations in Cai *et al.* (1992), where the authors had to come back to the equation initially derived by Westervelt (1963) to include the diffraction effect for weakly, moderately, and strongly scattering objects. The presented simulations show the ability to reconstruct the β profile; however, these findings, to our knowledge, were not experimentally confirmed.

Another group (Zhang *et al.*, 2001a) used Eq. (47) to express the secondary wave amplitude. However, they used the ratio of the secondary wave pressure amplitude after and before inserting the specimen as the projection data, adapting the insert substitution method introduced for the 2nd harmonic (Gong *et al.*, 1989) to the parametric array method. They calculated the sound field produced by a piston source, representing the primary beams as a superposition of Gaussian beams. This way the authors, for the first time, demonstrated, based on theoretical analysis, that the amplitude of the difference frequency wave is nearly proportional to the distance from the source (reducing possible diffraction errors) and has no side lobes. For these reasons, they concluded that the parametric array method provides a better source to image β, granting higher resolution and higher accuracy compared to the 2nd harmonic. The authors showed the feasibility of the proposed CT method for β imaging with computer simulations. A follow-up with experimental results was published in Zhang *et al.* (2001b), confirming theoretical considerations regarding the secondary wave profile. CT images of phantoms with different β configurations, reasonably agreeing with previous β measurement results of other methods, were presented. The authors did not take diffraction effects into account, considering their influence reduced due to the stable rise of the difference frequency component, and the use of the FAIS method. In Wang *et al.* (2003), the group extended their work from Zhang *et al.* (2001a) to reflection mode imaging, presenting the theoretical analysis and the developed imaging system. They used a compound transducer as a transmitter and receiver, recording the signals reflected from an aluminium plate located behind the sample of interest. The images showed promise, detecting a difference between healthy, fatty, and hepatocirrhosis liver tissue. The same strategy was utilized in Gong *et al.* (2004), acquiring the image of a three-layered medium in Fig. 13: porcine liver surrounded by porcine fat, submerged in water.

Barrière and Royer (2000, 2001) introduced a new setup for β measurement of liquid media. They showed that the interaction of two primary beams with a high frequency ratio (>10) is equivalent to the phase modulation of the high-frequency wave. In a configuration where the two source transducers are on opposite sides of the sample chamber, a low frequency pulse with a velocity potential ψ_2 modulates a high frequency plane wave with a velocity potential ψ_1. An important contribution of this paper is the analysis of the diffraction effects based on plane wave expansions. The authors showed that in the case of two primary beams with a high frequency ratio (>10), the diffraction effect on the secondary wave is identical to that on the high frequency carrier wave. Therefore, since the presented method compares the amplitude of the secondary wave $\psi_s(r)$ to the high frequency primary wave $\psi_1(r)$ to extract β, the effect of diffraction is cancelled out. These observations were confirmed when the measured β values of water and ethanol showed good agreement with previously reported values. The authors also extend this methodology with a comparative method. In this case, no calibration of the low frequency transducer is needed, and the relative amplitude to that in water is used. The authors state the uncertainty of their measurement to be within 5% for absolute measurements and 2% when the comparative method is adapted.

Bereza *et al.* (2008) and Burov *et al.* (2006) are the only works, to our knowledge, that register radiation of two plane waves intersecting at an angle (Fig. 14). The theory of such interaction is extensively treated in Hamilton and Blackstock (1987) and Tjotta and Tjotta (1987). Just as for the collinear case, nonlinearity results in the generation of sum and difference frequency waves. However, in this case, energy is scattered outside the region of primary wave interaction (Fig. 14), where it is described by the Westervelt equation. This approach allows for the reconstruction of the frequency components of the B/A distribution that depend on the orientation of the two sources and the receiver, as well as the transmit frequencies. To increase the range of reconstructed frequencies and decrease the number of required transducer configurations, the authors transmit broadband signals. Moreover, these signals were encoded such that propagation delays for the coded signals were different and predictable in each coordinate of the medium. This way, each point scatterer radiated a specific coded signal proportional to β. The authors showed *in silico* and on *ex vivo* heterogeneous media (e.g., hog fat in water) that the high-frequency portion of B/A distribution can be reconstructed with only three transducers involved in the measurement (e.g., Fig. 14). In the case of multiple transducers where a sharp angle exists between two sources, the reconstruction of absolute β values is also possible. Besides this,

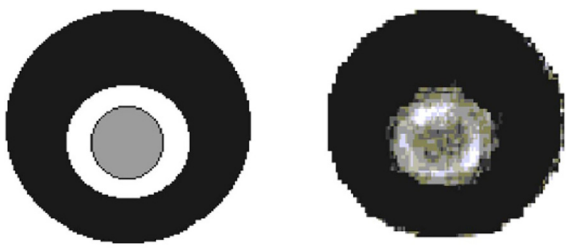

FIG. 13. (Color online) Reprinted from Gong *et al.* (2004). (a) Model of the imaged media: porcine liver surrounded with porcine fat, submerged in water. (b) The acquired reflection-mode tomographic image, utilizing the parametric array method.

https://doi.org/10.1121/10.0003627

the system is also capable of measuring the speed of sound c distribution with no additional measurements. Differently, this work registered the sum frequency, rather than the different frequency, since it allows for registration of a wider band of frequency components of β (Burov *et al.*, 2006). What is more, the registered signals contain information about the nonlinear parameter at a given location, unlike in the case of previous parametric array works and most FAM methods, which measure a cumulative signal.

Since the parametric array method allows generating frequencies much lower than the primary waves, most works based on Eqs. (46) and (47) neglect attenuation of the secondary waves α_s. As demonstrated by Zhang *et al.* (2001a) and Zhang *et al.* (2001b), when using collinear beams, the difference frequency waves rise almost linearly with distance from the source, making it easier to account for diffraction effects. Moreover, the secondary beam has no side lobes. Despite these advantages, it has been noticed in Zheng *et al.* (1999) that "nearly 40 dB in amplitude level difference exists between the primary waves and their difference-frequency wave," making the SNR level rather low and its practical application difficult. Varray (2011) noted that the length of the two transmitted pulses has to be sufficiently long for the generation of the secondary frequency components, setting a limitation to the resolution.

VII. PUMPING WAVES

Like the parametric array method, the pump wave method also exploits nonlinear effects produced when two plane waves interfere with each other. The principle of this technique is described best by the adiabatic dependence of speed of sound on B/A [Eq. (5)], already introduced for the thermodynamic method. Rearranging this equation with the use of the linear relation between pressure and particle velocity $\Delta P = \rho_0 c_0 u$ (Hamilton and Blackstock, 1987), we obtain

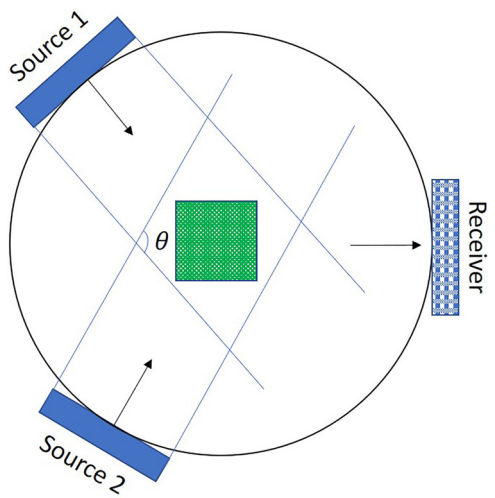

FIG. 14. (Color online) Schematic of the setup utilized in Burov *et al.* (2006), registering ultrasound scattered by two plane waves at an angle.

$$c = c_0 + \frac{B}{2A}\frac{\Delta P}{2\rho_0 c_0}. \tag{48}$$

One can now see how the speed of sound c changes with excess pressure ΔP. Unlike in the thermodynamic method, Ichida *et al.* (1983) created a variation in pressure ΔP by transmitting a high-power beam (pump wave) perpendicular to the probe beam [Fig. 15(a)], modifying the speed of sound c and, therefore, the phase of the probe beam. By registering the modified phase of the probe wave, they extracted B/A and created the very first images of the coefficient of nonlinearity in history.

The pumping wave techniques are presented hereafter in two sections: the classic pump wave technique and the SURF technique for echo-mode imaging. The main difference between these is that in the case of SURF, the probe wave has a much higher frequency than the pump wave. A summary of all the identified works is presented in Table VII. Note that pumping wave tomography corresponds to a line-by-line reconstruction, where the image is formed by translating the probe transmit and receive transducers along one direction [Fig. 15(a)]. This is different from conventional tomography used by FAM and the parametric array methods (Fig. 8).

A. Classic pump wave technique

In Ichida *et al.* (1983), the low power narrow carrier beam (named "probe" beam) was received by another transducer after its modulation by the high-power low-frequency plane wave, referred to as the pump wave [Fig. 15(a)]. The pump wave was sufficiently broad to insonify the entire object. This way, assuming a homogeneous density ρ_0 [Eq. (48)], B/A was the only parameter varying the speed of sound along the path of the probe beam. Figure 15(b) illustrates the modulated variations of the speed of sound Δc_1 and Δc_2 that the probe wave experiences as it propagates through a medium with the demonstrated B/A profile when pump waves $P_{transm1}$ and $P_{transm2}$ of different frequencies were utilized, respectively. The authors showed that the phase shift $\Delta\phi$ of the probe wave is the Fourier transform of the B/A distribution,

$$\Delta\phi\left(\frac{1}{\lambda_p}\right) = \frac{\pi}{\rho_0 {c_0}^2}\frac{P_s}{\lambda_c}\int_0^L B/A(z)\exp(j2\pi/\lambda_p)dz, \tag{49}$$

where z is the distance from the probe wave, λ_p and λ_c are the wavelengths of the pump and probe waves, correspondingly, P_s is the pump wave amplitude, and L is the distance the probe wave travelled in the studied medium. This way, the phase shift was measured for several frequencies transmitted by the pumping wave; the corresponding Fourier coefficients were then calculated and the B/A profile was reconstructed. Mechanical movement of the carrier probe allowed for generating a 2D image line by line. Interestingly, the authors of this work observed a high B/A

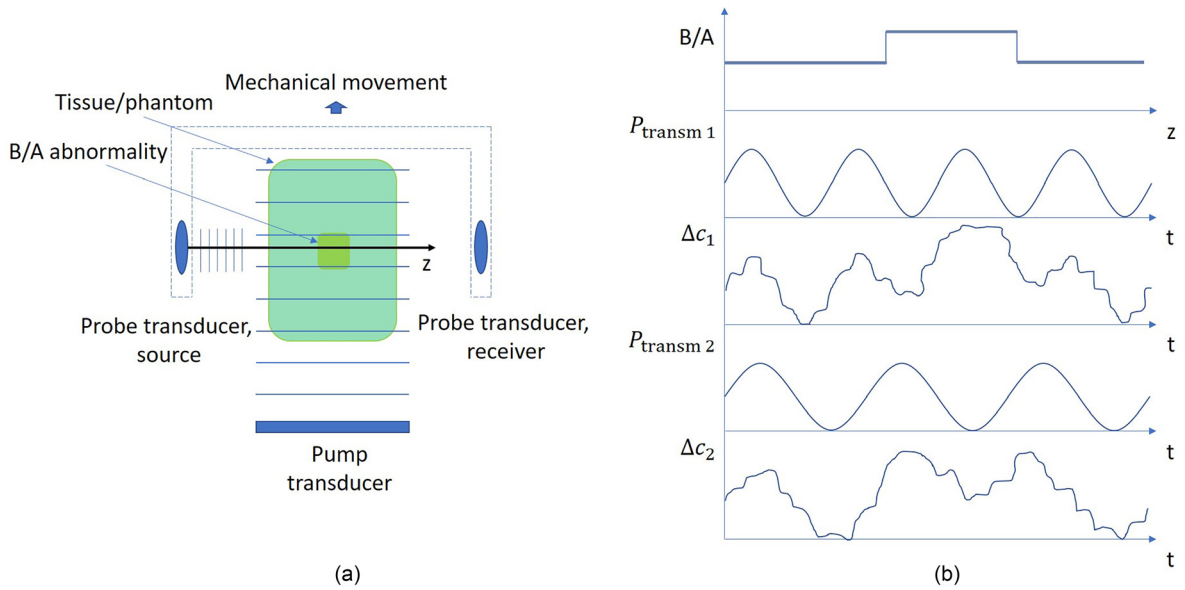

FIG. 15. (Color online) (a) Schematic of the first setup using pump waves, developed by Ichida *et al.* (1983). (b) A schematic illustration the speed of sound variation of the probe wave at points in space z with the given B/A when a pump wave is transmitted. Δc_1 and Δc_2 correspond to pump waves of different frequencies $P_{transm1}$ and $P_{transm2}$, respectively.

in muscle and bone, and low B/A of fat, contrary to the results of more recent measurements.

The previous scheme "required considerable time" (Ichida *et al.*, 1984) to acquire an image due to the frequency scanning of the pumping wave. A later modification (Ichida *et al.*, 1984) of the sinusoidal pumping wave to an impulsive pumping wave, containing many frequency components at once, allowed this method to work in real-time. In a further modification (Sato *et al.*, 1985), the location of the pumping wave was moved opposite the probe wave, next to the probe receiver (Fig. 16), allowing for a more compact and practical system. This configuration reduced B/A estimation errors due to distortion of the pumping wave's front on the way to the probe beam due to inhomogeneous tissue attenuation. Moreover, another complementary acquisition where the probe and pump transducers

TABLE VII. Summary of works utilizing pumping waves to measure B/A.

Group	Study	Type of assessment, imaged parameter	Investigated media	Uncert., %
Classic pump wave technique	Ichida *et al.*, 1983	Homogeneous, tomography, B/A	Water; images of a fish, pig tissue in water, heated pig tissue	3 (liquid)
	Ichida *et al.*, 1984	Tomography, B/A	Liquid phantom with inclusions, human forearm	—
	Sato *et al.*, 1985	Tomography, $\frac{B/A}{2\rho_0 c_0^3}$	Liquid phantom with inclusions, *in vivo* hamster	—
	Berkhout *et al.*, 1991; Kim *et al.*, 1990	*In silico* tomography	Heterogeneous phantoms of fluids, biological tissues	—
	Cain, 1986	Theoretical basis of reflection-mode tomography, B/A	—	—
	Houshmand *et al.*, 1988	*In silico* tomography, B/A	*In silico* phantoms with different 1D B/A and attenuation profiles	—
	Cain and Houshmand, 1989	*In silico* reflection-mode and transmit tomography, B/A	*In silico* phantoms with different 1D B/A profiles in lossless and attenuative media	—
	Kato and Watanabe, 1993, 1994	Homogeneous, heterogeneous 1D B/A profiles	Water, benzyn alcohol layer in water	—
SURF	Ueno *et al.*, 1990	Echo-mode 2D imaging, temperature	Temperature distribution in pig tissue and human abdominal tumor	20 (tissue)
	Fukukita *et al.*, 1996	Echo-mode 1D imaging, B/A	Agar phantom, liquids, 2-layered liquid phantom	5 (liquid)
	Kvam *et al.*, 2019b	Echo-mode 2D imaging, $\beta_p = \left(1 + \frac{B}{A}\right)k_s$	Phantom with inclusions	—

https://doi.org/10.1121/10.0003627

were interchanged allowed for tissue attenuation compensation. Together, all the mentioned studies performed by the same group have acquired B/A images of phantoms, fish, human arm, and a hamster *in vivo* (Ichida *et al.*, 1983; Ichida *et al.*, 1984; Sato *et al.*, 1985).

Several further publications were devoted to improving the previously presented method in an *in silico* environment. Berkhout *et al.* (1991) and Kim *et al.* (1990) showed that by additionally registering the frequency modulation of the signal one could also reconstruct the imaginary part of the Fourier components of the B/A distribution. These complete Fourier components acquired for a specific set of wave numbers showed the superior quality of the B/A profile reconstruction. Cain (1986) presented the theoretical basis for real-time B/A imaging in reflection mode using only one transducer as a source of the probe wave, the pump wave, and a receiver. The proposed transmit pulse consisted of two parts: a unipolar, high-pressure pump pulse coming right after the single-frequency, sinusoids probe wave (Fig. 17). The probe wave's length equals twice the distance from the transducer to the reflector. This way, when the pump pulse is just released from the transducer, the leading edge of the probe wave is in the same position, already back at the transducer surface, encountering the unipolar pump pulse. As the waves propagate, the pump pulse continues to interact with the reflected probe wave, producing phase changes, in other locations of the sample. Houshmand *et al.* (1988) continued this work, and for the same configuration studied the quality of the B/A reconstruction when using different shapes of the pump pulse. Houshmand *et al.* (1988) showed that broadband pulses provide the best estimates of the coefficient of nonlinearity and that a chirp is a good option, providing a good $B/A(z)$ estimate even for highly attenuating media. A following paper (Cain and Houshmand, 1989) focused on practical considerations suitable for both reflection and transmit modes: the limitations regarding pump width and pump amplitude as well as attenuation and distortion of the pump pulse as it propagates. The authors showed that compensation for the former effects is possible for several configurations of the pump and probe wave pulses, enabling satisfactory reconstruction of B/A profiles when a single reflector is present at the end of the imaged

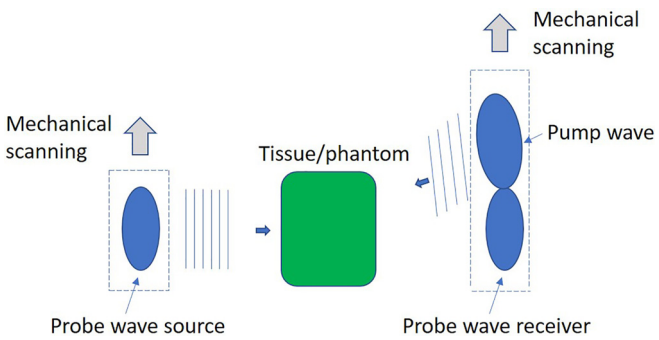

FIG. 16. (Color online) The first setup sending the pump wave nearly coaxially to the probe beam introduced by Sato *et al.* (1985).

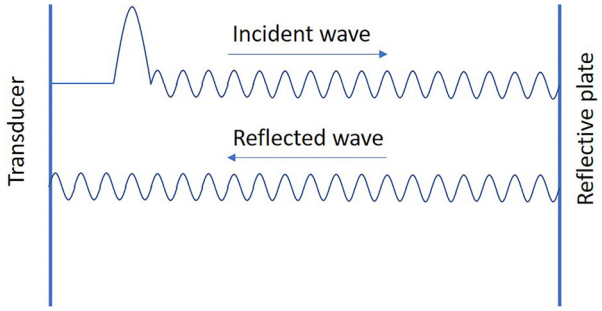

FIG. 17. (Color online) Illustration of the pulse that enables B/A reflection imaging with the pump waves with a single transducer, presented in Cain (1986).

B/A path. The authors noted that multiple reflections (e.g., tissue) pose a strong challenge in reflection-mode imaging, since they interact with the pump wave, adding noise to the image. This challenge, to our knowledge, was never overcome in experimental work, with the classic pump wave technique.

Kato and Watanabe (1993, 1994) introduced the general case of nonlinear interaction between two-plane waves intersecting at an angle θ in a homogeneous medium (Hamilton and Blackstock, 1987; Tjotta and Tjotta, 1987),

$$\Delta c = u_s \cos\theta + \frac{P_s}{2\rho_0 c_0}\frac{B}{A}, \tag{50}$$

where u_s and P_s the particle velocity and pressure of the pump wave, and Δc is the change in the probe wave's speed of sound. The equation above reduces to Eq. (48) in the perpendicular configuration used by the first pump wave work (Ichida *et al.*, 1983). For the plane wave case ($u_s = P_s/\rho_0 c_0$), in the phase domain, we can derive

$$\Delta\phi = \frac{\omega_p}{{c_0}^2}\int_0^L \left(\cos\theta + \frac{1}{2}\frac{B}{A}(z)\right) u_s dz, \tag{51}$$

where L is the interaction distance of the waves. Further, the authors showed that by registering the phase deviation of the probing wave $\Delta\phi$ at intersection angles $\theta = 0$ and $\theta = 180$, they were able to reconstruct the distribution of absolute $B/A(z)$ values for a path consisting of water and benzyl alcohol layers. Kato and Watanabe (1994) present the influence of diffraction effects on the B/A measurement. The system included two probe sources at opposite sides of the specimen, limiting the method to tomographic applications.

It was well noted by Kato and Watanabe (1993) that the pump wave method exhibited a rather large number of simulation studies (Berkhout *et al.*, 1991; Cain, 1986; Cain and Houshmand, 1989; Houshmand *et al.*, 1988; Kim *et al.*, 1990), and not so many experimental works (Ichida *et al.*, 1983; Ichida *et al.*, 1984; Kato and Watanabe, 1993; Sato *et al.*, 1985). The authors attributed this to rather small and difficult to measure phase changes induced by the pump pulse. A broad pump pulse is favorable for inducing stronger phase changes. However, it also decreases image resolution.

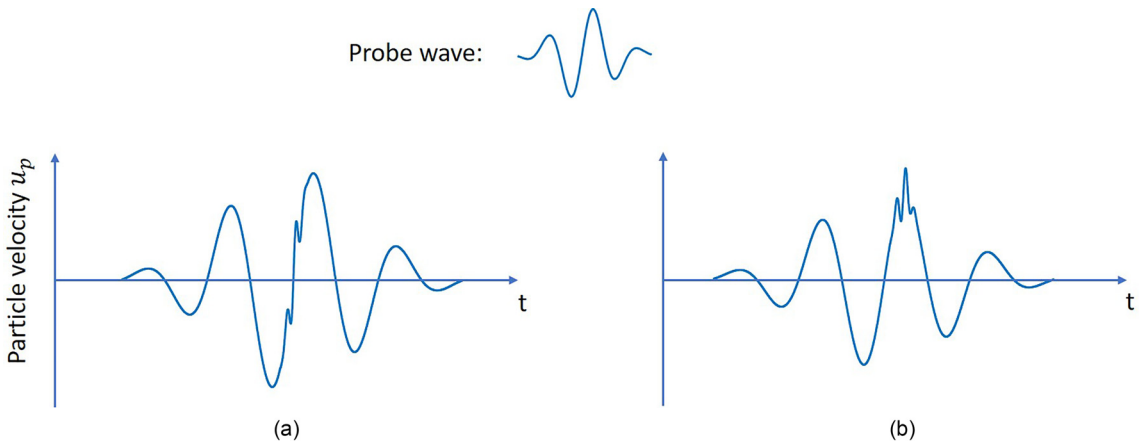

FIG. 18. (Color online) Examples of two configurations of pulse superposition used for the SURF method.

The current trade-off poses a requirement for an intense and stable pump source.

B. SURF technique for echo-mode imaging

SURF imaging can be seen as the successor of the pump wave method. The main difference is in that the probe wave has a much higher frequency than the pump wave (e.g., 2.5 MHz vs 300 kHz, Ueno *et al.*, 1990) and is superimposed on the probe wave at a chosen phase interval. This requires a dual frequency source (Fukukita *et al.*, 1996; Kvam *et al.*, 2019b), where the probe wave transducer also acts as a receiver in echo-mode. This technique requires two acquisitions with different configurations of the pulse superposition. For example, in Figs. 18(a) and 18(b), the probe wave is superimposed on the pump wave at the zero crossing of the particle velocity and peak particle velocity, respectively. Given that the velocity at a point of an acoustic waveform can be expressed as (Fukukita *et al.*, 1996; Kvam *et al.*, 2019b; Muir and Carstensen, 1980)

$$v = c_0 + \left(\frac{B}{2A}\right)\left(\frac{\Delta P}{\rho_0 c_0}\right) + u_p, \tag{52}$$

where u_p is the particle velocity, a time delay τ between the distorted and undistorted pump wave accumulates with

$$\tau = L\left(\frac{1}{c_0} - \frac{1}{v}\right) = L\beta u_p/(c_0)^2, \tag{53}$$

proportionally to the travelled distance L (Fig. 19). Therefore, the high-frequency probe pulse also distorts, undergoing either compression or expansion (depending on the phase of the pump wave), resulting in a shift of its center frequency. Moreover, the pump wave profile is affected by frequency-dependent attenuation, causing the center frequency of the pump wave to decrease with propagation. Fukukita *et al.* (1996) and Ueno *et al.* (1990) showed that B/A and α can be extracted from the ratio of the probe pulse spectra in two configurations of the probe wave superposition on the pump wave (Fig. 18). Moreover, since the frequencies of the detected probe pulses are close, the spectral ratio cancelled out scattering and diffraction effects. In their work, Fukukita *et al.* (1996) and Ueno *et al.* (1990) performed B/A and α measurements for several liquids, showing that B/A depth profiles for different liquid layers could be distinguished. In Ueno *et al.* (1990), *in vivo* images of the temperature distribution in pig tissue and a human abdominal tumor were inferred from measured B/A and attenuation. Unfortunately, no explicit images of B/A were provided.

Looking at Eq. (53) from another perspective, Kvam *et al.* (2019b) expressed v as

$$v = c_0\left(1 + \left(1 + \frac{B}{2A}\right)k_s P_s\right) = c_0(1 + \beta k_s P_s), \tag{54}$$

substituting $1/A = k_s = 1/\rho_0 c_0^2$, where k_s is the isentropic compressibility and $\beta k_s = \beta_p$ is the nonlinear bulk elasticity of the medium. Since in a realistic clinical setting, the density ρ_0, the compressibility k_s, and speed of sound c_0 are not known, the authors chose to measure the nonlinear bulk elasticity of the medium β_p rather than β. Inferring it from time delays τ, they modified Eq. (53), describing the accumulated time delay τ at point z_0,

$$\tau(z_0) = -\int_0^{z_0} \frac{\beta_p(z)}{c_0(z)} P_s(z)dz, \tag{55}$$

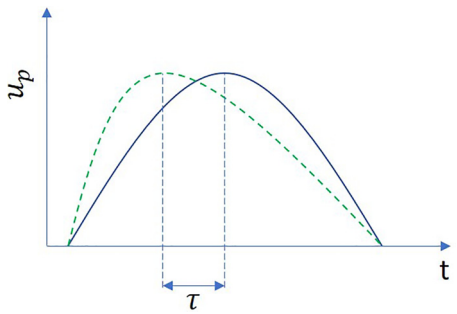

FIG. 19. (Color online) Illustration of the time delay τ between the distorted nonlinear (dashed line) wave and the undistorted (solid line) wave.

https://doi.org/10.1121/10.0003627

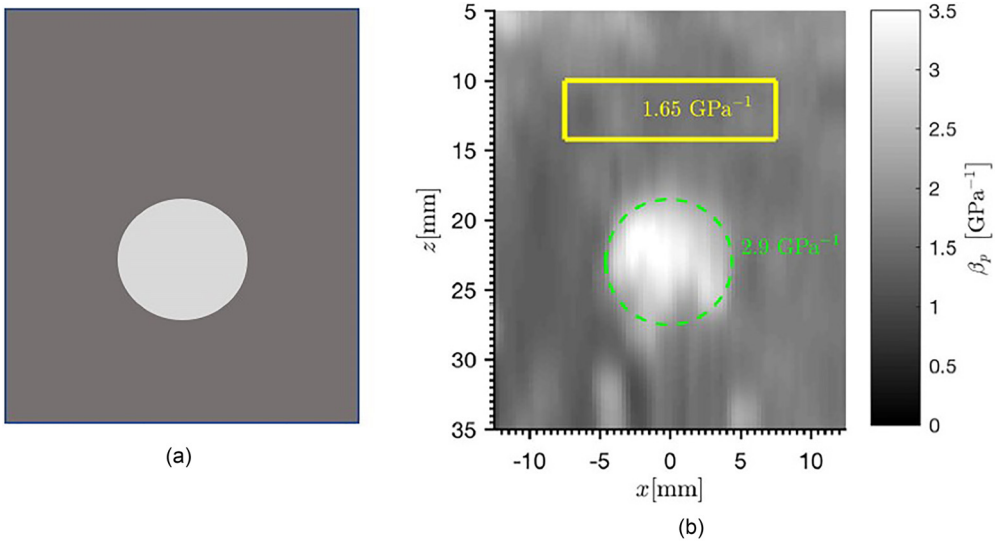

FIG. 20. (Color online) (a) Schematic of an agar-based tissue-mimicking phantom with an inclusion filled with corn oil. (b) Reprinted from Kvam *et al.* (2019b). The image of the phantom acquired with the SURF method.

for a plane wave probe pulse transmitted along z, superimposed with a positive phase of the pump wave, compared to that without a pump wave. The equation above neglects backward propagation delay and is accurate for the case when signals reflected from a single scatterer are compared. However, in reality, multiple scattering occurs as well as random interference, side lobes, reverberation noise, and refraction effects. Because of this, the authors chose not to infer the β_p variation from the derivative of τ with respect to the receive time, which would amplify the variations, but rather fit a model based on Eq. (55) to estimate β_p. An image of the β_p of a tissue-mimicking phantom is demonstrated in Fig. 20. The estimation required knowledge of the pump wave field in space $P(z)$, inferred from a measurement in a water tank.

Since the method compares signals with similar frequency content, it is considered relatively insensitive to attenuation and diffraction effects. The contribution of this work is significant since the method shows good contrast for an agar phantom with a corn oil inclusion *in silico* and *in vitro*, acquired with a linear 1D dual-frequency array. Besides this, Kvam *et al.* (2019a) found out that for most soft tissues the variability in B/A comes from the isentropic compressibility $k_s = 1/A$.

VIII. PHASE CONJUGATE BEAMS

Phase conjugate beams are time reversed beams, reradiated back to the source (Cunningham *et al.*, 2001) (Fig. 21). An optical image of a reradiated phase-conjugate beam was presented in Brysev *et al.* (2004). Phase conjugation provides the unique capability to compensate for phase distortion of the wave and achieves high-quality retrofocusing. Experimentally, this was demonstrated when a focused beam was transmitted through an aberration layer with random surface variations, and in a nonlinear nondispersive medium with inhomogeneities (Brysev *et al.*, 2004; Preobrazhensky and Pernod, 2003). Since phase conjugation provides amplification to the selected harmonic component (e.g., fundamental and 2nd harmonic), 2nd harmonic generation occurs during backwards propagation, allowing to for the registration of the 2nd or 4th harmonic of the transmitted signal. The registered higher harmonic amplitudes reflect B/A, and when the system is mechanically moved, it can produce C-scans (Fig. 21). Following this strategy, imaging of isoechogenic phantoms with heterogeneous B/A was proposed in Preobrazhensky and Pernod (2003), where the KZK equation was used to model wave propagation. Experimental images of isoechogenic liquid and liquid in gelatin phantoms (Krutyansky *et al.*, 2007; Preobrazhensky *et al.*, 2009) provided good contrast, reflecting the B/A distribution when the 2nd and 4th harmonics were registered. The fundamental images reflected varying attenuation or reflection coefficients. No experimental images of tissues were acquired. Such a possibility remains unclear since retrofocusing has been demonstrated for the nonlinear modes

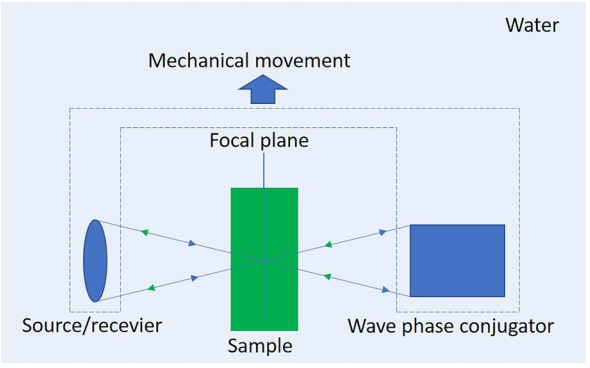

FIG. 21. (Color online) Typical phase conjugated beam setup. The arrows pointing to the right indicate the propagation of the originally transmitted signal; the arrows pointing to the left show the propagation of the phase conjugated beam.

only for nondispersive media (Preobrazhensky and Pernod, 2003). Diffraction effects can significantly deteriorate the quality of phase conjugation if the phase conjugator's diameter is too small (Brysev *et al.*, 2004).

IX. CONCLUSIONS

The first attempts to measure *B*/*A* were made in the early 1960s, when the finite amplitude (Beyer, 1960; Shutilov, 1959) and thermodynamic methods (Beyer, 1960) were first proposed, almost simultaneously. The parametric array (Nakagawa *et al.*, 1984) and the pump wave methods (Ichida *et al.*, 1983) were developed next, making the method of aqueous solutions (Sarvazyan *et al.*, 1990) and the phase conjugate method (Preobrazhensky and Pernod, 2003; Preobrazhensky *et al.*, 2009) the last ones to emerge. Several papers were published, comparing the performance of some of these methods (Arnold *et al.*, 1987; Law *et al.*, 1983, 1985; Nakagawa *et al.*, 1986; Zhang *et al.*, 2001a). Table VIII summarizes the main principle of *B*/*A* measurement of all the techniques, their advantages and disadvantages, the reported range of uncertainties, and whether or not experimental *B*/*A* images were acquired with the techniques. The latter possibility is particularly interesting from a clinical perspective since visualizing heterogeneous *B*/*A* distributions gives us the opportunity to localize suspicious tissue regions. It is worth mentioning that the data about measurement accuracy in Table VIII is rather unbalanced since some methods were much more utilized and evaluated than others.

The main disadvantage of the thermodynamic method is in that it cannot be used for *B*/*A* imaging and requires an advanced and complicated setup. At the same time, it is an accurate technique, which can be considered "the golden standard," establishing a reference to evaluate all the other methods. The method of aqueous solutions is the only technique that is more accurate (Sarvazyan *et al.*, 1990), but it requires a specific minuscule chamber and involves more complicated calculations and more extensive knowledge about the sample parameters. The work of Sarvazyan, in line with others (Sehgal *et al.*, 1986b), indicated that *B*/*A* reflects the strength of solute-solvent interactions, and grants information about molecule hydration. Moreover, Sarvazyan *et al.* (1990) observed that the replacement of an atomic group causes large changes in *B*/*A* concentration increment. These observations, together with a small sample volume, make this method a powerful option for molecular studies of biological samples. The absence of such tests may be explained by adequate alternatives currently applied in medicine, accurately detecting the chemical content of human fluids (Chen *et al.*, 2008; Delanghe, 2007; Saatkamp *et al.*, 2016). Most of these methods have difficulty distinguishing isomers (Chen *et al.*, 2008), while *B*/*A* is an excellent candidate for this task. Its utility for isomer distinction has already been demonstrated in Zhe *et al.* (2014) and may be of use when detecting early onset diabetes (Chen *et al.*, 2008) and porphyria type (Kühnel *et al.*, 1999).

In a situation when the pump wave and the probe wave propagate in the same direction, the parametric array method and pump wave method essentially merge (Cain *et al.*, 1986). In this review, we allot the technique to the parametric array method if *B*/*A* is inferred from the secondary wave pressure amplitude, and to the pump wave method when it is inferred through phase modulation of the probe wave. However, in the literature, this allocation may be different (e.g., SURF is regarded in Varray, 2011) as a parametric array method). Moreover, as FAM, the parametric array, and the pump wave methods all measure cumulative nonlinear effects of US propagation, in some papers (Kato and Watanabe, 1993; Varray *et al.*, 2011a) all three are associated with one group, referred to as FAM. In order to avoid confusion, here we refer to these three groups of methods as the extended finite amplitude methods (EFAM) for convenience. Even though the phase conjugate beam method is also based on harmonic accumulation, it is to be treated separately.

The phase conjugate beam method is the most recent method, counting only a few works. Its great advantage resides in the automatic compensation for phase deviation caused by an inhomogeneous medium or irregular surface, characteristic of tissue. At the same time, it seems that phase conjugation is challenging for dissipative media like tissue, currently limiting this method to studies of liquid samples. Only qualitative characterization of the samples' nonlinearity in conditions when the sample of interest has similar linear acoustic parameters as the reference medium, has been demonstrated at this point (Krutyansky *et al.*, 2007; Preobrazhensky *et al.*, 2009).

For all EFAMS, with few exceptions, attenuation measurement at the transmitted and received frequencies is strongly linked with *B*/*A* measurement of a lossy medium. Another factor affecting wave propagation, and therefore relevant for all EFAMS, is diffraction. In transmit mode, the influence of diffraction can be mitigated by comparing the registered signal in the sample to that in a reference medium with a similar speed of sound, following the principle of the comparative method and the FAIS. Creative alternatives eliminating the need for diffraction correction also involve large source transducers (FAM) (Chavrier *et al.*, 2006; Hunter *et al.*, 2016; Jackson *et al.*, 2014), or shifting of the diffraction pattern to the far field by attaching a steel delay line to the source (Wallace *et al.*, 2007), or measurements in the extreme near (Law *et al.*, 1981; Dunn *et al.*, 1982) or far fields (Cortela *et al.*, 2020; Dong *et al.*, 1999; King *et al.*, 2011). Since homogeneous EFAMS do not insonify the sample at high pressures, they can be suitable for *in vitro* assessment of organs for transplantation in transmission mode (e.g., liver in Hunter *et al.*, 2016).

Of all EFAMs, FAM is the most extensive group with the largest number of subgroups and modifications. This is attributed to the method's simplicity: it utilizes predominantly simple formulas within the framework of plane wave theory, and a simple setup with a source transmitting monochromatic signals. No composite waveforms (parametric

https://doi.org/10.1121/10.0003627

TABLE VIII. Summary of the main B/A measurement techniques. The graph *Uncert.*, % states the range of errors identified in these groups of method. Looking at Tables III, IV, V, VI, VII one can identify the works, where these uncertainties were taken from. In some cases, if the accuracy was not stated, errors were derived based on either the reference values provided in the corresponding papers, or B/A measured with the thermodymanic technique. In many cases, no information about the errors was available since the actual B/A was not known (e.g., self-made phantom, B/A images of a hamster, fish, etc).

Method	Main principle	Advantages	Disadvantages	Uncert., %	Images
Traditional thermodynamic. Sec. III A	B/A is composed of 2 terms	- Accurate, attenuation does not pose a big problem	- Requires knowledge of the isobaric volume coefficient of thermal expansion q and the specific heat at constant pressure Cp	3 (liq), 5 (tis)	—
	Proportional to the speed of sound	- Relatively insensitive to attenuation and diffraction effects	- Complicated setup		
	Changes Δc induced by an isobaric Temperature change and isothermal Pressure change [Eq. (12)]				
Isentropic thermodynamic. Sec. III B	B/A is proportional to the speed of sound changes Δc when pressure is varied adiabatically [Eq. (4)]	- Accurate, attenuation does not pose a big problem	- requires a complicated setup	0.85–4 (liq), 7 (tis)	—
		- Relatively insensitive to attenuation and diffraction effects			
Aqueous solutions. Sec. IV	Differential method, measuring the influence of small concentrations on B/A [Eq. (23)]	- Relatively insensitive to attenuation effects	- Very specific, complicated setup	0.3 (liq)	—
		- Small sample quantities			
		- The most accurate method			
Finite amplitude. Wave shape. Sec. V C	Determines B/A from the US wave shape	- More accurate compared to other FAM variations	- Light diffraction method: a complicated set up (A laser and an optical receiving system); - US equipment: transducer calibration and a broadband receiver required	7–8 (liq), 10 (tis)	—
Finite amplitude. Second harmonic measurements. Sec. V B	In most cases B/A is determined from formulas	- Relatively low accuracy	- In some cases, requires transducer calibration to estimate $P_1(0)$	2–20 (liq),	Tomography (e.g., Fig. 9)
	Based on the Fubini solution, modified to Incorporate losses and diffraction effects [Eqs. (26) – (30)]	- Affected by diffraction	- Diffraction and attenuation corrections	3–10 (tis)	C-scans, echo-mode imaging (e.g., Figs. 10, 11)
Finite amplitude. Fundamental nonlinear absorption. Sec. V C	Determines B/A by measuring the fundamental saturation as source pressure is increased [Eqs. (42), (44)]	- Calibration is needed only at the fundamental frequency - Does not require a wide transducer bandwidth	- Transducer calibration required	10 (liq), 6 (ph)	Echo-mode imaging
Parametric array. Sec. VI	Measures the amplitude of the difference frequency wave that is proportional to B/A	- Produces narrow, collimated beams	- The difference frequency beams have a low SNR	2–5 (liq), 10 (tis)	Tomography (e.g., Fig. 13)

TABLE VIII. (*Continued*)

Method	Main principle	Advantages	Disadvantages	Uncert., %	Images
		- Influenced less by diffraction effects	- The length of source pulses has to be sufficiently		
		- No side lobes	long to generate secondary components		
Classic pump wave.	Registers the phase modulation of	- Even in transmit mode, allows independent			
		B/*A* reconstruction along a single propagation line			
		- Not very sensitive to SNR since *B*/*A* is inferred			
Sec. VII A	The probe wave by the pump wave	from phase modulation rather than pressure units	- In practice, requires a separate pump transducer	3 (liq)	Tomography
Pump wave, SURF.	Registers the frequency shift or the time	- No diffraction correction needed	- In practice, requires a dual		
Sec. VII B	Delay of the probe wave in two pulse configurations	- Able to measure attenuation simultaneously	frequency transducer	5 (liq), 20 (tis)	Echo-mode imaging (e.g., Fig. 20)
Phase conjugate beams.	Determines *B*/*A* from higher harmonic amplitudes of the phase conjugated beam	- Compensates for phase distortion (automatic retrofocusing)	- Reflects qualitative *B*/*A* values	—	C-scans
Sec. VIII		- The phase conjugator amplifies the signal	- Only for nondissipative/weakly dissipative media		

array) or additional pump wave transducers, or composite transducers (pump wave) are needed to induce the nonlinear effects. All EFAMs enable *B*/*A* tomographic imaging (Table VIII). The first images were acquired with the pump wave method (Ichida *et al.*, 1983), reconstructing the *B*/*A* profile line-by-line. Later, FAM and the parametric method were also used to obtain *B*/*A* images in transmit, based on multiple angle reconstruction tomography (Radon transform). Pump wave tomography, compared to the parametric array and FAM tomography, allows for independent *B*/*A* reconstruction along a single propagation line without the contribution of other directions. This approach can result in real-time tomography (Ichida *et al.*, 1984) compared to reconstruction tomography. At the same time, reconstruction tomography allows improving the image resolution and quality due to numerous projections involved in the reconstruction process (Caponnetto and Bertero, 1997). Parametric array tomography allows for better resolution compared to FAM tomography (see Figs. 13 and 9) since the generated beams at the sum and difference frequencies are narrower compared to the second harmonic beam (Gong *et al.*, 2004; Wang *et al.*, 2003; Zhang *et al.*, 2001a). As for pump wave tomography, the image resolution is defined by the frequency of the pump wave and the size of the probe beam (Sato *et al.*, 1985). This way, we expect the resolution of pump wave tomography to be lower than for the parametric array and FAM methods since the probe beam is formed by the transmitted fundamental component with a wider beam. Discrimination between healthy ($B/A = 6.9$) and diseased liver ($B/A = 8.3$) has been achieved with parametric array and FAM tomography (Gong *et al.*, 2004), with even better image contrast for healthy liver and fat (Figs. 13 and 9). Unfortunately, all the pump wave tomographic works that we were able to identify showed rather poor quality images dating from 1983 to 1985 (Ichida *et al.*, 1983; Sato *et al.*, 1985). Therefore, it was difficult to compare pump wave tomography to the other types of tomography in this respect. Exceptionally, Bereza *et al.* (2008) and Burov *et al.* (2006) are the only works (the parametric array method), where *B*/*A* values were mapped to their specific locations by signal encoding.

Being a valuable asset, tomography still limits the exam to specific organs, such as the breast, and is rather time consuming for reconstruction. Paving the way for echo-mode imaging, several works have been devoted to reflection mode tomography, detecting the signals from a strong reflector on the side of the medium opposite from the source-receiver transducer (e.g., Cain, 1986; Gong *et al.*, 2004; Wang *et al.*, 2003). However, this resulted in little improvement with respect to *B*/*A*'s clinical applications.

Development to echo-mode imaging faced important challenges since the scatterer density distribution and echogenicity are the dominating factors influencing the strength of the reflected signal. Therefore, all echo-mode images were generated by limiting the scatterer effect by

https://doi.org/10.1121/10.0003627

normalizing or comparing the signal of interest to a reference signal, assumed to have a similar scattering pattern. This strategy also has the benefit of mitigating diffraction and attenuation effects. Another common assumption in the echo-mode works is that the nonlinear effect in backwards propagation is neglected since the amplitude of the reflected echoes is small compared to the forward propagating beam pressure (only for tissue, e.g., not solids). B/A echo-mode imaging was implemented with FAM, 2nd harmonic measurements (Akiyama, 2000; Fujii *et al.*, 2004; Gong *et al.*, 2004; Liu *et al.*, 2008; Toulemonde *et al.*, 2015; van Sloun *et al.*, 2015; Varray *et al.*, 2011b), Fundamental nonlinear absorption (Fatemi and Greenleaf, 1996; Nikoonahad and Liu, 1989, 1990) and SURF of the pump wave method (Fukukita *et al.*, 1987, 1996; Kvam *et al.*, 2019b; Ueno *et al.*, 1990) (Table IX). Among these, Fukukita *et al.* (1996) and Nikoonahad and Liu (1989, 1990) were only able to image B/A of liquid layers detecting signals reflected from wires (single-point scatterers) and Akiyama (2000), Fujii *et al.* (2004), Fukukita *et al.* (1996), Gong *et al.* (2004), and Liu *et al.* (2008) showed average B/A tissue values only, or values detected at a fixed-depth region, limiting these works to a global, single-parameter assessment of organs (e.g., fatty liver disease Fujii *et al.*, 2004).

The limited number of works presenting the B/A depth profile of tissue in their images points to the observation that even the normalized signals, corrected for scatterer effects, show to be nevertheless noisy (e.g., in Fujii *et al.*, 2004; Toulemonde *et al.*, 2014). Tissue, being a structure full of point scatterers located close together, favors interference of scattered signals and multiple scattering (Aubry and Derode, 2011), adding to the effects of grating lobes, reverberation noise (Kremkau and Taylor, 1986), and electronic noise. Many presented approaches (Akiyama, 2000; Fujii *et al.*, 2004; Gong *et al.*, 2004; Liu *et al.*, 2008; van Sloun *et al.*, 2015; Varray *et al.*, 2011b) for assessment of the B/A depth profile involve differentiation of the normalized signal with respect to time or space, amplifying the noise. Differently, Kvam *et al.* (2019b) formulated an optimization problem, based on the expression of the measured time delay τ, introducing penalties on the modelled process. Table IX shows that the only works able to assess the in-depth profile of B/A (or of a proportional parameter) of tissue or tissue-mimicking phantoms in echo-mode are Fatemi and Greenleaf (1996), Kvam *et al.* (2019b), Toulemonde *et al.* (2015), van Sloun *et al.* (2015), and Varray *et al.* (2011b). These demonstrate that current echo-mode imaging permits the delineation of tissue-mimicking phantom regions with different oil content/contrast agent content (Kvam *et al.*, 2019b; Toulemonde *et al.*, 2015; van Sloun *et al.*, 2015; Varray *et al.*, 2011b). Fatemi and Greenleaf (1996) were the only ones who performed B/A echo-mode imaging of heterogeneous tissues, where shadowing reflected the parameter of the nonlinearity of the preceding regions. Echo-mode in-depth temperature profiles in tissue, inferred from B/A, have been demonstrated only in Ueno *et al.* (1990).

Interestingly, some debate regarding the utility of B/A for temperature monitoring still exists, with certain studies showing a small B/A increment when tissue is coagulated (Jackson *et al.*, 2014; Saito and Kim, 2011), and others stating the contrary (Choi *et al.*, 2011; Lu *et al.*, 2004). Moreover, from another perspective, Gong *et al.* (2004) and

TABLE IX. Summary of the echo-mode methods implemented experimentally.

Method	Reference signal	Studied media	Probe
FAM. 2nd Harmonic measurements	- Fundamental at two harmonic frequency $2f_0$ (Akiyama, 2000; Fujii *et al.*, 2004; Gong *et al.*, 2004; Liu *et al.*, 2008)	- Homogeneous liquids and homogeneous bovine liver (Akiyama, 2000), - Homogeneous *in vivo* human liver (Fujii *et al.*, 2004)	- Sector array transducer (Fujii *et al.*, 2004) - Compound piezoelectric transducer (Gong *et al.*, 2004; Liu *et al.*, 2008)
		- Homogeneous tissue (Gong *et al.*, 2004; Liu *et al.*, 2008)[a]	- Two transducers (Akiyama, 2000)
	- Fundamental at f_0 (van Sloun *et al.*, 2015)	- Tissue-mimicking phantom with two layers	- Esaote LA332 commercial probe
	- 2nd harmonic in a reference medium (Varray *et al.*, 2011b)	- Two tissue-mimicking phantoms: with an inclusion and with a contrast-agent filled cavity	- Clinical probe
	- Fundamental at f_0 and 2nd harmonic in a reference medium (Toulemonde *et al.*, 2014, 2015)	- Tissue-mimicking phantom with three layers	- Commercial probe
FAM. Fundamental nonlinear absorption	- Low amplitude signal at the same frequency	- Liquid layers (Nikoonahad and Liu, 1989) - Liquid layers and *in vitro* heterogeneous tissue (Fatemi and Greenleaf, 1996)	- Commercial Acuson linear array probe
Pumping waves. SURF	- The probe pulse superimposed at another phase of the pump wave	- Liquid layers (Fukukita *et al.*, 1996)	- Dual frequency probe of 2 circular transducers (Fukukita *et al.*, 1996)
		- Agar phantom with inclusion (Kvam *et al.*, 2019b)	- Dual-frequency linear array (Kvam *et al.*, 2019b)

[a]The word "homogeneous" in this table refers to the assumption of homogeneity in depth. These studies presented B/A images that were acquired by mechanical movement of the probe.

Gong *et al.* (1993) demonstrated that B/A was able to provide better discrimination of porcine liver tissue compared to attenuation, velocity c_0, and density ρ_0, while Kvam *et al.* (2019a) concluded that for many soft tissues most of the estimated variability in B/A comes from variability in $1/A = \rho_0 c_0$. These controversial results indicate that more research is required to identify the boundaries of B/A applicability. Moreover, in our view, the utility of the thermodynamic technique and especially of the method for aqueous solutions may have been overlooked in biochemistry, molecular physics, and possible human fluid sample tests. Even though B/A cannot be used to determine the accurate and detailed chemical content of a substance, it is sensitive to structural change. Therefore, it would be particularly useful for the assessment of structural changes of the same substance (Zhe *et al.*, 2014) and has potential to diagnose diseases (Chen *et al.*, 2008; Kühnel *et al.*, 1999) through identification of the isomer type in human fluids.

This review brings us to the conclusion that more research is required to reformulate the boundaries of B/A applicability, possibly dispelling some current hopes for clinical applications and bringing new opportunities. The thermodynamic technique and the method for aqueous solutions are the most accurate, the latter being especially useful for studies of small solute concentrations. Transmission mode EFAMs allow less accurate B/A estimation, but with a simpler setup and wider perspective clinical applications. They can be of use when assessing the condition of transplantation organs (Hunter *et al.*, 2016), or measuring B/A *in vivo* as a uniform parameter (Fujii *et al.*, 2004). All EFAMS enable transmit tomography, limiting the exam to few clinical applications such as breast imaging. Development of an ultrasound B/A imaging modality is greatly hindered due to the fact that in echo-mode, the strength of the reflected signal is to a greater extent defined by the scatterer distribution and the variation of linear ultrasound parameters (c_0, ρ_0) than by B/A. Besides this, accurate imaging requires correction for diffraction effects, attenuation, various noise artifacts, and interference of signals coming from tissue scatterers. Strategies eliminating these effects would pave the way to B/A imaging in the clinic. Moreover, they may open new possibilities for imaging of the third-order nonlinear parameter C/A (Burov *et al.*, 2015; Burov *et al.*, 2013; Liu *et al.*, 2007; Xu *et al.*, 2003).

ACKNOWLEDGMENTS

This research was supported by the eMTIC collaboration and in part by the Russian Science Foundation (RSF) under Grant No. 19-12-00148 (O.A.S.).

Adler, L., and Hiedemann, E. (**1962**). "Determination of the nonlinearity parameter B/A for water and m-xylene," J. Acoust. Soc. Am. **34**(4), 410–412.
Akiyama, I. (**2000**). "Reflection mode measurement of nonlinearity parameter B/A," AIP Conf. Proc. **524**, 321–324.
Apfel, R. E. (**1983**). "The effective nonlinearity parameter for immiscible liquid mixtures," J. Acoust. Soc. Am. **74**(6), 1866–1868.
Apfel, R. E. (**1986**). "Prediction of tissue composition from ultrasonic measurements and mixture rules," J. Acoust. Soc. Am. **79**(1), 148–152.
Arnold, N., Cai, A., Nakagawa, Y., Hou, W., Wade, G., Yoneyama, M., and Nakagawa, M. (**1987**). "Acoustic tomography for imaging the nonlinear parameter," Pattern Recogn. Acoust. Imag. **768**, 93–99.
Aubry, A., and Derode, A. (**2011**). "Multiple scattering of ultrasound in weakly inhomogeneous media: Application to human soft tissues," J. Acoust. Soc. Am. **129**(1), 225–233.
Banchet, J., Cancian, J., and Cheeke, J. (**2000**). "Measurement of the acoustic nonlinearity parameter in 1-alkanols," Ultrasonics **38**, 301–304.
Banchet, J., and Cheeke, J. (**2000**). "Measurement of the acoustic nonlinearity parameter B/A in solvents: Dependence on chain length and sound velocity," J. Acoust. Soc. Am. **108**(6), 2754–2758.
Barrière, C., and Royer, D. (**2000**). "Nonlinear parameter measurement and transient acoustic field imaging using the parametric interaction in liquids," in *Proceedings of the 2000 IEEE Ultrasonics Symposium*, October 22–25, San Juan, Puerto Rico, pp. 603–606.
Barrière, C., and Royer, D. (**2001**). "Diffraction effects in the parametric interaction of acoustic waves: Application to measurements of the nonlinearity parameter B/A in liquids," Ultrasound Med. Biol **48**(6), 1706–1715.
Bartram, J. F. (**1972**). "A useful analytical model for the parametric acoustic array," J. Acoust. Soc. Am. **52**, 1042–1044.
Bereza, S. A., Burov, V. A., and Evtukhov, S. N. (**2008**). "Model experiments on acoustic tomography of the nonlinear parameter," Acoust. Phys. **54**(4), 449–459.
Berkhout, A. J., Ridder, J., and van der Wal, L. F. (**1991**). *Acoustical Imaging* (Plenum Press, New York).
Beyer, R. T. (**1960**). "Parameter of nonlinearity in fluids," J. Acoust. Soc. Am. **32**(6), 719–721.
Beyer, R. T. (**1973**). "Nonlinear acoustics," Am. J. Phys. **41**, 1060–1067.
Bjørnø, L. (**1986**). "Characterization of biological media by means of their non-linearity," Ultrasonics **24**, 254–259.
Bjørnø, L. (**2005**). "Contemporary aspects of the theory and application of nonlinear acoustics," Arch. Acoust. **30**(1), 73–85.
Bjørnø, L. (**2010**). "Introduction to nonlinear acoustics," Phys. Proc. **3**, 5–16.
Blackstock, D. (**1966**). "Convergence of the Keck-Beyer perturbation solution for plane waves of finite amplitude in a viscous fluid," J. Acoust. Soc. Am. **39**(2), 411–413.
Blackstock, D. T. (**1985**). "Generalized burgers equation for plane waves," J. Acoust. Soc. Am. **77**(6), 2050–2053.
Brysev, A. P., Krutyansky, L. M., Pernod, P., and Preobrazhensky, V. L. (**2004**). "Nonlinear ultrasonic phase-conjugate beams and their application in ultrasonic imaging," Acoust. Phys. **50**(6), 623–640.
Burgers, J. M. (**1948**). "A mathematical model describing the theory of turbulence," in *Advances in Applied Mechanics*, edited by R. von Mises and T. von Karman (Academic Press, New York), pp. 171–199.
Burns, P. N., Simpson, D. H., and Averkiou, M. A. (**2000**). "Nonlinear imaging," Ultrasound Med. Biol **26**(S1), S19–S22.
Burov, V. A., Evtukhov, S. N., Tkacheva, A. M., and Rumyantseva, O. D. (**2006**). "Acoustic tomography of the nonlinear parameter by a small number of transducers," Acoust. Phys. **52**, 655–669.
Burov, V. A., Shmelev, A. A., Kryukov, R. V., and Rumyantseva, O. D. (**2015**). "Role of nonlinear interactions in third-order acoustic tomography," Acoust. Phys. **61**(6), 636–650.
Burov, V. A., Shmelev, A. A., and Zotov, D. I. (**2013**). "A prototype for a tomography system using third-order acoustic nonlinear effects," Acoust. Phys. **59**(1), 27–44.
Byra, M., Wójcik, J., and Nowicki, A. (**2017**). "Ultrasound nonlinearity parameter assessment using plane wave imaging," in *Proceedings of the 2017 IEEE International Ultrasonics Symposium (IUS)*, September 6–9, Washington, DC, pp. 1511–1516.
Cai, A., Sun, J., and Wade, G. (**1992**). "Imaging the acoustic nonlinear parameter with diffraction tomography," IEEE Trans. Ultrason. Ferroelectr. Freq. Control **39**(6), 708–715.
Cain, C. A. (**1986**). "Ultrasonic reflection mode imaging of the nonlinear parameter B/A: I. A theoretical basis," J. Acoust. Soc. Am. **80**(28), 28–32.
Cain, C. A., and Houshmand, H. (**1989**). "Ultrasonic reflection mode imaging of the nonlinear parameter B/A. II: Signal processing," J. Acoust. Soc. Am. **86**(1), 28–32.
Cain, C. A., Nishiyama, H., and Katakura, K. (**1986**). "On ultrasonic methods for measurement of the nonlinear parameter B/A in fluid-like media," J. Acoust. Soc. Am. **80**(2), 685–688.

Caponnetto, A., and Bertero, M. (**1997**). "Tomography with a nite set of projections: Singular value decomposition and resolution," Inv. Prob. **13**, 1191–1205.
Cartersen, E. (**1998**). "Nonlinearities in the bioeffects of ultrasound," J. Acoust. Soc. Am. **103**, 3079.
Carstensen, E., Law, W., McKay, N., and Muir, T. (**1980**). "Demonstration of nonlinear acoustical effects at biomedical frequencies and intensities," Ultrasound Med. Biol. **6**, 359–368.
Chalikian, T. V., Sarvazyan, A. P., Funck, T., Belonenko, V. N., and Dunn, F. (**1992**). "Temperature dependences of the acoustic nonlinearity parameter *B*/*A* of aqueous solutions of amino acids," J. Acoust. Soc. Am. **91**, 52–58.
Chanamai, R., and McClements, D. J. (**1998**). "Ultrasonic attenuation of edible oils," J. Am. Oil Chem. Soc. **75**(10), 1447–1448.
Chavrier, F., Lafon, C., Birer, A., Barriere, C., Jacob, X., and Cathignol, D. (**2006**). "Determination of the nonlinear parameter by propagating and modeling finite amplitude plane waves," J. Acoust. Soc. Am. **119**(5), 2639–2644.
Chen, W., and Holm, S. (**2004**). "Fractional laplacian time-space models for linear and nonlinear lossy media exhibiting arbitrary frequency power-law dependency," J. Acoust. Soc. Am. **115**, 1424–1430.
Chen, J., Zhao, X., Fritsche, J., Yin, P., Schitt-Kopplin, P., Wang, W., Lu, X., Harling, H. U., Schleicher, E. D., Lehmann, R., and Xu, G. (**2008**). "Practical approach for the identification and isomer elucidation of biomarkers detected in a metabonomic study for the discovery of individuals at risk for diabetes by integrating the chromatographic and mass spectrometric information," Acta Clin. Belgica **80**, 1280–1289.
Chitnalah, A., Kourtiche, D., Jakjoud, H., and Nadi, M. (**2007**). "Pulse echo method for nonlinear ultrasound parameter measurement," Technol. Acoust. **13**, 1–8.
Choi, M., Guntur, S., LEE, J., Paeng, D., Lee, K., and Coleman, A. (**2011**). "Changes in ultrasonic properties of liver tissue in vitro during heating-cooling cycle concomitant with thermal coagulation," Ultrasound Med. Biol. **37**(12), 2000–2012.
Chung, S. H., Cerussi, A. E., Klifa, C., Baek, H. M., Birgul, O., Gulsen, G., Meritt, S. I., Hsiang, D., and Tromberg, B. (**2008**). "In vivo water state measurements in breast cancer using broadband diffuse optical spectroscopy," Phys. Med. Biol. **53**, 6713–6727.
Cleveland, R. O., and McAteer, J. A. (**2007**). *The Physics of Shock Wave Lithotripsy*, 2nd ed. (BC Decker Inc, London), Chap. 38.
Cobb, W. N. (**1983**). "Finite amplitude method for the determination of the acoustic nonlinearity parameter *B*/*A*," J. Acoust. Soc. Am. **73**(5), 1525–1531.
Coppens, A. B., Beyer, R. T., Seiden, M. B., Donohue, J., Guepin, F., Hodson, R. H., and Townsend, C. (**1965**). "Parameter of nonlinearity in fluids II," J. Acoust. Soc. Am. **38**, 797–804.
Cortela, G. A., Negreira, C. A., and Pereira, W. C. A. (**2020**). "Durability study of a gellan gum-based tissue-mimicking phantom for ultrasonic thermal therapy," J. Acoust. Soc. Am. **147**(3), 1531–1545.
Crocker, M. J. (**1997**). *Encyclopedia of Acoustics*, Vol. 1 (John Wiley and Sons, Inc., New York), pp. 193–202.
Cunningham, K. B., Hamilton, M. F., Brysev, A. P., and Krutyansky, L. M. (**2001**). "Time-reversed sound beams of nite amplitude," J. Acoust. Soc. Am. **109**(6), 2668–2674.
Davies, J. R., Tapson, J., and Mortimer, B. J. P. (**2000**). "A novel phase locked cavity resonator for *B*/*A* measurements in fluids," Ultrasonics **38**, 284–291.
Delanghe, J. (**2007**). "New screening diagnostic techniques in urinalysis," Acta Clin. Belgica **62**(3), 155–161.
Demi, L., van Dongen, K. W. A., and Verweij, M. (**2011**). "A contrast source method for nonlinear acoustic wave fields in media with spatially inhomogeneous attenuation," J. Acoust. Soc. Am. **129**(3), 1221–1230.
Devaney, A. J. (**1980**). "Quasi-plane waves and their use in radiation and scattering problems," Opt. Commun. **35**, 1–3.
Doinikov, A. A., Novell, A., Calmon, P., and Bouakaz, A. (**2014**). "Simulations and measurements of 3-D ultrasonic fields radiated by phased-array transducers using the Westervelt equation," IEEE Trans. Ultrason. Ferroelectr. Freq. Control **61**(9), 1470–1477.
Dong, Z., Junichi, K., and Wei, Z. (**2006**). "Model equation for acoustic nonlinear measurement of dispersive specimens at high frequency," Chin. Phys. Lett. **23**(10), 2807–2810.
Dong, F., Madsen, E., Macdonald, M., and Zagzebski, J. (**1999**). "Nonlinearity parameter for tissue-mimicking materials," Ultrasound Med. Biol. **25**(5), 831–838.
Dongen, K. W. V., and Verweij, M. D. (**2008**). "Sensitivity study of the acoustic nonlinearity parameter for measuring temperatures during high intensity focused ultrasound treatment," J. Acoust. Soc. Am. **123**(5), 3225.
Duck, F. A. (**1990**). *Physical Properties of Tissue: A Comprehensive Reference Book* (Academic Press, London).
Duck, F. A. (**2002**). "Nonlinear acoustics in diagnostic ultrasound," Ultrasound Med. Biol. **28**(1), 1–18.
Duck, F. A., and Starritt, H. C. (**1983**). "Acoustic shock generation by ultrasonic imaging equipment," Br. J. Radiol. **57**, 231–240.
Dunn, F., Law, W. K., and Frizzell, L. A. (**1982**). "Nonlinear ultrasonic propagation in biological media," Br. J. Cancer Suppl. **45**, 55–58.
Eggers, F., and Funck, T. (**1973**). "Ultrasonic measurements with milliliter liquid samples in the 0.5-100 MHz range," Rev. Sci. Instrum. **44**, 969–977.
Emery, J., Gassea, S., and Dugue, C. (**1979**). "Coefficient de nonlinearite acoustique dans les melanges eau-methanol et eau-ethanol" ("The acoustic coefficient of nonlinearity in water-methanol and water-ethanol mixtures"), J. Phys. **11**(40), 231–234.
Errabolu, R. V., Sehgal, C. M., Bahn, R. C., and Greenleaf, J. F. (**1988**). "Measurement of ultrasonic nonlinear parameter in excised fat tissues," Ultrasound Med. Biol **14**(2), 137–146.
Errabolu, R. L., Sehgal, C. M., and Greenleaf, J. F. (**1987**). "Dependence of ultrasonic nonlinear parameter *B*/*A* on fat," Ultrason. Imag. **9**, 180–194.
Everbach, E. C., and Apfel, R. E. (**1995**). "An interferometric technique for *B*/*A* measurement," J. Acoust. Soc. Am. **98**(6), 3428–3438.
Everbach, E. C., Zhu, Z., Jiang, P., Chu, B. T., and Apfel, R. E. (**1991**). "A corrected mixture law for *B*/*A*," J. Acoust. Soc. Am. **89**(1), 446–447.
Fatemi, M., and Greenleaf, J. F. (**1996**). "Real-time assessment of the parameter of nonlinearity in tissue using the 'nonlinear shadowing'," Ultrasound Med. Biol **22**(9), 1215–1228.
Fear, E. C., Hagness, S. C., Meaney, P. M., Okoniewski, M., and Stuchly, M. A. (**2002**). "Breast tumor detection with near-field imaging," IEEE Microw. Mag. **3**(1), 48–56.
Ficken, G. W., Jr., and Hiedemann, E. A. (**1956**). "Simple form of the sing-around method for the determination of sound velocities," J. Acoust. Soc. Am. **28**(5), 921–923.
Filonenko, E. A., and Khokhlova, V. A. (**2001**). "Effect of acoustic nonlinearity on heating of biological tissue by high-intensity focused ultrasound," Acoust. Phys. **47**(4), 468–475.
Fox, F. E., and Rock, G. D. (**1941**). "Ultrasonic absorption in water," J. Acoust. Soc. Am. **12**, 505–510.
Fox, F. E., and Wallace, W. A. (**1954**). "Absorption of finite amplitude sound waves," J. Acoust. Soc. Am. **26**, 994–1006.
Frøysa, K. (**1994**). "Weakly nonlinear propagation of a pulsed sound beam," J. Acoust. Soc. Am. **95**(1), 123–130.
Fubini-Ghiron, E. (**1935**). "Anomalies in the propagation of large amplitude acoustic waves," Alta Frequenza **4**, 530–581.
Fujii, Y., Taniguchi, N., Akiyama, I., Tsao, J., and Itoh, K. (**2004**). "A new system for in vivo assessment of the degree of nonlinear generation using the second harmonic component in echo signals," Ultrasound Med. Biol. **30**(11), 1511–1516.
Fukukita, H., Ueno, S., and Yano, T. (**1987**). "Application of nonlinear effect to ultrasonic pulse reflection method-modulation characteristics of received pulse," Jpn. J. Appl. Phys. **26**, 49–51.
Fukukita, H., Ueno, S., and Yano, T. (**1996**). "Ultrasound pulse reflection mode measurement of nonlinearity parameter *B*/*A* and attenuation coefficient," J. Acoust. Soc. Am. **99**(5), 2775–2782.
Germain, L., Jacques, R., and Cheeke, J. (**1989**). "Acoustic microscopy applied to nonlinear characterization of biological media," J. Acoust. Soc. Am. **86**(4), 1560–1565.
Ginter, S., Liebler, M., Steiger, E., Dreyer, T., and Riedlinger, R. E. (**2002**). "Full-wave modeling of therapeutic ultrasound: Nonlinear ultrasound propagation in ideal fluids," J. Acoust. Soc. Am. **111**, 2049–2059.
Gong, X., Feng, R., Zhu, C., and Shi, T. (**1984**). "Ultrasonic investigation of the nonlinearity parameter *B*/*A* in biological media," J. Acoust. Soc. Am. **76**(3), 949–950.

Gong, X. F., Liu, X. Z., and Zhang, D. (**1993**). "Influences of tissue composition and structural features of biological media on the ultrasonic nonlinearity parameter," Chin. J. Acoust. **12**(3), 265–270.
Gong, X., Zarembo, L. K., and Krasilnikov, V. A. (**1963**). "Measurement of the acoustic nonlinear parameter of liquid nitrogen," Akust. Zh. **9**, 382–383.
Gong, X., Zhang, D., Liu, J., Wang, H., Yan, Y., and Xu, X. (**2004**). "Study of acoustic nonlinearity parameter imaging methods in reflection mode for biological tissues," J. Acoust. Soc. Am. **116**(3), 1819–1825.
Gong, X., Zhu, Z., Shi, T., and Huang, J. (**1989**). "Determination of the acoustic nonlinearity parameter in biological media using FAIS and ITD methods," J. Acoust. Soc. Am. **86**(1), 1–5.
Goss, S. A., Frizell, L. A., and Dunn, F. (**1979**). "Ultrasonic absorption and attenuation in mammalian tissues," Ultrasound Med. Biol. **5**(2), 181–186.
Goss, S. A., and Fry, F. J. (**1981**). "Nonlinear acoustic behavior in focused ultrasonic fields: Observations of intensity dependent absorption in biological tissue," IEEE Trans. Sonics Ultrason. **28**, 21–25.
Greenspan, M., and Tschiegg, C. E. (**1957**). "Speed of sound in water by a direct method," J. Res. Natl. Bur. Standards **59**(4), 249–254.
Greenspan, M., and Tschiegg, C. E. (**1959**). "Tables of the speed of sound in water," J. Acoust. Soc. Am. **31**, 75–76.
Hagelberg, M. P., Holton, G., and Kao, S. (**1967**). "Calculation of *B*/*A* for water from measurements of ultrasonic velocity versus temperature and pressure to 10 000 kg/cm^2," J. Acoust. Soc. Am. **41**(3), 564–567.
Hamilton, M. F., and Blackstock, D. T. (**1987**). "On the coefficient of nonlinearity β in nonlinear acoustics," J. Acoust. Soc. Am **83**(1), 74–77.
Hamilton, M. F., and Blackstock, D. T. (**1998**). *Nonlinear Acoustics* (Academic Press, New York).
Harris, G., Liu, Y., Maruvada, S., and Gammell, P. (**2007**). "Finite amplitude method for measurement of nonlinearity parameter *B*/*A* using plane-wave tone bursts," in *Proceedings of the 2007 IEEE Ultrasonics Symposium*, October 28–31, New York, pp. 2072–2074.
Haumesser, L., and Meulen, F. V. (**2019**). "Reduced propagation path for *B*/*A* nonlinear parameter evaluation," Proc. Mtgs. Acoust. **38**, 045023.
Hikata, A., Kwun, H., and Elbaum, C. (**1980**). "Finite amplitude wave propagation in solid and liquid He 4," Phys. Rev. B **21**(9), 3932–3939.
Holton, G., Hagelberg, M. P., Kao, S., and Johnson, W. H. (**1968**). "Ultrasonic-velocity measurements in water at pressures to 10 000 kg/cm^2," J. Acoust. Soc. Am. **43**(1), 102–107.
Houshmand, H., McGough, R. J., Ebbini, E., Lee, H., and Cain, C. A. (**1988**). "Ultrasonic transmission mode imaging of the nonlinear parameter *B*/*A*: A simulation study," in *Proceedings of the 1988 Ultrasonics* Symposium, October 2–5, Chicago, IL, pp. 979–983.
Hunter, C., Sapozhnikov, O. A., Maxwell, A., Khokhlova, V. A., Wang, Y.-N., MacConaghy, B., and Kreider, W. (**2016**). "An ultrasonic caliper device for measuring acoustic nonlinearity," Phys. Proc. **87**, 93–98.
Ichida, N., Sato, T., and Linzer, M. (**1983**). "Imaging the nonlinear ultrasonic parameter of a medium," Ultrason. Imag. **5**, 295–299.
Ichida, N., Sato, T., Miwa, H., and Murakami, K. (**1984**). "Real-time nonlinear parameter tomography using impulsive pumping waves," IEEE Trans. Sonics Ultrason. **31**(5), 635–641.
Iinuma, K. (**1988**). "Ultrasonic method and apparatus for tissue characterization and imaging of nonlinear parameter," U.S. patent 4,771,786.
Ingenito, F., and Williams, A. O., Jr. (**1971**). "Calculation of second-harmonic generation in a piston beam," J. Acoust. Soc. Am. **49**, 319–328.
Jackson, E., Cleveland, R. O., and Coussios, C. C. (**2013**). "The origins of nonlinear enhancement in ex vivo tissue during high intensity focused ultrasound (HIFU) ablation," Proc. Mtgs Acoust. **19**, 075067.
Jackson, E., Coussios, C., and Cleveland, R. (**2014**). "Nonlinear acoustic properties of ex vivo bovine liver and the effects of temperature and denaturation," Phys. Med. Biol. **59**, 3223–3238.
Jain, R. K., Shah, S. A., and Finney, P. L. (**1984**). "Continuous noninvasive monitoring of pH and temperature in rat walker 256 carcinoma during normoglycemia and hyperglycemia," J. Nat. Cancer Inst. **73**(2), 429–436.
Jeong, H., Barnard, D., Cho, S., Zhang, S., and Li, X. (**2017**). "Receiver calibration and the nonlinearity parameter measurement of thick solid samples with diffraction and attenuation corrections," Ultrasonics **81**, 147–157.
Jeong, H., Zhang, S., Barnard, D., and Li, X. (**2015**). "Significance of accurate diffraction corrections for the second harmonic wave in determining the acoustic nonlinearity parameter," AIP Adv. **5**(9), 097179.
Jeong, H., Zhang, S., and Li, X. (**2016**). "A novel method for extracting acoustic nonlinearity parameters with diffraction corrections," J. Mech. Sci. Technol. **30**(2), 643–652.
Ji, P., Tan, E., Gan, W., and Yang, J. (**2011**). "A comparative analysis of preprocessing methods for the parametric loudspeaker based on the Khokhlov–Zabolotskaya–Kuznetsov equation for speech reproduction," IEEE Trans. Audio Speech Lang. Process. **19**, 937–946.
Kashkooli, H., Dolan, P. J., Jr., and Smith, C. W. (**1987**). "Measurement of the acoustic nonlinearity parameter in water, methanol, liquid nitrogen, and liquid helium-2 by two different methods: A comparison," J. Acoust. Soc. Am. **82**(6), 2086–2089.
Kato, A., and Watanabe, Y. (**1993**). "Measurement method of spatial distribution of nonlinearity parameter *B*/*A* using nonlinear interaction of two sound waves," Jpn. J. Appl. Phys. **32**, 2274–2278.
Kato, A., and Watanabe, Y. (**1994**). "Diffraction effect on phase deviation caused by nonlinear interaction between two sound waves in measuring spatial distribution of nonlinearity parameter *B*/*A*," Jpn. J. Appl. Phys. **33**, 2922–2928.
Keck, W., and Beyer, R. T. (**1960**). "Frequency spectrum of finite amplitude ultrasonic waves in liquids," Phys. Fluids **3**(3), 346–352.
Khelladi, H., Plantier, F., Daridon, J. L., and Djelouah, H. (**2009**). "Measurement under high pressure of the nonlinearity parameter *B*/*A* in glycerol at various temperatures," Ultrasonics **49**(8), 668–675.
Kim, D., Greenleaf, J. F., and Sehgal, C. M. (**1990**). "Ultrasonic imaging of the nonlinear parameter *B*/*A*: Simulation studies to evaluate phase and frequency modulation methods," Ultrasound Med. Biol **16**(2), 175–181.
Kim, H.-J., Schmerr, L. S., Jr., and Sedov, A. (**2006**). "Generation of the basis sets for multi-Gaussian ultrasonic beam models—An overview," J. Acoust. Soc. Am. **119**(4), 1971–1978.
King, R. L., Liu, Y., Maruvada, S., Herman, B. A., Wear, K. A., and Harris, G. R. (**2011**). "Development and characterization of a tissue-mimicking material for high-intensity focused ultrasound," IEEE Trans. Ultrason. Ferroelectr. Freq. Control **58**(7), 1397–1405.
Kourtiche, D., Alliès, L., Chitnalah, A., and Nadi, M. (**2001**). "Harmonic propagation of finite amplitude sound beams: Comparative method in pulse echo measurement of nonlinear *B*/*A* parameter," Meas. Sci. Technol. **12**, 1990–1995.
Kramer, S. M., McBride, S. L., and Mair, H. D. (**1988**). "Characteristics of wide-band planar ultrasonic transducers using plane and edge wave contributions," IEEE Trans. Ultrason. Ferroelectr. Freq. Control **35**(2), 253–263.
Krasilnikov, V. A., Shklovskaya-Kordy, V. V., and Zarembo, L. K. (**1957**). "On the propagation of ultrasonic waves of finite amplitude in liquids," J. Acoust. Soc. Am. **29**, 642–647.
Kremkau, F. W., and Taylor, K. J. W. (**1986**). "Artifacts in ultrasound imaging," J. Ultrasound Med. **5**, 227–237.
Krutyansky, L. M., Preobrazhensky, V. L., Pernod, P., and Matar, O. B. (**2007**). "Nonlinear imaging of isoechogenic phantoms using phase conjugation of the second acoustic harmonic," Phys. Wave Phenom. **15**(3), 186–190.
Kühnel, A., Groß, U., Jacob, K., and Doss, M. O. (**1999**). "Studies on coproporphyrin isomers in urine and feces in the porphyrias," Clin. Chim. Acta **282**, 45–58.
Kujawska, T., Wojcik, J., Filipczyński, L., and Etienne, J. (**2003**). "A new method for determination of the acoustic nonlinearity parameter *B*/*A* in multilayer biological media," in Proceedings of the 5th World Congress on Ultrasound, Paris, pp. 81–84.
Kuntz, H. L., Hixson, E. L., and Ryan, W. W. (**1983**). "The Rayleigh distance and geometric nearfield size of nonplane sound radiators," J. Acoust. Soc. Am. **74**, S82–S83.
Kushibiki, J., Ishibashi, M., Akashi, N., Sannomiya, T., Chubachi, N., and Dunn, F. (**1997**). "Transmission line method for the measurement of the acoustic nonlinearity parameter in biological liquids at very high frequencies," J. Acoust. Soc. Am. **102**(5), 3038–3044.
Kuznetsov, V. P. (**1970**). "Equations of nonlinear acoustics," Akust. Zh. **16**(4), 548–553 (in Russian).
Kvam, J., Holm, S., and Angelsen, B. A. J. (**2019a**). "Exploiting Ballou's rule for better tissue classification," J. Acoust. Soc. Am. **145**(4), 2103–2112.
Kvam, J., Solberg, S., Myhre, O., Rodriguez-Molares, A., and Angelsen, B. (**2019b**). "Nonlinear bulk elasticity imaging using dual frequency ultrasound," J. Acoust. Soc. Am. **146**(4), 2492–2500.

Law, W. K., Frizzell, L. A., and Dunn, F. (**1981**). "Ultrasonic determination of the nonlinearity parameter *B*/*A* for biological media," J. Acoust. Soc. Am. **69**(4), 1210–1212.
Law, W. K., Frizzell, L. A., and Dunn, F. (**1983**). "Comparison of thermodynamic and finite amplitude methods of *B*/*A* measurement in biological materials," J. Acoust. Soc. Am. **74**, 1295–1297.
Law, W. K., Frizzell, L. A., and Dunn, F. (**1985**). "Determination of the nonlinearity parameter *B*/*A* of biological media," Ultrasound Med. Biol. **11**(2), 307–318.
Li, X., Zhang, S., Jeong, H., and Cho, S. (**2017**). "Calibration of focused ultrasonic transducers and absolute measurements of fluid nonlinearity with diffraction and attenuation corrections," J. Acoust. Soc. Am. **142**, 984–990.
Liu, X., Gong, X., Yin, C., Li, J., and Zhang, D. (**2008**). "Noninvasive estimation of temperature elevations in biological tissues using acoustic nonlinearity parameter imaging," Ultrasound Med. Biol **34**(3), 414–424.
Liu, X., Li, J., Gong, X., Zhu, Z., and Zhang, D. (**2007**). "Theoretical and experimental study of the third-order nonlinearity parameter C/A for biological media," Phys. S **228**, 172–178.
Lu, Z., Daridon, J. L., Lagourette, B., and Ye, S. (**1998**). "A phase-comparison method for measurement of the acoustic nonlinearity parameter *B*/*A*," Meas. Sci. Technol. **9**, 1699–1705.
Lu, Z., Lagourette, B., and Daridon, J. L. (**2001**). "Acoustic nonlinearity parameter of liquid alkanes as a function of temperature, chain length and isomerism," Phys. Chem. Liquids **39**, 255–266.
Lu, Y., Liu, X., Gong, X., and Zhang, D. (**2004**). "Relationship between the temperature and the acoustic nonlinearity parameter in biological tissues," Chin. Sci. Bull. **49**(22), 2360–2363.
Ma, Q., Ma, Y., Gong, X., and Zhang, D. (**2005**). "Improvement of tissue harmonic imaging using the pulse-inversion technique," Ultrasound Med. Biol. **31**, 889–894.
Madigosky, W. M., Rosenbaum, I., and Lucas, R. (**1981**). "Sound velocities and *B*/*A* in fluorocarbon fluids and in several low density solids," J. Acoust. Soc. Am. **69**, 1639–1643.
Meulen, F. V., and Haumesser, L. (**2008**). "Evaluation of *B*/*A* nonlinear parameter using an acoustic self-calibrated pulse-echo method," Appl. Phys. Lett. **92**, 214106.
Mikhailov, I. G., and Shutilov, V. A. (**1959**). "Diffraction of light on harmonics of ultrasound waves, distorted in the process of propagation in liquid," Akust. Zh. **5**(1), 77–79 (in Russian).
Mikhailov, I. G., and Shutilov, V. A. (**1960**). "About the distortion of the shape of finite amplitudes ultrasound waves in various liquids," Akust. Zh. **6**(3), 340–346 (in Russian).
Muir, T. G., and Carstensen, E. L. (**1980**). "Prediction of nonlinear acoustic effects at biomedical frequencies and intensities," Ultrasound Med. Biol. **6**, 345–357.
Nakagawa, Y., Hou, W., Cai, A., Arnold, N., and Wade, G. (**1986**). "Nonlinear parameter imaging with finite-amplitude sound waves," in *Proceedings of the IEEE 1986 Ultrasonics Symposium*, November 17–19, Williamsburg, VA, pp. 901–904.
Nakagawa, Y., Nakagawa, M., Yoneyama, M., and Kikuchi, M. (**1984**). "Nonlinear parameter imaging computed tomography by parametric acoustic array," in *Proceedings of the IEEE 1984 Ultrasonics Symposium*, November 14–16, Chicago, IL, pp. 673–676.
Naugolnykh, K. (**2009**). "Nonlinear acoustics: From research in physics to application (historical incidents)," Acoust. Phys. **55**(3), 338–344.
Naugolnykh, K., and Ostrovskii, L. (**1998**). *Nonlinear Wave Processes in Acoustics* (Cambridge University Press, Cambridge, UK), Chap. 1, pp. 1–11.
Nikolini, C., Carlo, P., and Ridella, S. (**1987**). "The physical state of intranuclear water and ions: Changes during cell proliferation and chemically induced carcinogenesis," Toxicology Pathology **15**(2), 184–189.
Nikoonahad, M., and Liu, D. C. (**1989**). "Pulse-echo *B*/*A* measurement using variable amplitude excitation," in *Proceedings of the 1989 IEEE Ultrasonics Symposium*, October 3–6, Montreal, Canada, pp. 1047–1051.
Nikoonahad, M., and Liu, D. C. (**1990**). "Pulse-echo single frequency acoustic nonlinearity parameter (*B*/*A*) measurement," IEEE Trans Ultrason. Ferroelectr. Freq. Control **37**(3), 127–134.
Nomoto, O., and Negishi, K. (**1965**). "Diffraction of light by ultrasonic waves of finite amplitude," Acta Acust. united Acust. **15**(4), 223–235.
Panfilova, A., Shelton, S. E., Caresio, C., van Sloun, R. J. G., Molinari, F., Wijkstra, H., Dayton, P. A., and Mischi, M. (**2019**). "On the relationship between dynamic contrast-enhanced ultrasound parameters and the underlying vascular architecture extracted from acoustic angiography," Ultrasound Med. Biol **45**(2), 539–548.
Panfilova, A., van Sloun, R., Wilbeboer, R., Wijkstra, H., and Mischi, M. (**2018**). "A fixed-distance plane wave method for estimating the ultrasound coefficient of nonlinearity," Proc. Mtgs. Acoust. **34**, 020001.
Pantea, C., Osterhoudt, C. F., and Sinha, D. N. (**2013**). "Determination of acoustical nonlinear parameter of water using the finite amplitude method," Ultrasonics **53**, 1012–1019.
Plantier, F., Daridon, J.-L., and Lagourette, B. (**2002a**). "Measurement of the *B*/*A* nonlinearity parameter under high pressure: Application to water," J. Acoust. Soc. Am. **111**(2), 707–715.
Plantier, F., Daridon, J.-L., and Lagourette, B. (**2002b**). "Nonlinear parameter (*B*/*A*) measurements in methanol, 1-butanol and 1-octanol for different pressures and temperatures," J. Phys. D **35**, 1063–1067.
Plantier, F., Daridon, J.-L., and Lagourette, B. (**2003**). "Measurement of the acoustic nonlinearity parameter in liquid alkanes under pressure and comparison with the Lee-Kesler correlation," J. Acoust. Soc. Am. **35/36**, 109–116.
Preobrazhensky, V., and Pernod, P. (**2003**). "Nonlinear acoustics of phase conjugate waves in heterogeneous media (NGA approach)," in Proceedings of the 5th World Congress on Ultrasonics, WCU 2003, pp. 875–878.
Preobrazhensky, V., Pernod, P., Pyl'nov, Y. B., Krutyansky, L., Smagin, N., and Preobrazhensky, S. (**2009**). "Nonlinear acoustic imaging of isoechogenic objects and flows using ultrasound wave phase conjugation," Acta Acust. united Ac. **95**, 36–45.
Purrington, R. D., and Norton, G. V. (**2012**). "A numerical comparison of the Westervelt equation with viscous attenuation and a causal propagation operator," Math Comput. Simul. **82**, 1287–1297.
Rudnick, I. (**1952**). "Theory of the attenuation of very high amplitude sound waves," Technical Report 1, Bodine Engine Co., Los Angeles, CA.
Rudnick, I. (**1958**). "On the attenuation of finite amplitude waves in a liquid," J. Acoust. Soc. Am. **30**, 564–567.
Saatkamp, C. J., de Almeida, M. L., Bispo, J. A. M., Pinheiro, A. L. B., Fernandes, A. B., and Silveira, L., Jr. (**2016**). "Quantifying creatinine and urea in human urine through raman spectroscopy aiming at diagnosis of kidney disease," J. Biomed. Opt. **21**(3), 037001–037007.
Saito, S. (**1993a**). "Measurement of the acoustic nonlinearity parameter *B*/*A* in liquid media using focused ultrasound," J. Acoust. Soc. Am. **93**(1), 162–172.
Saito, S. (**1993b**). "Measurement of acoustic nonlinearity parameter using focused ultrasound detected by a concave receiver," J. Acoust. Soc. Jpn. **16**(4), 239–246.
Saito, S. (**2010**). "Finite amplitude method for measuring the nonlinearity parameter *B*/*A* in small-volume samples using focused ultrasound," J. Acoust. Soc. Am. **127**(1), 51–61.
Saito, S., and Kim, J. H. (**2011**). "Two-dimensional measurement of the nonlinearity parameter *B*/*A* in excised biological samples," Rev. Sci. Instrum. **82**(6), 064901.
Saito, S., Yamamoto, A., and Nakamura, K. (**2005**). "*B*/*A* measurement for liquid media using an LN transducer with inverted-domain layer," Jpn. J. Appl. Phys. **44**(6B), 4431–4435.
Sapozhnikov, O. A. (**2015**). "High-intensity ultrasonic waves in fluids: Nonlinear propagation and effects," in *Power Ultrasonics. Applications of High-Intensity Ultrasound*, edited by J. A. Gallego-Juárez and K. F. Graff (Woodhead Publishing, Cambridge, UK), Chap. 2, pp. 9–35.
Sarvazyan, A. P. (**1982**). "Development of methods of precise ultrasonic measurements in small volumes of liquids," Ultrasonics **20**, 151–154.
Sarvazyan, A. P. (**1991**). "Ultrasonic velocity of biological compounds," Ann. Rev. Biophys. Biophys. Chem. **20**, 321–342.
Sarvazyan, A. P., Chalikian, T. V., and Dunn, F. (**1990**). "Acoustic nonlinearity parameter *B*/*A* of aqueous solutions of some amino acids and proteins," J. Acoust. Soc. Am. **88**, 1555–1561.
Sato, T., Fukusimal, A., Ichidal, N., Ishikawal, H., Miwa, H., Igarashi, Y., Shimura, T., and Murakami, K. (**1985**). "Nonlinear parameter tomography system using counterpropagating probe and pump waves," Ultrason. Imaging **7**(1), 49–59.
Sato, T., and Yamakoshi, Y. (**1986**). "Nonlinear tissue imaging," in *Proceedings of the 1986 Ultrason*ics S*ymposium*, November 17–19, Williamsburg, VA, pp. 890–900.

Sehgal, C. M., Bahn, R. C., and Greenleaf, J. F. (**1984**). "Measurement of the acoustic nonlinearity parameter *B*/*A* in human tissues by a thermodynamic method," J. Acoust. Soc. Am. **76**, 1023–1029.
Sehgal, C. M., Brown, G. M., Bahn, R. C., and Greenleaf, J. F. (**1986a**). "Measurement and use of acoustic nonlinearity and sound speed to estimate composition of excised livers," Ultrasound Med. Biol **12**(11), 865–874.
Sehgal, C. M., Porter, B. R., and Greenleaf, J. F. (**1986b**). "Ultrasonic nonlinear parameters and sound speed of alcohol–water mixtures," J. Acoust. Soc. Am **79**(2), 566–570.
Shen, C., and Li, P. (**2001**). "Tissue harmonic image analysis based on spatial covariance," IEEE Trans. Ultrason. Ferroelectr. Freq. Control **48**, 1648–1656.
Shklovskaya-Kordi, V. V. (**1963**). "Acoustical methods for determining internal pressure in liquids," Akust. Zh. **9**(1), 107–111 (in Russian).
Shutilov, V. A. (**1959**). "Optical studies of the shape of ultrasonic waves of large amplitude in liquids," Akust. Zh. **5**(2), 231–240 (in Russian).
Szabo, T. L. (**1994a**). "Causal theories and data for acoustic attenuation obeying a frequency power law," J. Acoust. Soc. Am. **97**(1), 14–24.
Szabo, T. L. (**1994b**). "Time domain equations for lossy media obeying a frequency power law," J. Acoust. Soc. Am **96**(1), 491–500.
Takahashi, S. (**1995**). "Measurement of acoustic nonlinearity parameter by observation waveforms," Jpn. J. Appl. Phys. **34**, 2790–2792.
Takenouchi, M., Suzuki, H., and Tagami, H. (**1986**). "Hydration characteristics of pathologic stratum corneum-evaluation of bound water," Soc. Invest. Dermatol. **87**(5), 574–576.
Thuras, A. L., Jenkins, R. T., and O'Neil, H. T. (**1935**). "Extraneous frequencies generated in air carrying intense waves," J. Acoust. Soc. Am. **6**, 173–180.
Tjotta, J. N., and Tjotta, S. (**1981**). "Nonlinear equations of acoustics, with application to parametric acoustic arrays," J. Acoust. Soc. Am. **69**, 1644–1652.
Tjotta, J. N., and Tjotta, S. (**1987**). "Interaction of sound waves. part 1: Basic equations and plane waves," J. Acoust. Soc. Am. **82**(4), 1425–1428.
Toulemonde, M., Varray, F., Basset, O., Tortoli, P., and Cachard, C. (**2014**). "High frame rate compounding for nonlinear *B*/*A* parameter ultrasound imaging in echo mode—Simulations," in *Proceedings of the 2014 IEEE International Conference on Acoustics, Speech and Signal Processing*, May 4–9, Florence, Italy, pp. 5153–5157.
Toulemonde, M., Varray, F., Basset, O., Tortoli, P., and Cachard, C. (**2015**). "Nonlinearity parameter *B*/*A* of biological tissue ultrasound imaging in echo mode," AIP. Conf. Proc. **1685**, 040016.
Treeby, B. E., and Cox, B. T. (**2010**). "k-Wave: Matlab toolbox for the simulation and reconstruction of photoacoustic wave fields," J. Biomed. Opt. **15**(2), 021314.
Ueno, S., Hashimoto, M., Fukukita, H., and Yano, T. (**1990**). "Ultrasound thermometry in hyperthermia," in IEEE Ultrasonics Symposium, December 4–7, Honolulu, HI, pp. 1645–1651.
van Sloun, R., Demi, L., Shan, C., and Mischi, M. (**2015**). "Ultrasound coefficient of nonlinearity imaging," IEEE Trans. Ultrason. Ferroelectr. Freq. Control **62**(7), 1331–1341.
van Sloun, R. J. G., Demi, L., Postema, A. W., de la Rosette, J. J., Wijkstraa, H., and Mischi, M. (**2017**). "Ultrasound-contrast-agent dispersion and velocity imaging for prostate cancer localization," Med. Imag. Anal. **35**, 610–619.
Varray, F. (**2011**). "Simulation in nonlinear ultrasound: Application to nonlinear parameter imaging in echo mode configuration," Ph.D. thesis, Université Claude Bernard, Lyon, France.
Varray, F., Basset, O., Tortoli, P., and Cachard, C. (**2011a**). "Extensions of nonlinear *B*/*A* parameter imaging methods for echo mode," IEEE Trans. Ultrason. Ferroelectr. Freq. Control **58**(6), 1232–1244.
Varray, F., Chenot, J., Basset, O., Tortoli, P., Melodelima, D., and Cachard, C. (**2011b**). "Nonlinear parameter imaging to characterize HIFU ablation: Preliminary in vitro results in porcine liver," in *Proceedings of the 2011 IEEE International Ultrasonics Symposium*, October 18–21, Orlando, FL, pp. 1361–1363.
Verboven, E. (**2017**). "Development of ultrasound contrast agent based radiotherapy," Ph.D. thesis, KU Leuven, Leuven, Belgium.
Waag, R. C. (**1984**). "A review of tissue characterization from ultrasonic scattering," IEEE Transact. Biomed. Eng. **31**(12), 884–893.
Wallace, K., Lloyd, C., Holland, M., and Miller, J. G. (**2007**). "Finite amplitude measurements of the nonlinear parameter *B*/*A* for liquid mixtures spanning a range relevant to tissue harmonic mode," Ultrasound Med. Biol. **33**(4), 620–629.
Wang, H., Zhu, X., Gong, X., and Zhang, D. (**2003**). "Computed tomography of the acoustic nonlinearity parameter *B*/*A* for biological tissues via difference frequency wave from a parametric array in reflection mode," Chin. Sci. Bull. **48**(22), 2427–2430.
Wen, J. J., and Breazeale, M. A. (**1988**). "A diffraction beam field expressed as the superposition of gaussian beams," J. Acoust. Soc. Am. **83**(5), 1752–1756.
Westervelt, P. J. (**1963**). "Parametric acoustic arrays," J. Acoust. Soc. Am. **35**(1), 535–537.
Williams, A. O. (**1951**). "The piston source at high frequencies," J. Acoust. Soc. Am. **23**(1), 1–6.
Wilson, W. D. (**1959**). "Speed of sound in distilled water as a function of temperature and pressure," J. Acoust. Soc. Am. **31**, 1067–1072.
Wu, J., and Tong, J. (**1998**). "Measurements of the nonlinearity parameter *B*/*A* of contrast agents," Ultrasound Med. Biol. **24**(1), 153–159.
Xia, L. (**2019**). "Analysis of acoustic nonlinearity parameter *B*/*A* in liquids containing ultrasound contrast agents," J. Acoust. Soc. Am. **146**(2), 1394–1403.
Xu, X., Mao, F., Gong, X., and Zhang, D. (**2003**). "Theoretical calculation and experimental study on the third-order nonlinearity parameter C/A for organic liquids and biological fluids," J. Acoust. Soc. Am. **113**(3), 1743–1748.
Yoshizumi, K., Sato, T., and Ichida, N. (**1987**). "A physicochemical evaluation of the nonlinear parameter *B*/*A* for media predominantly composed of water," J. Acoust. Soc. Am. **82**(1), 302–305.
Yu, J., Cai, X., Wang, Y., and Ma, Y. (**2014**). "Simulation and phantom study of the acoustic nonlinear *B*/*A* parameter for biological tissues by using comparative method," Int. J. Biosci. Biochem. Bioinf. **4**, 438–447.
Zabolotskaya, E. A., and Khokhlov, R. V. (**1969**). "Quasi-plane waves in the nonlinear acoustics of confined beams," Akust. Zh. **15**(1), 40–47 (in Russian)
Zeqiri, B., Cook, A., Rétat, L., Civale, J., and ter Haar, G. (**2015**). "On measurement of the acoustic nonlinearity parameter using the finite amplitude insertion substitution (FAIS) technique," Metrologia **52**, 406–422.
Zhang, D., Chen, X., and Gong, X. (**2001a**). "Acoustic nonlinearity parameter tomography for biological tissues via parametric array from a circular piston source–theoretical analysis and computer simulations," J. Acoust. Soc. Am. **109**(3), 1219–1225.
Zhang, J., and Dunn, F. (**1987**). "*In vivo B*/*A* determination in a mammalian organ," J. Acoust. Soc. Am. **81**(5), 1635–1637.
Zhang, J., and Dunn, F. (**1991**). "A small volume thermodynamic system for *B*/*A* measurement," J. Acoust. Soc. Am **89**(1), 73–79.
Zhang, D., and Gong, X. (**1994**). "Computer simulation of acoustic nonlinear parameter tomography," Acta Acustica **2**, 169–175.
Zhang, D., and Gong, X. (**1999**). "Experimental investigation of the acoustic nonlinearity parameter tomography for excised pathological biological tissues," Ultrasound Med. Biol. **25**(4), 593–599.
Zhang, D., and Gong, X. (**2006**). "Acoustic nonlinear imaging and its application in tissue characterization," in *Ultrasonic and Advanced Methods for Nondestructive Testing and Material Characterization* (World Scientific, New Jersey), pp. 139–153.
Zhang, D., Gong, X., and Chen, X. (**2001b**). "Experimental imaging of the acoustic nonlinearity parameter *B*/*A* for biological tissues via a parametric array," Ultrasound Med. Biol. **27**(10), 1359–1365.
Zhang, D., Gong, X., and Ye, S. (**1996**). "Acoustic nonlinearity parameter tomography for biological specimens via measurements of the second harmonics," J. Acoust. Soc. Am. **99**(4), 2397–2402.
Zhang, J., Kuhlenschmidt, M. S., and Dunn, F. (**1991**). "Influences of structural factors of biological media on the acoustic nonlinearity parameter *B*/*A*," J. Acoust. Soc. Am. **89**(1), 80–91.
Zhao, J., Li, X., Yu, J., and Wang, Y. (**2014**). "Nonlinear ultrasound simulation based on full-wave model and comparisons with kzk," Int. J. Biosci. Biochem. Bioinf. **4**(5), 322–325.
Zhao, X., and McGough, R. J. (**2014**). "The Khokhlov-Zabolotskaya-Kuznecov equation with power law attenuation," in *Proceedings of the 2014 IEEE International Ultrasonics Symposium*, September 3–6, Chicago, IL, pp. 2225–2228.
Zhe, Z., Gong, C., and Dong, Z. (**2014**). "Molecular structure dependence of acoustic nonlinearity parameter *B*/*A* for silicone oils," Chin. Phys. B **23**(5), 054302.

Zheng, Y., Maev, R. G., and Solodov, I. Y. (**1999**). "Nonlinear acoustic applications for material characterization: A review," Can. J. Phys. **77**, 927–967.
Zhu, Z., Roos, M. S., Cobb, W. N., and Jensen, K. (**1983**). "Determination of the acoustic nonlinearity parameter *B*/*A* from phase measurements," J. Acoust. Soc. Am. **74**(5), 1518–1521.
Zorebski, E., and Zorebski, M. (**2009**). "Acoustic nonlinearity parameter *B*/*A* determined by means of thermodynamic method under elevated pressures for alkanediols," Ultrasonics **54**(1), 368–374.
Zorebski, E., Zorebski, M., and Dzida, M. (**2016**). "Acoustic nonlinearity parameter *B*/*A*, internal pressure, and acoustic impedance determined at pressures up to 100 mPa for 1-ethyl-3-methylimidazolium bis [(trifluoromethyl)sulfonyl]imide," Arch. Acoust. **41**(1), 59–66.
Zorebski, E., Zorebski, M., and Ernst, S. (**2005**). "Speed of ultrasound in liquids measured at a constant acoustic pathlength. comparison and discussion of errors," J. Phys. IV France **129**, 79–82.